

Amorphous Electron-Accepting Materials for Organic Optoelectronics

Promotoren

Prof. dr. E. J. R. Sudhölter, hoogleraar in de nano-organische chemie, DelftChemTech, Technische Universiteit Delft.

Prof. dr. H. Zuilhof, hoogleraar in de organische chemie, Laboratorium voor Organische Chemie, Wageningen Universiteit.

Samenstelling promotiecommissie

Prof. dr. H. van Amerongen	Wageningen Universiteit.
----------------------------	--------------------------

Prof. dr. L. D. A. Siebbeles	Technische Universiteit Delft
------------------------------	-------------------------------

Dr. J. M. Kroon	Energieonderzoek Centrum Nederland (ECN), Petten
-----------------	--

Prof. dr. ir. R. A. J. Janssen	Technische Universiteit Eindhoven
--------------------------------	-----------------------------------

Dit onderzoek is uitgevoerd binnen de onderzoeksschool VLAG

Amorphous Electron-Accepting Materials for Organic Optoelectronics

Ganesan Palaniswamy

Proefschrift
ter verkrijging van de graad van doctor
op gezag van de Rector Magnificus
van Wageningen Universiteit,
Prof. dr. M. J. Kropff,
in het openbaar te verdedigen
op vrijdag 22 juni 2007
des namiddags te 13.30 uur in de Aula

Palaniswamy, G.

Amorphous electron-accepting materials for organic optoelectronics

Ph.D. Thesis submitted to Wageningen University – with summaries in English and Dutch

ISBN 978-90-8504-687-5

To my beloved Parents

என் அன்பு பெற்றோருக்கு சமர்ப்பணம்

Contents

Chapter 1	Introduction	1
Chapter 2	Tetrahedral <i>n</i> -Type materials : Efficient Quenching of the Excitation of <i>p</i> -Type Polymers in Amorphous Films	21
Chapter 3	Femtosecond Time-Resolved Photophysics of 1,4,5,8-Naphthalene Diimides	41
Chapter 4	Amorphous Siloxanes with Naphthalene Diimide Acceptor Moieties	59
Chapter 5	Naphthalene Diimide Side-Chain Polymers: Synthesis, Microwave Conductivity and Morphology Studies	87
	Glossary of Acronyms	105
	Summary	107
	Samenvatting	111
	Curriculum Vitae	115
	List of Publications	117
	Acknowledgments	119

Chapter 1

Introduction

Abstract

This chapter gives a brief overview of the central properties of organic (opto-) electronic materials and of the working principles of devices that are based on such materials. Specific attention is devoted to organic photovoltaic cells and in particular to heterojunction cells. The importance of the nanoscale morphology in such heterojunction devices is discussed, together with expected advantages of amorphous materials to obtain films with the desired morphology. Finally the outline of the thesis is given.

1.1. Organic Electronics

The discovery of conductivity in doped π -conjugated polymers has opened the field of organic electronics.^{1, 2} This revolutionary discovery has led to the outburst of research in which π -conjugated oligomers and polymers are investigated as an active layer in organic electronic and optoelectronic devices, such as organic field-effect transistors, organic light emitting diodes and all-organic (plastic) solar cells. The use of such π -conjugated materials in these devices has been proven to have great potential for possible commercial applications.³ These devices most commonly have an electron-donating *p*-type material and an electron-accepting *n*-type π -conjugated material. Examples of the first class include polythiophene (PT) and its derivatives like poly(3-hexylthiophene) (P3HT),⁴⁻¹² and poly-[2,5-thienylene vinylene] (PTV);¹³⁻¹⁵ derivatives of poly(phenylenevinylene) (MDMO-PPV¹⁶⁻²² and MEH-PPV²³⁻²⁹), various derivatives of polyfluorene,³⁰⁻³⁸ phthalocyanines,³⁹⁻⁴² pentacene,⁴³⁻⁴⁸ and poly(triarylamine) derivatives⁴⁹⁻⁵³ (Figure 1.1). Examples of *n*-type π -conjugated material are fullerenes and their derivatives like PCBM,^{16, 20, 54-61} and C₇₀,^{19, 62-64} perylene diimides,⁶⁵⁻⁷² naphthalene diimides,^{71, 73-78} and *n*-type polymers such as CNEPPV⁷⁹⁻⁸² (Figure 1.2).

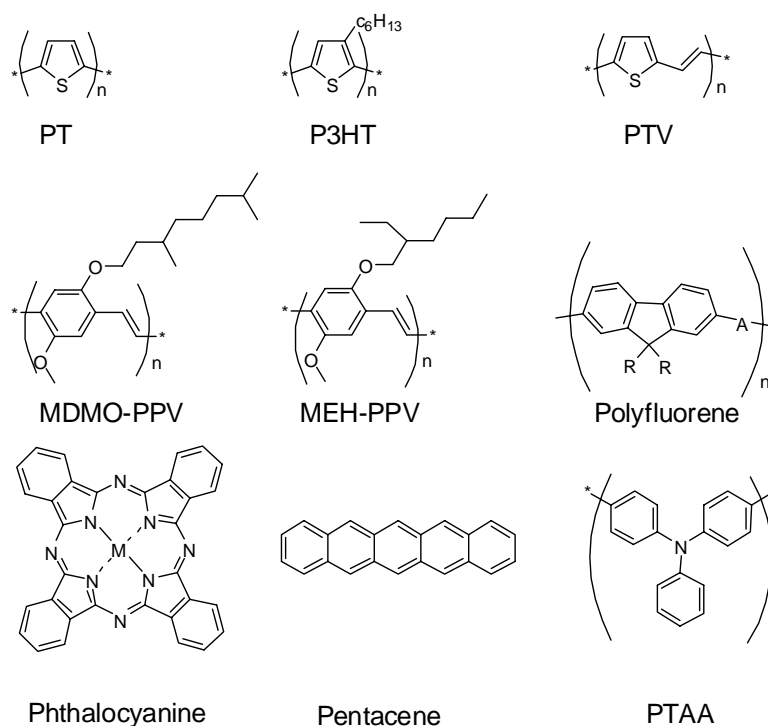


Figure 1.1. Examples of organic *p*-type materials.

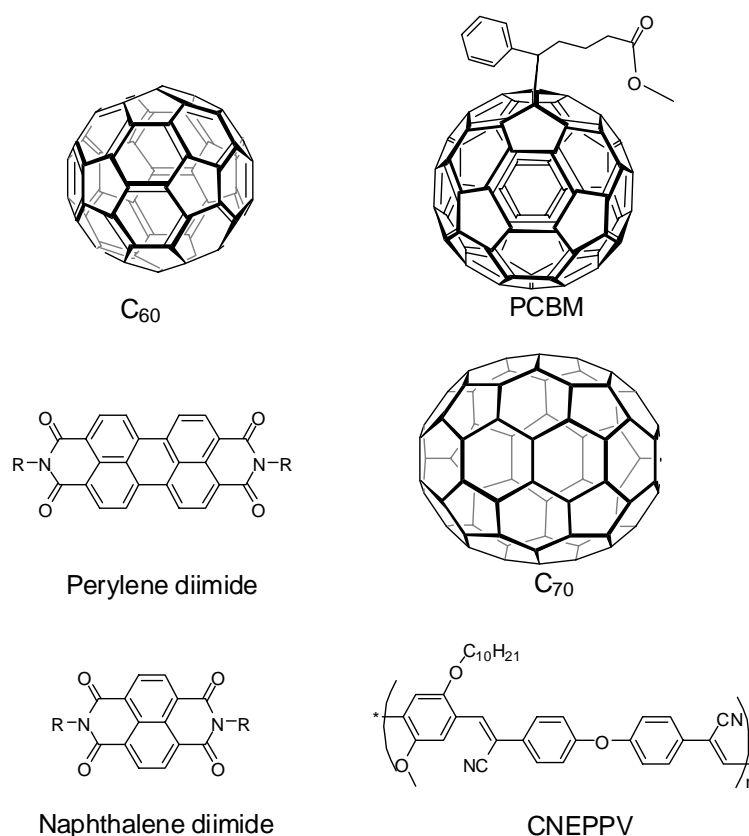


Figure 1.2. Examples of organic *n*-type materials.

Schematic representations of three organic-material based devices, namely organic light-emitting diode (OLED), organic field-effect transistor (OFET) and organic solar cell, are given in Figure 1.3. The working principles of the OLED and OFET are described, in short, below. Organic solar cells are discussed in more detail.

Light Emitting Diode (LED) devices usually consists of single or multiple layers of organic thin films, sandwiched between a glass substrate coated with indium-tin oxide (ITO), and a low work function metal (Figure 1.3.a.). Usually, the active layer consists of a conductive light-emitting layer (e.g. *p*-type polymers) and charge-transporting materials (e.g. aluminum quinoxalate). Upon applying a voltage electrons and holes flow from the electrodes to meet in the organic active layer. These charges recombine in the active layer and promote the organic molecule/polymer to its electronically excited state, which decays to the ground state by emitting light. The materials properties determine the color of the emitted light.

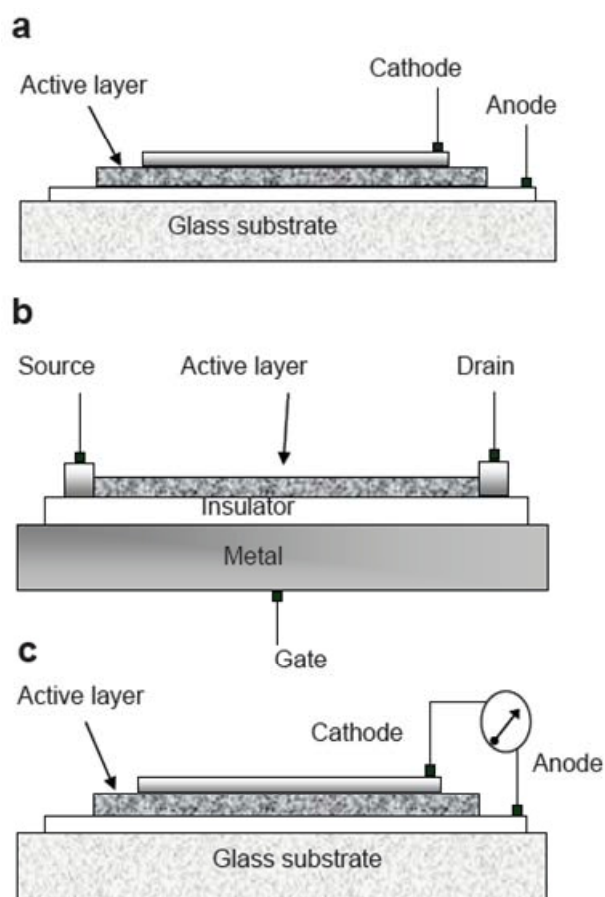


Figure 1.3. Schematic representation of organic electronic and opto-electronic devices. (a) Light Emitting Diode (LED) (b) A metal-insulator-semiconductor Field-Effect Transistor (FET) and (c) Photovoltaic device (PV).

Commonly known FETs (depicted schematically in Figure 1.3.b) are the metal-insulator-semiconductor FET (MISFET), which is also called as metal-oxide-semiconductor FET (MOSFET). In such a FET, the conducting channel of the organic semiconductor is electrically separated from the gated metal electrode by an oxide layer. The current flows between the two Ohmic contacts with the source and drain regions, through the semiconductor. This current flow is modulated by applying a voltage on the gated metal electrode. Depending on the bias of the voltage, the charge carriers are either accumulated or depleted, near the interface of the semiconductor and the insulator. If a negative voltage is applied, then holes are accumulated in the channel; if a positive voltage is applied, then the holes are depleted and electrons are accumulated. The current flow in

the channel, at a given source-drain potential, is proportional to the accumulated charges, which in turn are dependent on the applied gate voltage. As the accumulation and depletion cycle (switching speed) should be fast enough for commercial applications, high charge mobility semiconductors are required for this kind of applications.

1.2. Solar cells

The exponential growth of energy needs in the world and the depletion of the fossil fuel reserves have brought a compelling situation to this planet to find an alternative energy source. Among the alternatives, solar energy is the most attractive one, as it aims at utilizing the nearly inexhaustible energy that we obtain from the Sun.

The "photovoltaic effect" is the basic physical phenomenon through which a solar cell converts sunlight directly into a voltage. In 1839, nineteen-year-old Edmund Becquerel, a French experimental physicist, discovered the photovoltaic effect while experimenting with an electrolytic cell made up of two metal electrodes.⁸³ Becquerel found that certain materials would produce small amounts of electric current when exposed to light. After this invention, a first realistic silicon based *p-n* junction solar cell was developed at the Bell Labs in 1954.⁸⁴ Nowadays various devices based on single crystalline, poly crystalline, nano-crystalline, amorphous, ribbon and thin film silicon are used with varying overall energy efficiencies ranging between 9.5 and 24.7 % of energy conversion (as of Dec. 2006).⁸⁵ Apart from silicon-based photovoltaic devices, other inorganic devices based on a combination of materials such as GaAs, InP, *etc.* are also known, with recorded efficiencies above 32 %. Although significant progress has been made for inorganic photovoltaic devices, for many climatological conditions they are still not cost effective, partially due to the requirement of highly pure silicon. In contrast to the inorganic photovoltaic devices, organic photovoltaic devices have advantages like light-weight, easy processability, flexibility in shape and low cost of production of the relevant dyes. A wide range of available organic motifs have been stimulating research in this field over the past three decades. The main differences between the inorganic and organic solar cells are:

- a. Organic materials show a much lower charge-carrier mobilities compared to silicon. This disadvantage is partially compensated by the higher optical absorption extinction coefficient of organic materials. Due to these higher

extinction coefficients, even ~100 nm thin films are sufficient to absorb a significant fraction of the solar light, as required to make a working organic solar cell.

- b. In low-band gap silicon solar cells, the photoexcitation results directly in the separation of charges. Whereas in organic solar cells, photoexcitation results in the formation of electron-hole pairs, which are called excitons. Exciton binding energies for organic solar cells are typically higher than 0.4 eV, while for the silicon analog it is about 0.025 eV.^{86, 87}

Over the years roughly four types of (organic) solar cells with a variety of materials have been developed:

1. Schottky-type cell
2. Dye-sensitized solar cell or Grätzel cell
3. Bilayer heterojunction cell and
4. Bulk heterojunction cells

Out of these four cells, the Grätzel cells form a separate class of solar cells since they use nanoparticles of titanium dioxide, an organic dye molecule and a redox couple, making it essentially a dye-sensitized electrochemical solar cell. A schematic diagram of these four types of cells is given in Figure 1.4. In these solar cells the process of conversion of light energy into electrical energy consists of a series of four consecutive steps namely: (1) absorption of light, which leads to formation of excitons; (2) exciton diffusion; (3) dissociation of the excitons into charges (holes and electrons), and (4) charge transport through the active layer to the respective electrodes. The overall electrical current flow is the result of all the four processes and its efficiency is described by the equation:

$$\eta_j = \eta_{\text{abs}} \times \eta_{\text{diss}} \times \eta_{\text{cc}}$$

where η_j is the observed photocurrent efficiency, η_{abs} the efficiency of photon absorption, η_{diss} is the efficiency of exciton diffusion and η_{cc} is the efficiency of charge separation and collection at the electrode.

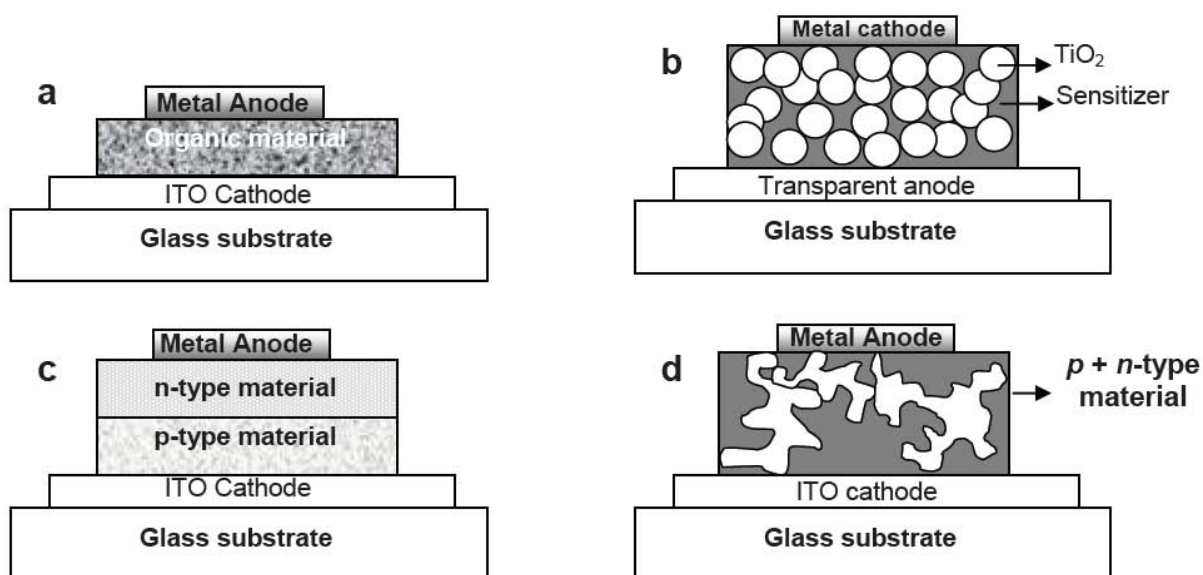


Figure 1.4. Schematic representation of different types of solar cells. (a) Schottky-type cell (b) Grätzel cell (c) Bilayer heterojunction cell (d) Bulk heterojunction cell.

In Schottky-type cells (Figure 1.4.a),⁸⁸⁻⁹⁰ a single active organic material is sandwiched between two electrodes of different work functions. This type of cell is intrinsically inefficient, since the photo-generation of charges takes place only at the metal-organic interface. Since the exciton can typically diffuse less than 20 nm,⁹¹⁻⁹⁴ only those charges created within 20 nm from the electrode contribute to the observed photocurrent. The efficiency is further reduced because of the exciton quenching at the interface. Due to these effects, this type of cells has not got much attention.

In the dye-sensitized solar cells (Figure 1.4.b), widely known as Grätzel cells, the dye (usually a ruthenium complex) absorbs the light and injects an electron into the titanium dioxide nanoparticles. The electron lost by the dye is regenerated by a redox couple (I^-/I_3^-), in which iodide is converted into iodine. The injected electrons are conducted through the nanocrystalline film of TiO_2 and collected at the transparent anode ($SnO_2:F$). The iodine travels to the cathode and reconverted into iodide. The energy conversion efficiency of this kind of solar cells has reached values up to 10.4%.^{85,95} A major drawback of this kind of solar cell is the usage of an organic liquid to dissolve the redox couple, due to which the whole system should be sealed perfectly to prevent

evaporation of the solvent. Studies with non-volatile ionic liquids to replace these have been started, but up to now this has only yielded a significantly lower efficiency.^{96-99, 100}

In a bilayer device, also known as a heterojunction cell (Figure 1.4.c), the electron-donor (*p*-type) and the electron-acceptor (*n*-type) materials are coated on top of each other and sandwiched between two electrodes. The *p*- and *n*-type materials form a planar interface where charge separation occurs. An example of such a heterojunction cell, based on a phthalocyanine donor and a perylene diimide acceptor, got attention when it was reported by Tang *et al.* showing an energy efficiency of 1 %.¹⁰¹ Various other molecular and polymeric materials were investigated and described elsewhere.^{40, 102, 103} In silicon-based *p-n* junction cells, the majority of free charge carriers are generated upon doping. After band gap excitation the electron-hole pair separates at the junction. In the organic heterojunction cells no controlled doping is applied and the charges are formed at the junction by electron transfer from the photo-excited donor to the acceptor, or from the donor to the photo-excited acceptor. Therefore, in these heterojunction cells it is a prerequisite that the donor and acceptor materials are chosen such that the driving force for photo-induced electron transfer is favorable. With this class heterojunction devices, an efficiency up to 3.6 % has been observed, in which the *p-n* junction is formed by thermal evaporation of the donor phthalocyanines and the acceptor C₆₀.¹⁰⁴

The bulk heterojunction solar cells (Figure 1.4.d.) operate on the same principles as the bilayer devices, but provide a larger donor-acceptor interfacial area to enable efficient charge separation. In the bilayer devices the donor and acceptor materials are in contact with anode and cathode electrodes, respectively. This enables an easy charge collection. In bulk heterojunction cells the donor and acceptor materials should form a continuous pathway for charge transport. Therefore, the morphology of the mixed donor and acceptor layer is of utmost importance. By far the most successful bulk heterojunction cells are mainly based on a combination of a conjugated electron-donor polymer (MDMO-PPV or P3HT) with a derivative of C₆₀ or C₇₀. With such combination of organic materials energy efficiencies up to 5.2 %¹⁰⁵ have been achieved.^{19, 106-108} The highest efficiencies reported were obtained by optimization of the solvent used for the spin-coating process and by application of proper post-production techniques like temperature annealing, in order to get an interpenetrating network and a bicontinuous phase. These results confirm that by changing the morphology, the performance of the

photovoltaic devices could be improved. In the following session the morphology of the bulk heterojunction is discussed in more detail.

1.3. Morphology of bulk heterojunction films

It is known that small molecular semiconducting materials tend to crystallize.¹⁰⁹ This tendency of crystallization is less in neutral organic molecules compared to salts, since the only intermolecular interactions are the Van der Waals attractions. However, control over it is essential for organic solar cells, as such crystallization of organic molecules plays an important role in the optical absorption properties and charge mobilities. Besides, such a crystallization in the bulk heterojunction film may lead to phase separation. There are three main criteria, which effect the final morphology of the bulk heterojunctions.

1. Molecular chemical structure of the individual components
2. Inter- and intramolecular ordering and interactions and
3. Inter-component interactions and their miscibility

Apart from the above, the film preparation conditions (like solvent, spin-coating conditions, etc.) and post-production techniques (like annealing) also influence the morphology and thus the final performance of the materials.^{106, 108, 110} These influences can be classified into thermodynamic and kinetic parameters.¹¹¹

In short, the structural ordering of the components and their electrical properties within a scale of 10 – 100 nm (representing the exciton diffusion length and the typical thickness of the film, respectively) has a dominant effect on the final device performance. Therefore, it is essential that there is an intimate mixing between the donor and the acceptor components with phase separation in the order of the exciton diffusion length (10 nm) or in other words supramolecular dimensions. Changes in physical parameters and post-production processes can improve the morphology, mainly of the electron-donating polymers, which brings more ordering in these polymers. This improved ordering in the polymers increases the hole mobility, which in turn results in a higher energy efficiency. At the same time, this leads to phase separation and crystallization of the electron-accepting component (e.g. PCBM). This kind of phase separation and

crystallization hampers the formation of a bicontinuous phase within the film, and to form such a bicontinuous phase higher amounts of PCBM (upto 80 % by weight) are then necessary.

There have been many attempts to improve the morphology by changing parameters like solvent, donor-acceptor molar ratios and annealing conditions. These attempts have resulted in a better understanding of the device performance in relation to the morphology. But there are not many attempts made to understand the morphology by changing the molecular structure of the active component, especially in the acceptor part. Therefore, this thesis aims at understanding the change in morphology on changing the molecular structure of the acceptor in such a way that amorphous materials are obtained.

1.4. Amorphous materials for opto-electronic applications

Amorphous molecular materials or molecular glasses are interesting for opto-electronic applications because of their following properties.¹¹²

1. They are in a thermodynamically non-equilibrium state and hence may exhibit glass-transition phenomena usually associated with amorphous polymers.
2. They may possess a variety of states such as the amorphous glass, super-cooled liquid or crystal.
3. They may be characterized by the presence of free volume and by the disorder of both intermolecular distance and orientation.
4. They may form uniform, transparent amorphous thin films by vapor deposition and spin-coating methods.
5. In contrast to single crystals and liquid crystals that show anisotropic properties, amorphous molecular materials may exhibit isotropic properties as well as homogeneous properties due to the absence of grain boundaries.
6. In contrast to polymers, they are pure materials with well-defined molecular structures and definite molecular weights without any polydispersity.

There have been many attempts to use organic amorphous materials¹¹³⁻¹¹⁸ for (opto-) electronic devices. A more detailed review can be found elsewhere.¹¹² In this thesis

electron-accepting materials, based on two different classes of amorphous low-molecular weight molecular materials and on an amorphous side-chain polymer, are described. All the materials described in this thesis contain the naphthalene diimide (NDI) unit as the acceptor moiety. This unit has been chosen due their high electron mobilities and electron-accepting capabilities from a variety of donor materials.^{71, 73-78}

1.5. Outline of thesis

Apart from this introductory Chapter 1, this thesis consists of four experimental chapters.

In Chapter 2, the synthesis of a new class of amorphous materials with a central tetrahedral core is described (Figure 1.5). This tetrahedral core in the molecule gives amorphous properties to the resulting material, which decouples the optoelectronic properties from the molecular structure. Extensive studies on such materials are made, specifically in a blend with *p*-type polymers, for which we report the fluorescence quenching efficiency, morphology and time-resolved microwave conductivity.

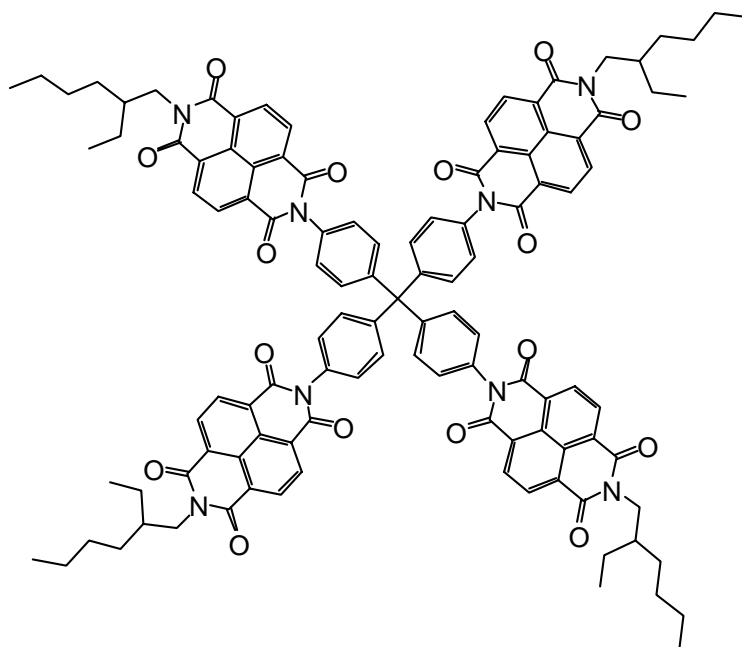


Figure 1.5. Tetrahedral molecule described in Chapter 2.

Chapter 3 describes the photophysics of this tetrahedral molecule and two of its model compounds. Both steady-state and time-resolved absorption and fluorescence techniques have been used to delineate the excited state processes and the time scale in which they occur in these molecules. Femtosecond transient absorption spectroscopy reveals electron transfer from phenyl to the naphthalenediimide moiety. This conclusion of room temperature measurements were confirmed with low temperature (77 K) fluorescence lifetime measurements.

In Chapter 4, the syntheses of another new class of well-defined amorphous materials based on the hydrosilylation of linear and cyclic siloxanes (Figure 1.6) are described. The interactions between the NDI chromophores are influenced by the size of the cycle and have an effect on the film morphology. A series of NMR and photophysical studies were carried out, both in solution and in thin films, in order to ascertain their molecular structure and geometry.

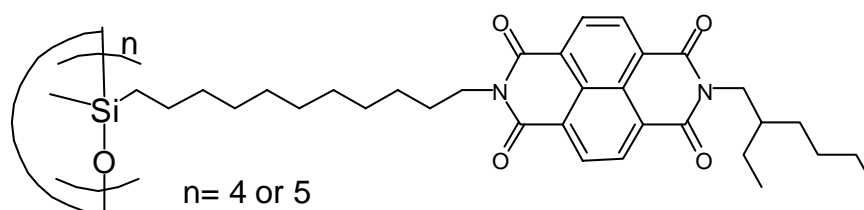


Figure 1.6. Cyclic siloxane-based *n*-type materials described in Chapter 4.

Chapter 5 describes the synthesis of side-chain polymers (Figure 1.7) based on poly(styrene/1-alkene-*alt*-maleic anhydride) by grafting the NDI chromophores to the polymer backbone. These polymers are obtained in their imide form, without any free carboxylic acid functional groups. The polymers are studied in a blend with *p*-type polymers, to investigate fluorescence quenching, morphology and their photo-induced conductivity using time-resolved microwave conductivity measurements.

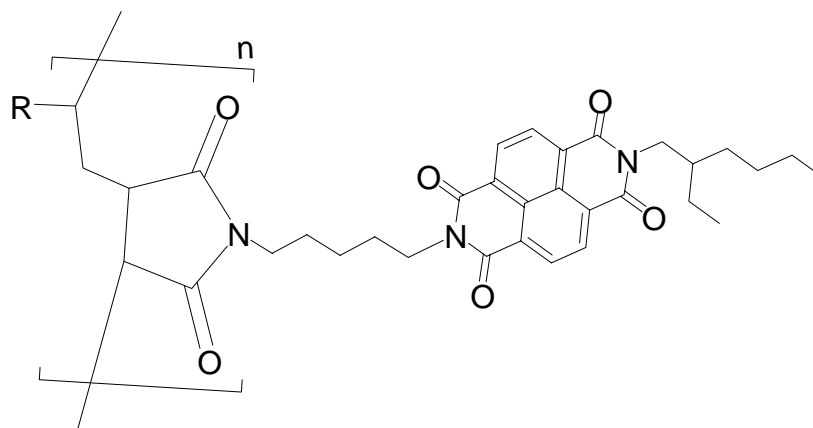


Figure 1.7. Side-chain polymers studied in Chapter 5.

1.6. References

1. Chiang, C. K.; Fincher, C. R.; Park, Y. W.; Heeger, A. J.; Shirakawa, H.; Louis, E. J.; Gau, S. C.; Macdiarmid, A. G. *Phys. Rev. Lett.* **1977**, *39*, 1098-1101.
2. Shirakawa, H.; Louis, E. J.; Macdiarmid, A. G.; Chiang, C. K.; Heeger, A. J. *J. Chem. Soc.-Chem. Commun.* **1977**, 578-580.
3. <http://www.oled-info.com/history>
4. Liu, J. S.; Tanaka, T.; Sivula, K.; Alivisatos, A. P.; Frechet, J. M. J. *J. Am. Chem. Soc.* **2004**, *126*, 6550-6551.
5. Ramos, A. M.; Rispens, M. T.; van Duren, J. K. J.; Hummelen, J. C.; Janssen, R. A. *J. Am. Chem. Soc.* **2001**, *123*, 6714-6715.
6. Sirringhaus, H.; Brown, P. J.; Friend, R. H.; Nielsen, M. M.; Bechgaard, K.; Langeveld-Voss, B. M. W.; Spiering, A. J. H.; Janssen, R. A. J.; Meijer, E. W.; Herwig, P.; de Leeuw, D. M. *Nature* **1999**, *401*, 685-688.
7. Roman, L. S.; Andersson, M. R.; Yohannes, T.; Inganas, O. *Adv. Mater.* **1997**, *9*, 1164-1168.
8. McCullough, R. D.; Lowe, R. D.; Jayaraman, M.; Anderson, D. L. *J. Org. Chem.* **1993**, *58*, 904-912.
9. Roncali, J. *Chem. Rev.* **1992**, *92*, 711-738.
10. Tsumura, A.; Koezuka, H.; Ando, T. *Appl. Phys. Lett.* **1986**, *49*, 1210-1212.

11. Bredas, J. L.; Themans, B.; Fripiat, J. G.; Andre, J. M.; Chance, R. R. *Phys. Rev. B* **1984**, *29*, 6761-6773.
12. Glenis, S.; Horowitz, G.; Tourillon, G.; Garnier, F. *Thin Solid Films* **1984**, *111*, 93-103.
13. Fuchigami, H.; Tsumura, A.; Koezuka, H. *Appl. Phys. Lett.* **1993**, *63*, 1372-1374.
14. Murase, I.; Ohnishi, T.; Noguchi, T.; Hirooka, M. *Polymer Communications* **1987**, *28*, 229-231.
15. Jen, K. Y.; Maxfield, M.; Shacklette, L. W.; Elsenbaumer, R. L. *J. Chem. Soc.-Chem. Commun.* **1987**, 309-311.
16. Hoppe, H.; Niggemann, M.; Winder, C.; Kraut, J.; Hiesgen, R.; Hinsch, A.; Meissner, D.; Sariciftci, N. S. *Adv. Funct. Mater.* **2004**, *14*, 1005-1011.
17. Van Duren, J. K. J.; Yang, X. N.; Loos, J.; Bulle-Lieuwma, C. W. T.; Sieval, A. B.; Hummelen, J. C.; Janssen, R. A. J. *Adv. Funct. Mater.* **2004**, *14*, 425-434.
18. Rispens, M. T.; Meetsma, A.; Rittberger, R.; Brabec, C. J.; Sariciftci, N. S.; Hummelen, J. C. *Chem. Commun.* **2003**, 2116-2118.
19. Wienk, M. M.; Kroon, J. M.; Verhees, W. J. H.; Knol, J.; Hummelen, J. C.; van Hal, P. A.; Janssen, R. A. J. *Angew. Chem.-Int. Edit.* **2003**, *42*, 3371-3375.
20. Martens, T.; D'Haen, J.; Munters, T.; Beelen, Z.; Goris, L.; Manca, J.; D'Olieslaeger, M.; Vanderzande, D.; De Schepper, L.; Andriessen, R. *Synth. Met.* **2003**, *138*, 243-247.
21. Van Hal, P. A.; Wienk, M. M.; Kroon, J. M.; Verhees, W. J. H.; Slooff, L. H.; van Gennip, W. J. H.; Jonkheijm, P.; Janssen, R. A. J. *Adv. Mater.* **2003**, *15*, 118-121.
22. Munters, T.; Martens, T.; Goris, L.; Vrindts, V.; Manca, J.; Lutsen, L.; De Ceuninck, W.; Vanderzande, D.; De Schepper, L.; Gelan, J.; Sariciftci, N. S.; Brabec, C. J. *Thin Solid Films* **2002**, *403*, 247-251.
23. Nguyen, T. Q.; Martini, I. B.; Liu, J.; Schwartz, B. J. *J. Phys. Chem. B* **2000**, *104*, 237-255.
24. Kohler, A.; dos Santos, D. A.; Beljonne, D.; Shuai, Z.; Bredas, J. L.; Holmes, A. B.; Kraus, A.; Mullen, K.; Friend, R. H. *Nature* **1998**, *392*, 903-906.
25. Scott, J. C.; Kaufman, J. H.; Brock, P. J.; DiPietro, R.; Salem, J.; Goitia, J. A. *J. Appl. Phys.* **1996**, *79*, 2745-2751.

26. Yu, G.; Gao, J.; Hummelen, J. C.; Wudl, F.; Heeger, A. J. *Science* **1995**, *270*, 1789-1791.
27. Yu, G.; Heeger, A. J. *J. Appl. Phys.* **1995**, *78*, 4510-4515.
28. Yu, G.; Pakbaz, K.; Heeger, A. J. *Appl. Phys. Lett.* **1994**, *64*, 3422-3424.
29. Parker, I. D. *J. Appl. Phys.* **1994**, *75*, 1656-1666.
30. Charas, A.; Morgado, J.; Martinho, J. M. G.; Alcacer, L.; Cacialli, F. *Chem. Commun.* **2001**, 1216-1217.
31. Scherf, U.; List, E. J. W. *Adv. Mater.* **2002**, *14*, 477-487.
32. List, E. J. W.; Guentner, R.; de Freitas, P. S.; Scherf, U. *Adv. Mater.* **2002**, *14*, 374-378.
33. Setayesh, S.; Grimsdale, A. C.; Weil, T.; Enkelmann, V.; Mullen, K.; Meghdadi, F.; List, E. J. W.; Leising, G. *J. Am. Chem. Soc.* **2001**, *123*, 946-953.
34. Bernius, M. T.; Inbasekaran, M.; O'Brien, J.; Wu, W. S. *Adv. Mater.* **2000**, *12*, 1737-1750.
35. Grell, M.; Knoll, W.; Lupo, D.; Meisel, A.; Miteva, T.; Neher, D.; Nothofer, H. G.; Scherf, U.; Yasuda, A. *Adv. Mater.* **1999**, *11*, 671-675.
36. Bliznyuk, V. N.; Carter, S. A.; Scott, J. C.; Klarner, G.; Miller, R. D.; Miller, D. C. *Macromolecules* **1999**, *32*, 361-369.
37. Redecker, M.; Bradley, D. D. C.; Inbasekaran, M.; Woo, E. P. *Appl. Phys. Lett.* **1998**, *73*, 1565-1567.
38. Pei, Q. B.; Yang, Y. *J. Am. Chem. Soc.* **1996**, *118*, 7416-7417.
39. Xue, J. G.; Uchida, S.; Rand, B. P.; Forrest, S. R. *Appl. Phys. Lett.* **2004**, *84*, 3013-3015.
40. Peumans, P.; Yakimov, A.; Forrest, S. R. *J. Appl. Phys.* **2003**, *93*, 3693-3723.
41. Rostalski, J.; Meissner, D. *Sol. Energy Mater. Sol. Cells* **2000**, *61*, 87-95.
42. Wohrle, D.; Meissner, D. *Adv. Mater.* **1991**, *3*, 129-138.
43. Lloyd, M. T.; Mayer, A. C.; Tayi, A. S.; Bowen, A. M.; Kasen, T. G.; Herman, D. J.; Mourey, D. A.; Anthony, J. E.; Malliaras, G. G. *Org. Electron.* **2006**, *7*, 243-248.
44. Dimitrakopoulos, C. D.; Malenfant, P. R. L. *Adv. Mater.* **2002**, *14*, 99-117.
45. Vertsimakha, Y.; Verbitsky, A. *Synth. Met.* **2000**, *109*, 291-294.
46. Nelson, S. F.; Lin, Y. Y.; Gundlach, D. J.; Jackson, T. N. *Appl. Phys. Lett.* **1998**, *72*, 1854-1856.

47. Lin, Y. Y.; Gundlach, D. J.; Nelson, S. F.; Jackson, T. N. *IEEE Electron Device Lett.* **1997**, *18*, 606-608.
48. Gundlach, D. J.; Lin, Y. Y.; Jackson, T. N.; Nelson, S. F.; Schlom, D. G. *IEEE Electron Device Lett.* **1997**, *18*, 87-89.
49. Chan, L. H.; Lee, R. H.; Hsieh, C. F.; Yeh, H. C.; Chen, C. T. *J. Am. Chem. Soc.* **2002**, *124*, 6469-6479.
50. Liu, S.; Jiang, X. Z.; Ma, H.; Liu, M. S.; Jen, A. K. Y. *Macromolecules* **2000**, *33*, 3514-3517.
51. Thelakkat, M.; Hagen, J.; Haarer, D.; Schmidt, H. W. *Synth. Met.* **1999**, *102*, 1125-1128.
52. Bellmann, E.; Shaheen, S. E.; Thayumanavan, S.; Barlow, S.; Grubbs, R. H.; Marder, S. R.; Kippelen, B.; Peyghambarian, N. *Chem. Mater.* **1998**, *10*, 1668-1676.
53. Kolb, E. S.; Gaudiana, R. A.; Mehta, P. G. *Macromolecules* **1996**, *29*, 2359-2364.
54. Waldauf, C.; Schilinsky, P.; Perisutti, M.; Hauch, J.; Brabec, C. J. *Adv. Mater.* **2003**, *15*, 2084-2088.
55. Svensson, M.; Zhang, F. L.; Veenstra, S. C.; Verhees, W. J. H.; Hummelen, J. C.; Kroon, J. M.; Inganas, O.; Andersson, M. R. *Adv. Mater.* **2003**, *15*, 988-991.
56. Padinger, F.; Rittberger, R. S.; Sariciftci, N. S. *Adv. Funct. Mater.* **2003**, *13*, 85-88.
57. Brabec, C. J.; Winder, C.; Sariciftci, N. S.; Hummelen, J. C.; Dhanabalan, A.; van Hal, P. A.; Janssen, R. A. J. *Adv. Funct. Mater.* **2002**, *12*, 709-712.
58. Dhanabalan, A.; van Duren, J. K. J.; van Hal, P. A.; van Dongen, J. L. J.; Janssen, R. A. J. *Adv. Funct. Mater.* **2001**, *11*, 255-262.
59. Gebeyehu, D.; Brabec, C. J.; Padinger, F.; Fromherz, T.; Hummelen, J. C.; Badt, D.; Schindler, H.; Sariciftci, N. S. *Synth. Met.* **2001**, *118*, 1-9.
60. Neugebauer, H.; Brabec, C.; Hummelen, J. C.; Sariciftci, N. S. *Sol. Energy Mater. Sol. Cells* **2000**, *61*, 35-42.
61. Brabec, C. J.; Padinger, F.; Hummelen, J. C.; Janssen, R. A. J.; Sariciftci, N. S. *Synth. Met.* **1999**, *102*, 861-864.
62. Haddock, J. N.; Zhang, X. H.; Domercq, B.; Kippelen, B. *Org. Electron.* **2005**, *6*, 182-187.
63. Wang, X. J.; Perzon, E.; Oswald, F.; Langa, F.; Admassie, S.; Andersson, M. R.; Inganas, O. *Adv. Funct. Mater.* **2005**, *15*, 1665-1670.

- 64. Yao, Y.; Shi, C. J.; Li, G.; Shrotriya, V.; Pei, Q. B.; Yang, Y. *Appl. Phys. Lett.* **2006**, *89*, 153507.
- 65. Del Cano, T.; Hashimoto, K.; Kageyama, H.; De Saja, J. A.; Aroca, R.; Ohmori, Y.; Shirota, Y. *Appl. Phys. Lett.* **2006**, *88*, 071117.
- 66. Rybtchinski, B.; Sinks, L. E.; Wasielewski, M. R. *J. Am. Chem. Soc.* **2004**, *126*, 12268-12269.
- 67. Li, X. Y.; Sinks, L. E.; Rybtchinski, B.; Wasielewski, M. R. *J. Am. Chem. Soc.* **2004**, *126*, 10810-10811.
- 68. Im, C.; Tian, W.; Bassler, H.; Fechtenkotter, A.; Watson, M. D.; Mullen, K. *Synth. Met.* **2003**, *139*, 683-686.
- 69. Van der Boom, T.; Hayes, R. T.; Zhao, Y. Y.; Bushard, P. J.; Weiss, E. A.; Wasielewski, M. R. *J. Am. Chem. Soc.* **2002**, *124*, 9582-9590.
- 70. Angadi, M.; Gosztola, D.; Wasielewski, M. R. *Mater. Sci. Eng. B-Solid State Mater. Adv. Technol.* **1999**, *63*, 191-194.
- 71. Angadi, M. A.; Gosztola, D.; Wasielewski, M. R. *J. Appl. Phys.* **1998**, *83*, 6187-6189.
- 72. Neuteboom, E. E.; Meskers, S. C. J.; van Hal, P. A.; van Duren, J. K. J.; Meijer, E. W.; Janssen, R. A. J.; Dupin, H.; Pourtois, G.; Cornil, J.; Lazzaroni, R.; Bredas, J. L.; Beljonne, D. *J. Am. Chem. Soc.* **2003**, *125*, 8625-8638.
- 73. Ganesan, P.; Yang, X. N.; Loos, J.; Savenije, T. J.; Abellon, R. D.; Zuilhof, H.; Sudhölter, E. J. R. *J. Am. Chem. Soc.* **2005**, *127*, 14530-14531.
- 74. Katz, H. E.; Bao, Z. N.; Gilat, S. L. *Accounts Chem. Res.* **2001**, *34*, 359-369.
- 75. Katz, H. E.; Johnson, J.; Lovinger, A. J.; Li, W. J. *J. Am. Chem. Soc.* **2000**, *122*, 7787-7792.
- 76. Katz, H. E.; Lovinger, A. J.; Johnson, J.; Kloc, C.; Siegrist, T.; Li, W.; Lin, Y. Y.; Dodabalapur, A. *Nature* **2000**, *404*, 478-481.
- 77. Laquindanum, J. G.; Katz, H. E.; Dodabalapur, A.; Lovinger, A. J. *J. Am. Chem. Soc.* **1996**, *118*, 11331-11332.
- 78. Wasielewski, M. R.; Wiederrecht, G. P.; Svec, W. A.; Niemczyk, M. P. *Sol. Energy Mater. Sol. Cells* **1995**, *38*, 127-134.
- 79. Offermans, T.; van Hal, P. A.; Meskers, S. C. J.; Koetse, M. M.; Janssen, R. A. J. *Phys. Rev. B* **2005**, *72*, 045213.

80. Loos, J.; Yang, X. N.; Koetse, M. M.; Sweelssen, J.; Schoo, H. F. M.; Veenstra, S. C.; Grogger, W.; Kothleitner, G.; Hofer, F. *J. Appl. Polym. Sci.* **2005**, *97*, 1001-1007.
81. Quist, P. A. C.; Savenije, T. J.; Koetse, M. M.; Veenstra, S. C.; Kroon, J. M.; Siebbeles, L. D. A. *Adv. Funct. Mater.* **2005**, *15*, 469-474.
82. Veenstra, S. C.; Verhees, W. J. H.; Kroon, J. M.; Koetse, M. M.; Sweelssen, J.; Bastiaansen, J.; Schoo, H. F. M.; Yang, X.; Alexeev, A.; Loos, J.; Schubert, U. S.; Wienk, M. M. *Chem. Mater.* **2004**, *16*, 2503-2508.
83. Goetzberger, A.; Hebling, C.; Schock, H. W. *Mater. Sci. Eng. R-Rep.* **2003**, *40*, 1-46.
84. Chapin, D. M.; Fuller, C. S.; Pearson, G. L. *J. Appl. Phys.* **1954**, *25*, 676-677.
85. Green, M. A.; Emery, K.; King, D. L.; Hishikawa, Y.; Warta, W. *Prog. Photovolt: Res. Appl.* **2007**, *15*, 35-40.
86. Gregg, B. A. *J. Phys. Chem. B* **2003**, *107*, 4688-4698.
87. Gregg, B. A.; Hanna, M. C. *J. Appl. Phys.* **2003**, *93*, 3605-3614.
88. Morizumi, T.; Kudo, K. *Appl. Phys. Lett.* **1981**, *38*, 85-86.
89. Chamberlain, G. A.; Cooney, P. J.; Dennison, S. *Nature* **1981**, *289*, 45-47.
90. Ghosh, A. K.; Feng, T. *J. Appl. Phys.* **1978**, *49*, 5982-5989.
91. Kerp, H. R.; Donker, H.; Koehorst, R. B. M.; Schaafsma, T. J.; van Faassen, E. E. *Chem. Phys. Lett.* **1998**, *298*, 302-308.
92. Haugeneder, A.; Neges, M.; Kallinger, C.; Spirk, W.; Lemmer, U.; Feldmann, J.; Scherf, U.; Harth, E.; Gugel, A.; Mullen, K. *Phys. Rev. B* **1999**, *59*, 15346-15351.
93. Halls, J. J. M.; Pichler, K.; Friend, R. H.; Moratti, S. C.; Holmes, A. B. *Appl. Phys. Lett.* **1996**, *68*, 3120-3122.
94. Yoshino, K.; Yin, X. H.; Muro, K.; Kiyomatsu, S.; Morita, S.; Zakhidov, A. A.; Noguchi, T.; Ohnishi, T. *Jpn. J. Appl. Phys. Part 2 - Lett.* **1993**, *32*, L357-L360.
95. Nazeeruddin, M. K.; Pechy, P.; Renouard, T.; Zakeeruddin, S. M.; Humphry-Baker, R.; Comte, P.; Liska, P.; Cevey, L.; Costa, E.; Shklover, V.; Spiccia, L.; Deacon, G. B.; Bignozzi, C. A.; Gratzel, M. *J. Am. Chem. Soc.* **2001**, *123*, 1613-1624.
96. Bach, U.; Lupo, D.; Comte, P.; Moser, J. E.; Weissortel, F.; Salbeck, J.; Spreitzer, H.; Gratzel, M. *Nature* **1998**, *395*, 583-585.
97. Kroeze, J. E.; Hirata, N.; Schmidt-Mende, L.; Orizu, C.; Ogier, S. D.; Carr, K.; Gratzel, M.; Durrant, J. R. *Adv. Funct. Mater.* **2006**, *16*, 1832-1838.

98. Snaith, H. J.; Schmidt-Mende, L.; Gratzel, M.; Chiesa, M. *Phys. Rev. B* **2006**, *74*, 045306.
99. Mohmeyer, N.; Kuang, D. B.; Wang, P.; Schmidt, H. W.; Zakeeruddin, S. M.; Gratzel, M. *J. Mater. Chem.* **2006**, *16*, 2978-2983.
100. Stathatos, E.; Lianos, R.; Zakeeruddin, S. M.; Liska, P.; Gratzel, M. *Chem. Mater.* **2003**, *15*, 1825-1829.
101. Tang, C. W. *Appl. Phys. Lett.* **1986**, *48*, 183-185.
102. Pettersson, L. A. A.; Roman, L. S.; Inganas, O. *J. Appl. Phys.* **1999**, *86*, 487-496.
103. Harima, Y.; Yamashita, K.; Suzuki, H. *Appl. Phys. Lett.* **1984**, *45*, 1144-1145.
104. Peumans, P.; Forrest, S. R. *Appl. Phys. Lett.* **2001**, *79*, 126-128.
105. Reyes-Reyes, M.; Kim, K.; Dewald, J.; Lopez-Sandoval, R.; Avadhanula, A.; Curran, S.; Carroll, D. L. *Org. Lett.* **2005**, *7*, 5749-5752.
106. Ma, W. L.; Yang, C. Y.; Gong, X.; Lee, K.; Heeger, A. J. *Adv. Funct. Mater.* **2005**, *15*, 1617-1622.
107. Brabec, C. J.; Sariciftci, N. S.; Hummelen, J. C. *Adv. Funct. Mater.* **2001**, *11*, 15-26.
108. Reyes-Reyes, M.; Kim, K.; Carroll, D. L. *Appl. Phys. Lett.* **2005**, *87*, 083506.
109. Baker, K. N.; Fratini, A. V.; Resch, T.; Knachel, H. C.; Adams, W. W.; Socci, E. P.; Farmer, B. L. *Polymer* **1993**, *34*, 1571-1587.
110. Al-Ibrahim, M.; Ambacher, O.; Sensfuss, S.; Gobsch, G. *Appl. Phys. Lett.* **2005**, *86*.
111. Yang, X.; Loos, J. *Macromolecules* **2007**, *40*, 1353-1362.
112. Shirota, Y. *J. Mater. Chem.* **2000**, *10*, 1-25.
113. Castro, C. M.; Delgado, M. C. R.; Hernandez, V.; Shirota, Y.; Casado, J.; Navarrete, J. T. L. *J. Phys. Chem. B* **2002**, *106*, 7163-7170.
114. Wang, S. J.; Oldham, W. J.; Hudack, R. A.; Bazan, G. C. *J. Am. Chem. Soc.* **2000**, *122*, 5695-5709.
115. Robinson, M. R.; Wang, S. J.; Heeger, A. J.; Bazan, G. C. *Adv. Funct. Mater.* **2001**, *11*, 413-419.
116. Hughes, G.; Bryce, M. R. *J. Mater. Chem.* **2005**, *15*, 94-107.
117. Grigalevicius, S. *Synth. Met.* **2006**, *156*, 1-12.
118. Grazulevicius, J. V. *Polym. Adv. Technol.* **2006**, *17*, 694-696.

Chapter 2

Tetrahedral *n*-Type Materials: Efficient Quenching of the Excitation of *p*-Type Polymers in Amorphous Films

Abstract

A new approach towards the design and synthesis of amorphous *n*-type materials is presented. The tetrahedral core in the molecule gives amorphous properties to the resulting material, which decouples the optoelectronic properties from the molecular structure. This allows a systematic improvement of the optoelectronic properties. As a starting point the non-directionality available via tetrahedral cores, as present in tetra(phenyl)methane, is used. This chapter presents the first steady-state and transient optical data and ground-state electrochemical properties of a novel naphthalene diimide-based *n*-type material. In addition, morphology and transient charge carrier studies were performed on blended films of this tetrahedral molecule and polymeric *p*-type materials.

2.1. Introduction

The possibility to tailor the properties of molecular materials by adjusting the HOMO and LUMO levels in order to achieve an efficient charge separation has enabled over the past decade a surge in the efforts directed towards the development of all-organic solar cells.¹⁻⁵ Basically two types of such solar cells have been envisaged: 1) *p-n* double layer cells, in which two layers of *p*- and *n*-type materials are deposited on top of each other,⁶ and 2) bulk heterojunction cells, in which the *p*-type and *n*-type materials are blended, so as to form a bi-continuous phase to allow charge transport to opposite electrodes.^{7, 8}

The most well-known of the latter type of cells are based on a polymeric *p*-type material, such as MDMO-PPV and P3HT, and *n*-type materials like the bucky - ball derivatives. The success of these devices⁹ hinges on many aspects, including proper electronic states of *p*-type and *n*-type materials, efficient light absorption by the *p*-type and *n*-type material, and an appropriately small degree of phase separation in the order of few tens of nanometer to obtain an efficient charge separation and a bi-continuous phase. Limitations include a) phase separation of the *n*-type material, which requires high amounts of the bucky-ball derivatives (~80 weight %) to obtain the optimal bi-continuous phase and charge transport, b) limited visible light absorption by C₆₀-derivates,¹⁰ and c) the fact that the spherical-shape of the bucky ball that allows charge transport in nearly all directions with equal probability is intrinsically linked to its optical absorption properties and therefore hard to improve systematically.

One of the major difficulties faced with organic materials is their crystallization and aggregation behavior in films. In case of photovoltaic devices, it has been realized that the crystallization¹¹ of the *n*-type material poses a problem and therefore, morphology and processing conditions of the active organic layer are important for obtaining an efficient device. In our current work we have attempted to overcome the crystallization problem using amorphous materials with 1,4,5,8-naphthalene tetracarboxylic diimide (NDI) moieties. NDIs are air-stable electron conductors¹² that are capable of accepting electrons from electronically excited ruthenium complexes¹³ and porphyrins¹⁴ when they are covalently bound to the donor molecule.

This chapter presents the data of this new approach, in which the shape of the (NDI-containing) *n*-type molecule, that yields the amorphous properties,¹⁵ to the resulting

material, which decouples the optoelectronic properties from the molecular structure. This allows a systematic improvement of the latter. This approach uses the non-directionality available via tetrahedral cores, such as those of tetra(phenyl)methane. In contrast to a polymeric approach, like in the case of *p*-type materials, small molecules have the advantage that they can be obtained in pure form and have a defined structural arrangement in films. To prevent crystallization of *p*-type materials in OLEDs, such a tetrahedral approach has been used in various instances.^{16, 17} Although, this tetrahedral approach has been studied for OLED purposes, literature towards photovoltaic devices remains scarce especially with *n*-type materials. In this chapter the synthesis, first steady-state and transient optical studies and ground-state electrochemical properties of a novel *n*-type material, with naphthalenediimide chromophores are presented. In addition, the morphology and transient charge carrier mobility studies were done with films of blended polymeric *p*-type materials and the tetrahedral molecule.

2.2. Results and discussion

2.2.1. Synthesis

Tetra(phenyl)methane, **5**, was synthesized starting from trityl chloride. Upon heating to 220 °C trityl chloride undergoes a nucleophilic attack by aniline. The resulting product on treatment with HCl yields an intermediate salt. This was converted into a diazonium salt using isoamyl nitrite at -10 °C. The resulting diazonium salt was reduced subsequently using hypophosphorous acid to obtain tetra(phenyl)methane **5** in a good yield (>80 %). Tetra(nitrophenyl)methane, **6**, was synthesized by nitration of **5** using fuming nitric acid with an isolated yield of 38 %. The central tetrahedral core **7** was synthesized by reducing **6**.¹⁸ As the reduction of **6** with H₂ in presence of PdO and Pd/C was not efficient, a modified procedure¹⁹ with Raney-nickel was followed to get **7** (Scheme 2.1.).

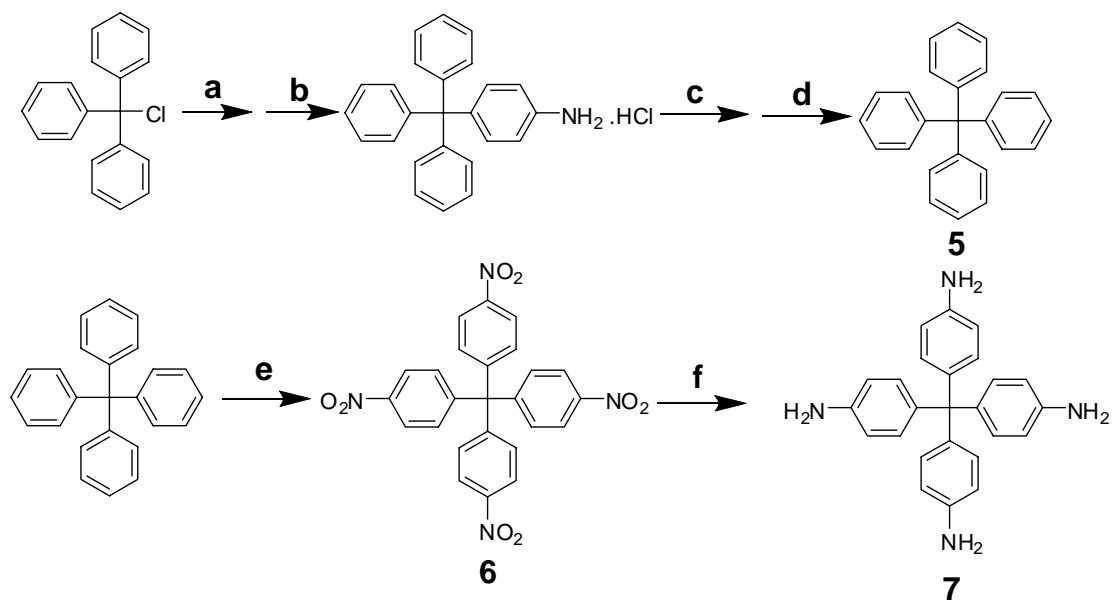
Only about 25 % average yield was achieved in the synthesis of naphthalene monoimide monoanhydride **3**, mainly due to formation of diimide **4** and the open ring product of **3**. Synthesis of the tetrahedral molecule **1** was achieved by reacting **3** and **7** (Scheme 2.2.) under argon atmosphere, with a reasonable isolated yield of 43 % (99.97 % pure). While products with 2-fold or 3-fold substitution rather than complete 4-fold

substitution reduced the yield of this reaction, their structural similarity also hampered the purification of the desired product, thus further bringing down the isolated yields of the desired product.

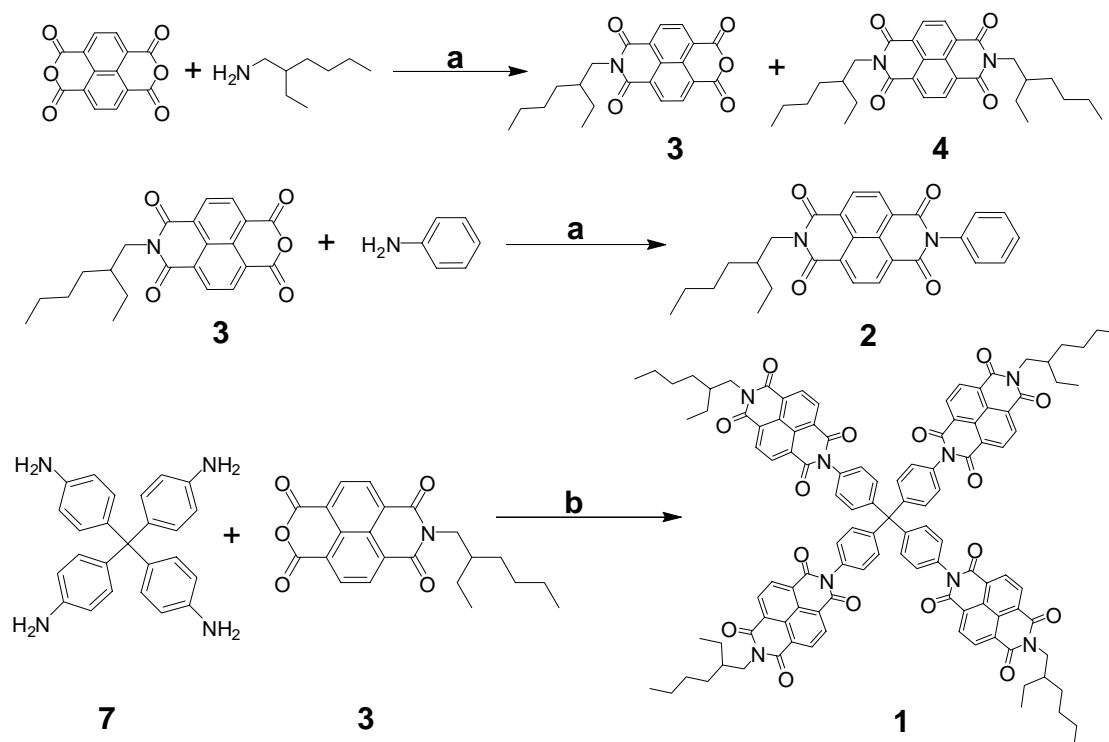
For spectroscopic comparisons, a model compound, **2** was synthesized by the reaction of aniline with **3**. For the same purposes compound **4**, a by-product in the synthesis of **3** was further purified using column chromatography on silica gel column with CH_2Cl_2 as eluent.

2.2.2. Effect of substituents on imide nitrogen on solubility

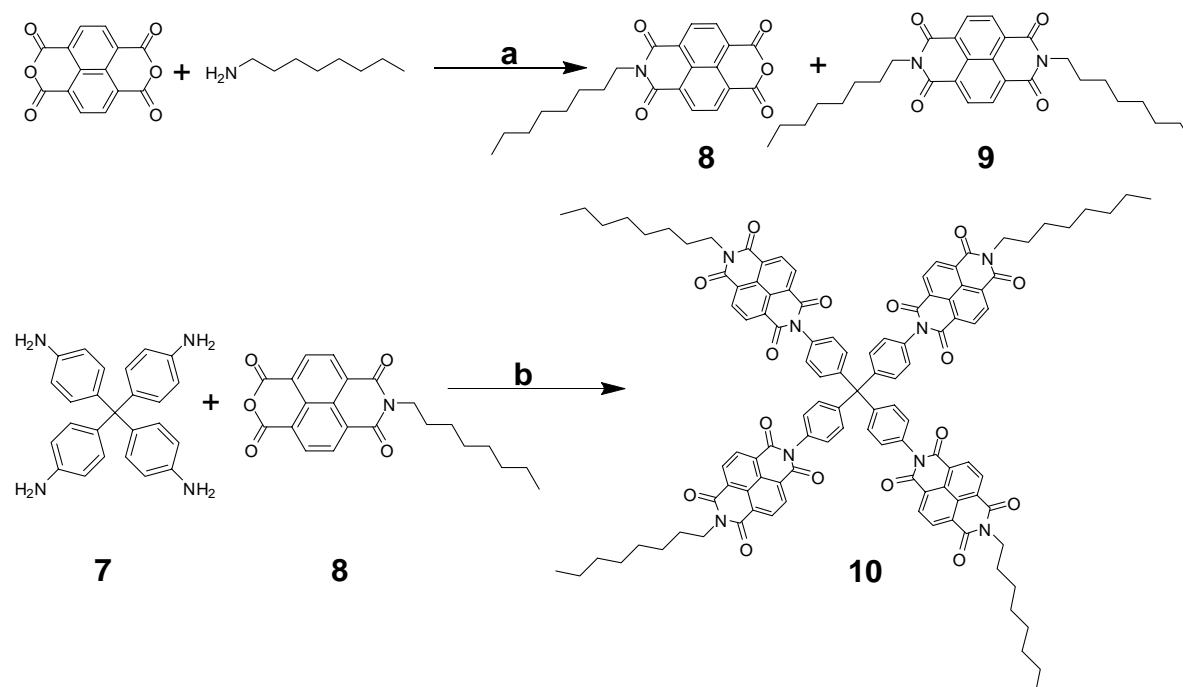
Although the type of substitution on the imide nitrogen in NDIs does not make much difference in terms of its basic photo and electrochemical behavior, it might play a significant role in the solubility of the molecules. Therefore a tetrahedral molecule without branching in the alkyl chain **10**, an analogue of **1**, was also synthesized as depicted in Scheme 2.3. The 2-ethyl hexyl chain in **1** was replaced with *n*-octyl chain in **10**. The monoimide **8**, and the dialkyl molecule **9**, both with *n*-octyl substituents, are soluble in solvents like CHCl_3 , CH_2Cl_2 , THF, DMF, DMSO, CB, ODCB, *etc.*



Scheme 2.1. Synthesis of the central tetrahedral core compound **7**. (a) Aniline, 220 °C; (b) 2 N HCl/MeOH, reflux; (c) $\text{H}_2\text{SO}_4/\text{EtOH}$, -10 °C, isoamyl nitrite; (d) 50 % H_3PO_2 in water, reflux; (e) fuming HNO_3 , acetic acid/acetic anhydride; (f) Hydrazine monohydrate, THF, Raney-nickel.



Scheme 2.2. Synthesis of tetrahedral molecule **1** and model compounds **2** and **4**. (a) Reflux in DMF for 15 h under N_2 ; (b) Reflux in DMF for 15 h under argon.



Scheme 2.3. Synthesis of tetrahedral NDI **10** without alkyl chain branching. (a) Reflux in DMF for 15 h under N_2 ; (b) Reflux in DMF for 15 h under argon.

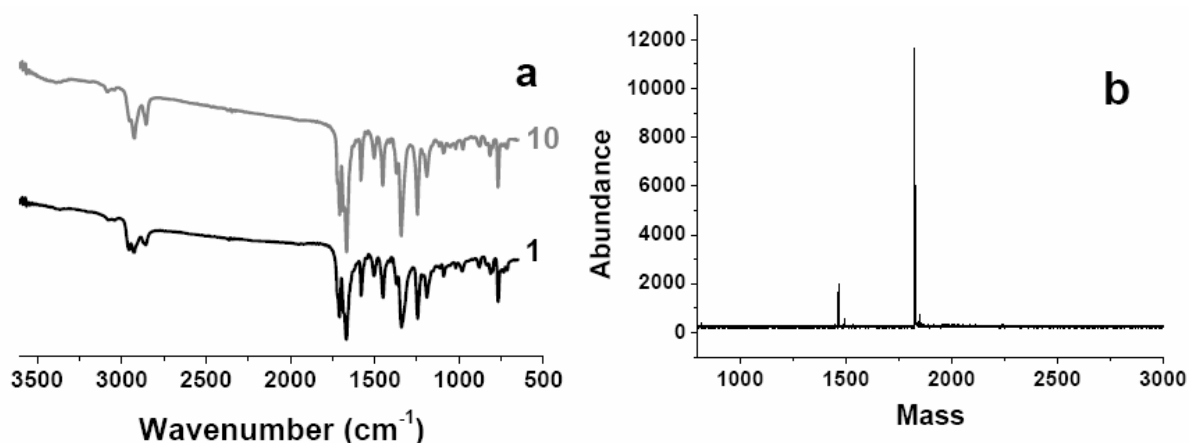


Figure 2.1. (a) Infrared spectra of **1** and **10**; (b) MALDI-TOF spectra of **10**.

An insoluble product was obtained from the reaction between **7** and **8** making purification of the desired molecule impossible. The infrared spectrum (Figure 2.1a) of the product was almost the same as that of **1** giving strong indication for the formation of **10**. The presence of **10** was further confirmed by Matrix-Assisted Laser Desorption/Ionization – Time of Flight (MALDI-TOF) analysis (Figure 2.1b), where the desired mass of 1826 for M^+ was observed, together with the mass at 1465 for the three-fold substituted byproduct.

While the above two experiments prove the formation of **10**, it also proves that the branched alkyl chain is crucial for a better solubility of the tetrahedral molecule.

2.2.3 UV-Vis and fluorescence spectroscopy

Absorption spectra of **1** show π - π^* transitions (Figure 2.2.) with vibrational features at 343, 361 and 381 nm, similar to **2** and **4**. All the three molecules show weak fluorescence with a small Stokes shift. These are in agreement with literature data for 1,4,5,8-naphthalenetetracarboxylicdiimides.²⁰ Compound **1** and **2** show the singlet emission with maxima at 391 nm and a charge-transfer (CT) fluorescence with a maxima around 550 nm (discussed in detail in Chapter 3). In summary, the absorption (0.7 μ M) spectra of **1** and **2** are near-identical to those of a model compound, **4** but the fluorescence spectra show additional CT fluorescence. Interestingly, at higher concentrations (7 μ M) the excitation spectrum of **1** shows the formation of ground-state complexes that give rise to complex fluorescence with $\lambda_{\text{max}} \sim 470$ nm, which is absent at

lower concentrations. Such ground-state complex formation is also evident from absorption spectra at higher concentrations. This complex formation is likely advantageous for charge transport, as it indicates significant π - π interactions between adjacent molecules of **1**.

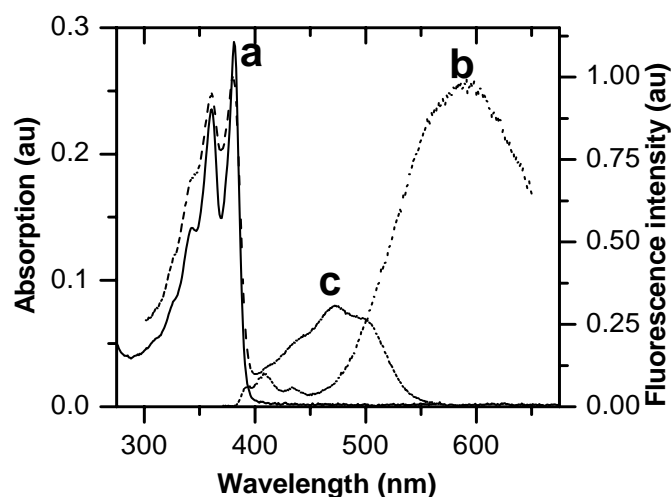


Figure 2.2. (a) Absorption; (b) Fluorescence ($\lambda_{\text{exc}} = 350$ nm); (c) excitation spectra ($\lambda_{\text{emi}} = 590$ nm) of **1** in chloroform.

2.2.4. Electrochemistry

Cyclic voltammetry studies indicate that **1** undergoes two one-electron reductions (Figure 2.3), with the first reduction at -1.23 V and the second reduction at -1.72 V *vs.* ferrocene-ferrocenium (Fc/Fc⁺) ion. In chloroform, the Fc/Fc⁺ is not electrochemically reversible as the potential difference between oxidation and reduction was around 250 mV. This may be due to a charge transport problem with tetrabutylammonium perchlorate, as its solubility is limited in chloroform. Similar electrochemical irreversibility also observed with reduction and oxidation of **1** and therefore, the reduction of the chromophore should be completely reversible like other known diimides.^{21, 22} Molecules **2** and **4** also show two reduction waves, which are shown in Figure 2.3 and the potentials are listed in Table 2.1.

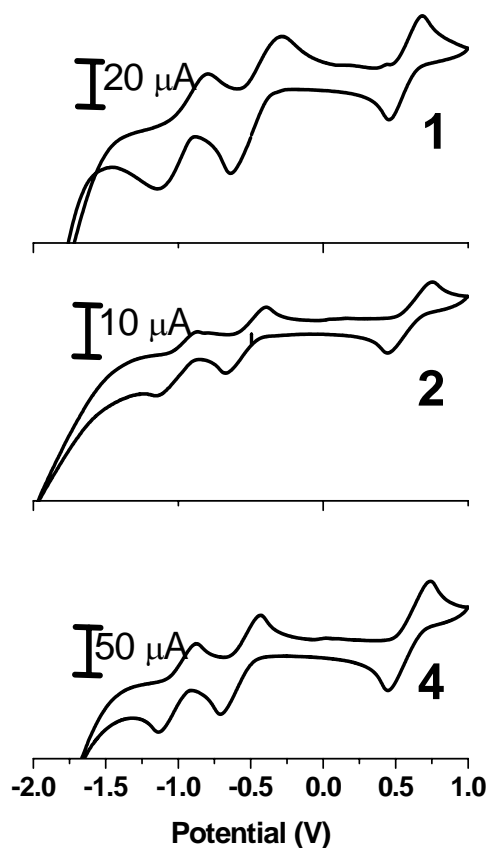


Figure 2.3. Cyclic voltammograms of **1**, **2** and **4** (1 mM solution in chloroform with 0.1 M tetrabutylammonium perchlorate and ferrocene, at a scan rate of 30 mV.s⁻¹). Ferrocene oxidation and reduction are seen at 0.61 V and 0.41 V respectively.

Table 2.1. Reduction potentials of **4**, **2** and **1** *vs.* Fc/Fc⁺ in chloroform

Molecule	1 st reduction potential	2 nd reduction potential
4	-1.28 V	-1.71 V
2	-1.24 V	-1.69 V
1	-1.23 V	-1.72 V

As observed from the reduction potentials, **2** and **1** are more easily reduced than **4** by 0.04 V and 0.05 V respectively. Theoretical calculations done at B3LYP/6-31G(d)

level of theory reveal that the dihedral angle between the phenyl ring and the naphthalenediimide ring is 80° in **2**, and is 83° in **1** (Figure 2.4.). Since these two rings are not completely perpendicular to each other, there is a possibility of electron flow between these two rings, which might be the cause for the slight differences in the reduction potentials of **2** and **1**, in comparison with that of **4**.

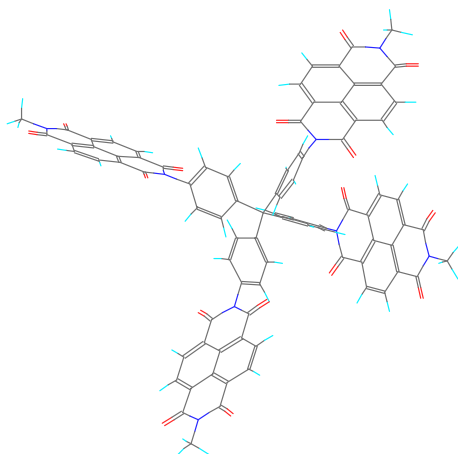


Figure 2.4. Structure of **1** (alkyl chains were replaced with methyl group for ease of calculation) - energy minimized at B3LYP/6-31G(d) level of theory.

2.2.5. Laser Flash Photolysis

With laser flash photolysis studies, the absorption spectra of the transient species formed after excitation with a short laser pulse are obtained, in different time domains. In the present study compounds **1**, **2** and **4** are studied in the nanosecond time domain and they show two distinct peaks at 450 nm and 480 nm in their transient absorption spectra (Figure 2.5.). We assign these peaks to the triplet state as they are very similar to literature data for NDIs with alkyl substituents.²³ Presence of a phenyl ring in **1** and **2** does not significantly affect the absorption spectra of the triplet state (Figure 2.5a.). This indicates that the substitution at the imide nitrogen does not affect the excited state properties of the naphthalenediimide moiety, in the nanosecond time domain.

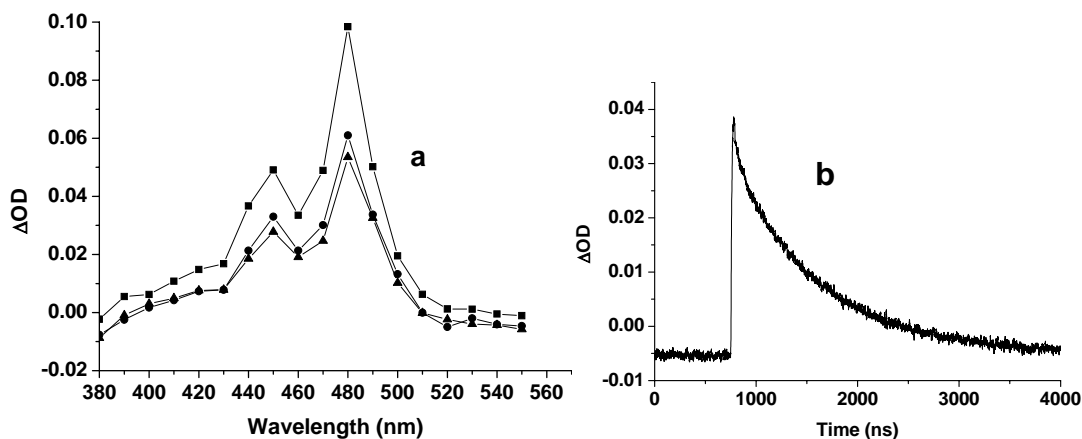


Figure 2.5. (a) Transient absorption spectra of **4** (■), **2** (▲) and **1** (●) in chloroform, taken 40 ns after the excitation pulse ($\lambda_{\text{exc}}=355$ nm). (b) decay profile of **1** at 480 nm.

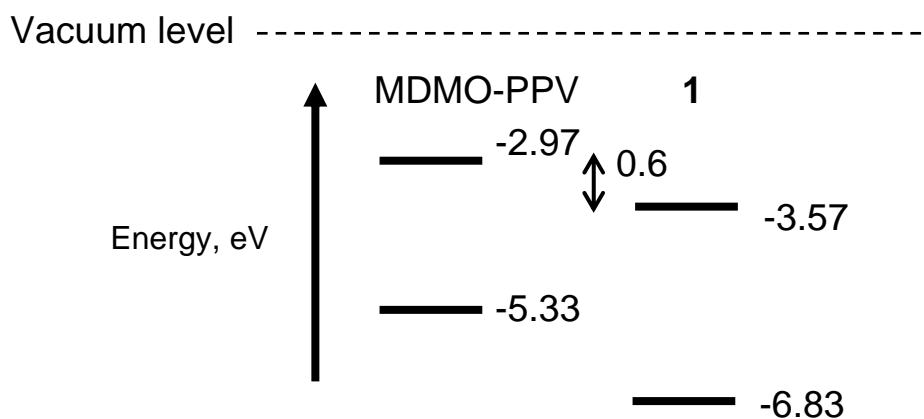
The transient decays were single exponential for all the three molecules with lifetimes of 495, 448 and 895 ns for **4**, **2**, and **1** respectively. While **4** and **2** have a similar triplet lifetime, compound **1** has a longer lifetime. This might be due to the restriction in the rotational freedom of the molecule, which slows down the triplet relaxation processes.

2.2.6. Fluorescence quenching properties

From the absorption spectrum and electrochemical data, the HOMO and LUMO levels (Scheme 2.4.) of the donor and acceptor molecules were estimated with respect to the vacuum level. Compared to the LUMO level of the electron-donating polymer MDMO-PPV,²⁴ the LUMO level of **1** is 0.6 eV lower in energy. Therefore, according to equation 1, this combination of Donor-Acceptor system has a driving force of 0.6 eV for electron transfer upon excitation of MDMO-PPV. A similar driving force is found with P3HT, another electron-donating polymer since the LUMO of P3HT (-3.53 eV)^{25, 26} is closer to the LUMO of MDMO-PPV.

$$\Delta G = (E_{D+}) - (E_{A-}) - (\Delta G_{00}) \quad \text{----- Equation 1}$$

where E_{D+} is the adiabatic ionization potential of the donor, E_{A-} is the adiabatic electron affinity of the acceptor and ΔG_{00} is the lowest energy excited state.



Scheme 2.4. HOMO and LUMO levels of the electron-donating polymer MDMO-PPV and **1**, as calculated from absorption spectra and electrochemical data.

Knowing the driving force for the photo-induced electron transfer, fluorescence quenching studies, an indicative experiment to confirm electron transfer, were done with electron-donor polymers MDMO-PPV and P3HT. It was found that $\sim 99\%$ of the donor fluorescence has been quenched (Figure 2.6.) by the acceptor **1**, in films. Upon increasing the weight ratio of **1** from 20 to 80 %, an increased fluorescence quenching was observed. This is a strong indication of possible electron transfer from the polymer to **1**.

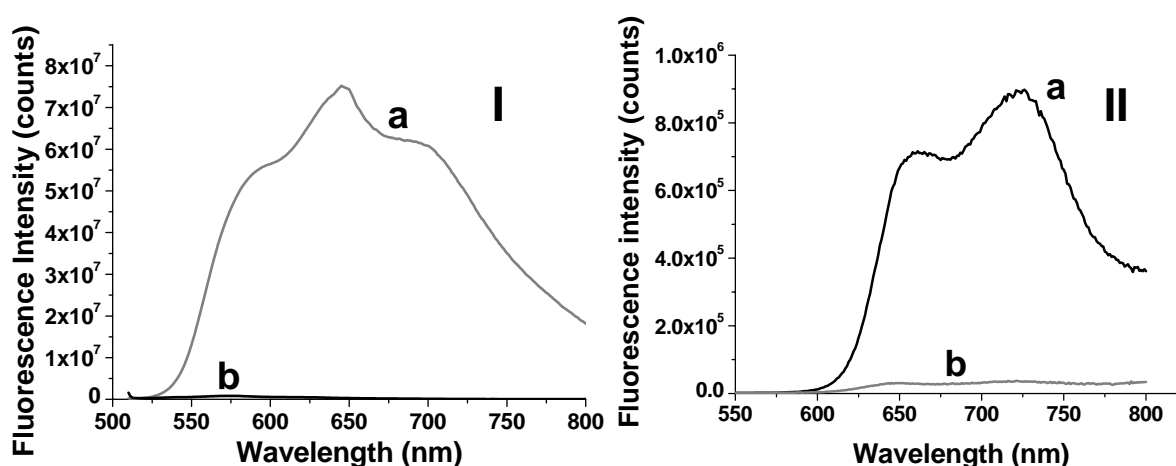


Figure 2.6. MDMO-PPV and P3HT fluorescence quenching in films spin coated from chlorobenzene solutions (2000 rpm for 60 s) **I.** Fluorescence of (a) pure MDMO-PPV film (b) 1:1 mixture of MDMO-PPV and **1**; **II.** (a) Fluorescence of (a) pure P3HT film (b) 1:1 mixture of P3HT and **1** ($\lambda_{\text{exc}} = 450 \text{ nm}$).

2.2.7. Morphology

Bright field transmission electron microscopy (BF-TEM) images were obtained for films with various ratios of donor and acceptor. Films were obtained with **1** from 20 to 80 weight % in MDMO-PPV and P3HT, by spin coating and by drop casting from chlorobenzene and chloroform solutions. Figure 2.7. shows a very uniform film without any aggregation or phase separation either from the donor or acceptor molecule.

Films with MDMO-PPV and **1**, spincoated from chloroform, had inhomogeneous features, whereas the films spin coated from chlorobenzene were very uniform till 80 weight % of **1**. This kind of solvent effect is also known for solar cells with blends of MDMO-PPV and C₆₀ derivatives.⁷ With **1** and MDMO-PPV, spin coated from chlorobenzene, the films remained uniform even after annealing at 130 °C (Figure 2.7b), which is in contrast with C₆₀-derivative containing films, which on annealing resulted in crystallization and phase separation in μm scale domains.¹¹

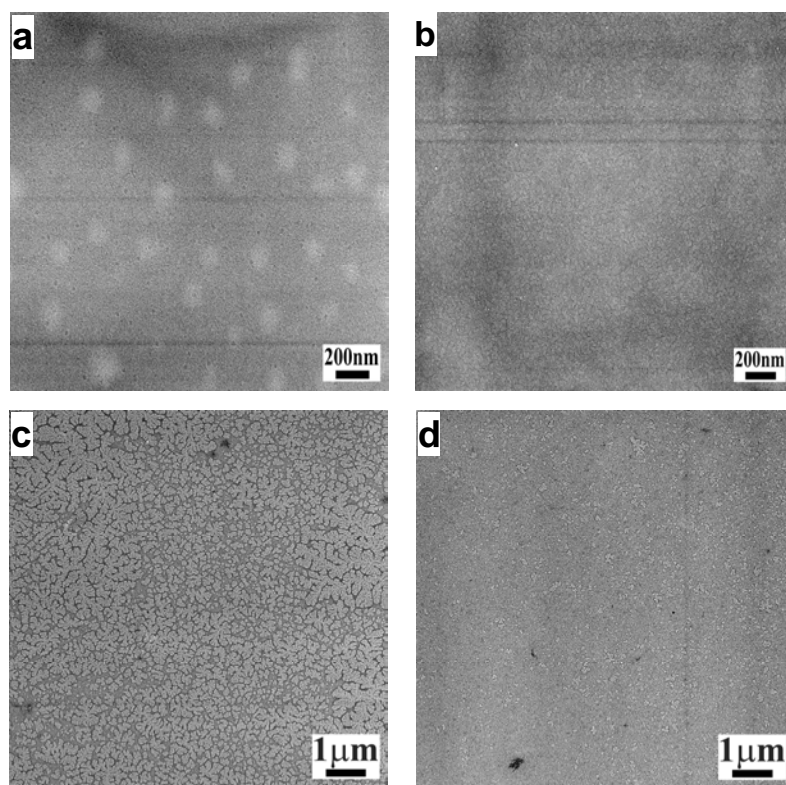


Figure 2.7. BF-TEM images of 1:1 mixtures of p-type and n-type materials (a) 1:1 mixture of MDMO-PPV and **1**, spin coated from chloroform; (b) 1:1 mixture of MDMO-PPV and **1**, spin coated from chlorobenzene and annealed at 130 °C for 1 h; (c) pristine P3HT film; (d) 1:1 mixture of P3HT and **1** spin coated from chlorobenzene. (all films were spin coated, on a glass substrate with a ~100 nm layer of PEDOT:PSS, at 2000 rpm for 60 s).

Films with P3HT and **1** show some features similar to those expected for phase separation, however, careful examination shows that this is due to de-wetting of P3HT on PEDOT:PSS thin films. On spin coating the pristine P3HT film on PEDOT:PSS, de-wetting was also observed as indicated by features of $\sim 1\ \mu\text{m}$ dimension. (Figure 2.7c). Since electron donor-acceptor mixtures upon spin-coating gave very thin films ($\sim 40\text{--}90\ \text{nm}$), water soluble PEDOT:PSS layer was necessary to float the films in order to load the films on the TEM grid. This would also simulate the solar cells, where PEDOT:PSS is coated as a hole transport layer (HTL). Apart from this de-wetting issue, the films were very uniform without any phase separation or crystallization arising from the acceptor molecule **1** (Figure 2.7d) indicating the miscibility of **1** with the electron donating polymer, P3HT.

The above morphological studies have proven that the tetrahedral approach indeed prevents phase separation and crystallization in a larger extent, like the case of C_{60} derivatives, and yields a very uniform morphology upon mixing the tetrahedral *n*-type materials based on NDI with *p*-type polymers.

2.2.8. Flash Photolysis – Time Resolved Microwave Conductivity (FP-TRMC) studies

The encouraging results from fluorescence quenching and morphology studies of **1** prompted us to directly study the formation of transient charge carriers and their lifetimes in films with an often investigated polymeric *p*-type material, P3HT,²⁷⁻³⁰. This can be accomplished via flash photolysis time-resolved microwave conductivity measurements (FP-TRMC).³¹ FP-TRMC probes the amount and mobility of charge carriers formed upon excitation with a short laser pulse (pulse FWHM = 4 ns; $\lambda_{\text{exc}} = 500\ \text{nm}$) via the time-resolved absorption of microwaves that are passed through the irradiated sample. As obvious from Figure 2.8., pulsed excitation leads to near-instantaneous, highly efficient formation of long-lived charge carriers, with lifetimes in the order of tens of microseconds. This can be related to the high intrinsic charge mobility of pure **1**. Using 3 MeV electron pulses, a mobility of $0.03\ \text{cm}^2\ \text{V}^{-1}\text{s}^{-1}$ was measured for **1**, at a frequency of 30 GHz,³² which is very high for an amorphous material. This is a strong indication of an efficient electron transport between neighboring molecules of **1**.

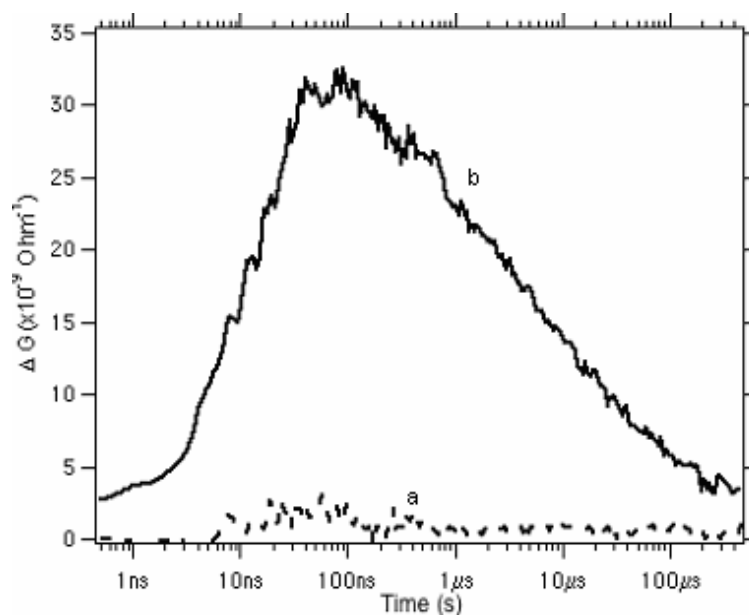


Figure 2.8. Change in conductivity ΔG obtained from FP-TRMC measurements ($\lambda_{\text{exc}} = 500 \text{ nm}$, intensity = $28 \mu\text{J cm}^{-2}$ per pulse) for films of (a) pure P3HT and (b) 1:1 mixture of P3HT and **1**.

2.3. Experimental

^1H and ^{13}C NMR were measured either on a Bruker DPX 300 (300 MHz) or on a Bruker DPX 400 (400 MHz) spectrometer. HRMS data were obtained with a Finnigan MAT 95 spectrometer. MALDI-TOF measurements were done using a Bruker-Ultraflex spectrometer with a α -cyano - hydroxyl cinnamic acid matrix. UV spectra were measured with a Perkin-Elmer Lambda 18 UV/Vis spectrophotometer. Fluorescence spectra were measured using a Spex Fluorolog 3.22 spectrophotometer. All the spectra were corrected for the sensitivity of the detector and the background. Electrochemical measurements were done with an Autolab PGSTAT 100 with a platinum disc as working electrode, Ag/AgCl as reference electrode and glassy carbon as counter electrode. Platinum disc electrodes were polished before each measurement. Measurements were carried out at a scan rate of 30 mVs^{-1} in a nitrogen environment. TEM images were obtained with a JEOL JEM FX-2000 system and the images were recorded with traditional negative plates. The FP-TRMC setup has been described in reference 31. Nanosecond laser flash photolysis studies were carried out with an excitation wavelength

of 355 nm from the 3 ω pulse of a Nd:YAG laser (Brilliant FWHM = 4 ns, Quantal Inc.), and the signals were detected using a LP920 spectrophotometer (Edinburgh Instruments Limited) fitted with a 450 W Xe arc lamp as a probe and a red-sensitive photomultiplier (R928, Hamamatsu) and a ICCD camera (DH720, Andor Technology) as detectors.

All the starting materials were purchased from Sigma-Aldrich and used as is, unless specified otherwise. Solvents used for spectroscopic measurements were of spectrophotometric grade purchased from Sigma-Aldrich, which were freshly distilled over drying agent before use. Ferrocene (Fluka), internal standard in CV measurements, was sublimed before use. Aniline was distilled under reduced pressure before synthesis of compound **2**.

2.3.1. Synthesis and characterization

N-(2-ethylhexyl) naphthalene monoimide monoanhydride 3: Naphthalene dianhydride (20.02 g, 74.65 mmol) was taken in a three-necked flask with 200 ml of freshly distilled DMF. The slurry was heated to about 140 °C under N₂ atmosphere. To this slurry 2-ethylhexylamine (9.65 g, 74.64 mmol) was added drop wise for about 10 minutes and the reaction mixture was refluxed for 15 h, under N₂ atmosphere. The reaction mixture was cooled and the precipitated diimide was filtered off. The solvent, DMF, was evaporated under low pressure and the residue dissolved in dichloromethane to remove any insoluble material. Dichloromethane evaporated and the crude material was purified on silica column with dichloromethane as eluent to obtain 7.1 g (25 % yield) of the desired product **3** as a pale yellow-orange solid.

¹H NMR (400 MHz, CDCl₃) δ 8.83 (s, 4H, Naphth-H), 4.11 (m, 2H, -N-CH₂-), 1.94(m, 1H, -CH₂-CH-CH₂), 1.35(m, 8H, 4 \times CH₂), 0.95(t, 3H, J = 7.4 Hz), 0.89(t, 3H, J = 7.2 Hz); **¹³C NMR** δ 162.6, 158.8, 133.1, 131.3, 128.8, 127.9, 126.9, 122.7, 44.8, 37.9, 30.6, 28.5, 23.9, 22.9, 14.0, 10.5; **HRMS** calculated for C₂₂H₂₁NO₅ 379.1420, found 379.1420.

N, N'-bis(2-ethylhexylamine)naphthalenediimide 4: This is obtained as a byproduct in the synthesis of **3**. It was further purified on a silica column with dichloromethane as eluent, for spectroscopic measurements.

¹H NMR (300 MHz, CDCl₃) δ 8.67 (s, 4H, Naphth-H), 4.00 (m, 4H, -N-CH₂-), 1.86(m, 2H, -CH₂-CH-CH₂), 1.28(m, 16H, 8 \times CH₂), 0.88(m, 12H, 4 \times CH₃); **¹³C NMR** δ 163.59,

131.38, 130.97, 130.74, 127.10, 126.96, 44.98, 38.32, 31.09, 31.07, 29.01, 26.09, 24.42, 23.41, 14.44, 10.98; **HRMS** calculated for $C_{30}H_{38}N_2O_4$ 490.2830, found 490.2832.

N-Phenyl N'-(2-ethylhexyl)naphthalenediimide 2: Compound **3** (1.03 g, 2.71 mmol) and aniline (0.26 g, 2.79 mmol) were taken in a three-necked flask with 10 ml of DMF and refluxed for 15 h under nitrogen. Subsequently, DMF was evaporated under reduced pressure and the residue was purified on a silica column with dichloromethane as eluent to get 1.01 g of **2** (89.9 % yield).

¹H NMR (400 MHz, $CDCl_3$) δ 8.83 (s, 4H, Naphth-H), 7.59 (m, 3H, *p* and *m*-phenyl), 7.36 (dt, 2H, *o*-phenyl) 4.17 (m, 2H, -N- CH_2), 1.98(m, 1H, - CH_2 -CH- CH_2), 1.35(m, 8H, 4 \times CH₂), 0.93(t, 6H); **¹³C NMR** δ 163.6, 163.4, 135.0, 131.8, 131.5, 130.0, 129.6, 129.2, 128.9, 128.5, 127.5, 127.3, 127.2, 127.1, 45.1, 38.3, 37.5, 32.2, 31.1,30.1, 29.8, 29.0, 24.5, 23.5, 23.1, 14.5, 11.0; **HRMS** calculated for $C_{28}H_{26}N_2O_4$ 454.1894, found 454.1893.

tetra-4-[N-(2-ethylhexyl)naphthalene-1,4:5,8-tetracarboxylic diimide-N'-yl]phenylmethane 1: Compound **3** (0.55 g, 1.45 mmol) was placed in a three-necked flask with 10 ml of freshly distilled DMF under argon. To this **7** (0.13 g, 0.342 mmol) dissolved in 10 ml of DMF was added drop-wise at 140 °C. After the addition, the mixture was refluxed under argon atmosphere over night. DMF was evaporated under reduced pressure and the residue loaded on alumina column (6.7 % deactivated by addition of 13.5 ml water in 500 g of alumina) and eluted with neat chloroform to obtain 0.27 g of **1** at 43.3 % yield (with respect to **7**).

¹H NMR (400 MHz, $CDCl_3$) δ 8.81 (s, 16H, Naphth-H), 7.63 (dd, 8H, Ar-H), 7.63 (dd, 8H, Ar-H) 4.18 (m, 8H, -N- CH_2), 1.98(m, 4H, - CH_2 -CH- CH_2), 1.38(m, 32H, 4 \times 4 \times CH₂), 0.97(t, 12H, *J* = 7.4 Hz), 0.90(t, 12H, *J* = 7.1 Hz); **¹³C NMR** δ 163.1, 162.9 146.4, 133.1, 132.4, 131.4, 131.1, 127.9, 127.1, 126.8, 126.7, 64.6, 44.6, 37.8, 30.7, 28.6, 24.0, 23.0, 14.1, 10.6; **MALDI-TOF** calculated for $[M+H]^+$ 1825.73, found 1825.82.

tetra(phenyl)methane 5: A mixture of triphenylmethylchloride (18.36 g, 66 mmol) and aniline (16.8 g, 177 mmol) were heated to 220 °C for five minutes and cooled to 90 °C. This was treated with 100 ml of 2 N HCl and 90 ml of methanol and refluxed briefly. The gray solid filtered and dissolved in 130 ml of ethanol and 20 ml of

concentrated sulfuric acid. The mixture was cooled to $-10\text{ }^{\circ}\text{C}$ and 15 ml of isoamyl nitrite was added. After stirring the mixture for about thirty minutes, 30 ml of 50 % hypophosphorous acid was added at $-10\text{ }^{\circ}\text{C}$ and heated to reflux. An olive colored solid was filtered off. This crude product was washed with ethanol and 1,4-dioxane to yield *tetra*(phenyl)methane solid at 84.8 % yield. Melting Point: $280.9\text{ }^{\circ}\text{C}$ (literature $281\text{--}282\text{ }^{\circ}\text{C}$).

tetra(*p*-nitrophenyl)methane 6: To **5** (15 g, 46.8 mmol) 75 ml of fuming nitric was added in portions at $-10\text{ }^{\circ}\text{C}$ with vigorous stirring. To this mixture 25 ml of acetic anhydride and 50 ml of glacial acetic acid were slowly added and stirred for about 15 minutes. Finally the reaction mixture was diluted with 100 ml of glacial acetic acid. The resulting yellow solid was washed with acetic acid and methanol. The crude product was recrystallized using DMF to get yellow crystals of **6** (8.9 g, 38.0 % yield).

^1H NMR (300 MHz, d_6 -DMSO) δ 8.51 (d, 8H, Ar-H, $J = 9.0\text{ Hz}$), 7.85 (d, 8H, Ar-H, $J = 8.9\text{ Hz}$) δ ; **^{13}C NMR** δ 146.6, 136.9, 132.1, 113.6, 62.2; **HRMS** calculated for $\text{C}_{25}\text{H}_{16}\text{N}_4\text{O}_8$ 500.0968, found 500.0969.

tetra(*p*-aminophenyl)methane 7: To **6** (1.5 g, 2.99 mmol) in 100 ml of THF, 2.00 g (excess) of hydrazine monohydrate and $\sim 10\text{ g}$ of Raney-nickel were added and refluxed for about 3 h. The mixture was hot filtered and washed with ethanol. Solvent was evaporated and the residue was washed with ethanol and dried to get 0.7 g of **7** in a 61.3 % yield.

^1H NMR (300 MHz, d_6 -DMSO) δ 6.65 (d, 8H, Ar-H, $J = 8.7\text{ Hz}$), 6.35 (d, 8H, Ar-H, $J = 8.7\text{ Hz}$), 4.80 (s, 8H, Ar- NH_2); **^{13}C NMR** δ 149.9, 145.0, 130.4, 122.7, 64.2; **HRMS** calculated for $\text{C}_{25}\text{H}_{24}\text{N}_4$ 380.2001, found 380.2004.

2.4. Conclusions

The use of a tetrahedral architecture for electron accepting molecules with NDIs, upon mixing with *p*-type polymers, has resulted in uniform film formation without phase separation or crystallization together with efficient fluorescence quenching. In addition, the non-directionality required for optimal charge separation in a film, and for charge transport through the film could also be obtained. This approach could further be optimized by variation of the aromatic diimides or other *n*-type materials with more extended π -systems, without compromising the non-directionality that is essential for the

formation of amorphous blends, while yielding layers with an absorption spectrum with a better overlap with the solar emission spectrum. As such this approach adds significant flexibility to the construction of amorphous blends of *n*-type and *p*-type materials for optoelectronic devices such as all-organic solar cells.

2.5. References

1. Brabec, C. J. *Sol. Energy Mater. Sol. Cells* **2004**, *83*, 273-292.
2. Gregg, B. A. *J. Phys. Chem. B* **2003**, *107*, 4688-4698.
3. Hoppe, H.; Sariciftci, N. S. *J. Mater. Res.* **2004**, *19*, 1924-1945.
4. Nelson, J. *Curr. Opin. Solid State Mat. Sci.* **2002**, *6*, 87-95.
5. Sun, S.; Fan, Z.; Wang, Y.; Haliburton, J. *J. Mater. Sci.* **2005**, *40*, 1429-1443.
6. Hayashi, Y.; Yamada, I.; Takagi, S.; Takasu, A.; Soga, T.; Jimbo, T. *Jpn. J. Appl. Phys. Part 1 - Regul. Pap. Short Notes Rev. Pap.* **2005**, *44*, 1296-1300.
7. Brabec, C. J.; Sariciftci, N. S.; Hummelen, J. C. *Adv. Funct. Mater.* **2001**, *11*, 15-26.
8. Svensson, M.; Zhang, F. L.; Veenstra, S. C.; Verhees, W. J. H.; Hummelen, J. C.; Kroon, J. M.; Inganas, O.; Andersson, M. R. *Adv. Mater.* **2003**, *15*, 988-991.
9. Shaheen, S. E.; Brabec, C. J.; Sariciftci, N. S.; Padinger, F.; Fromherz, T.; Hummelen, J. C. *Appl. Phys. Lett.* **2001**, *78*, 841-843.
10. Wienk, M. M.; Kroon, J. M.; Verhees, W. J. H.; Knol, J.; Hummelen, J. C.; van Hal, P. A.; Janssen, R. A. J. *Angew. Chem.-Int. Edit.* **2003**, *42*, 3371-3375.
11. Yang, X. N.; van Duren, J. K. J.; Rispen, M. T.; Hummelen, J. C.; Janssen, R. A. J.; Michels, M. A. J.; Loos, J. *Adv. Mater.* **2004**, *16*, 802-806.
12. Katz, H. E.; Lovinger, A. J.; Johnson, J.; Kloc, C.; Siegrist, T.; Li, W.; Lin, Y. Y.; Dodabalapur, A. *Nature* **2000**, *404*, 478-481.
13. Johansson, O.; Borgstrom, M.; Lomoth, R.; Palmblad, M.; Bergquist, J.; Hammarstrom, L.; Sun, L. C.; Akermark, B. *Inorg. Chem.* **2003**, *42*, 2908-2918.
14. Mori, Y.; Sakaguchi, Y.; Hayashi, H. *J. Phys. Chem. A* **2002**, *106*, 4453-4467.
15. Shirota, Y. *J. Mater. Chem.* **2005**, *15*, 75-93.
16. Wang, S. J.; Oldham, W. J.; Hudack, R. A.; Bazan, G. C. *J. Am. Chem. Soc.* **2000**, *122*, 5695-5709.
17. Chan, L. H.; Lee, R. H.; Hsieh, C. F.; Yeh, H. C.; Chen, C. T. *J. Am. Chem. Soc.* **2002**, *124*, 6469-6479.

18. Neugebauer, F. A.; Fischer, H.; Bernhardt, R. *Chem. Ber.-Recl.* **1976**, *109*, 2389-2394.
19. Langhals, H.; Wagner, C.; Ismael, R. *New J. Chem.* **2001**, *25*, 1047-1049.
20. Barros, T. C.; Brochsztain, S.; Toscano, V. G.; Berci, P.; Politi, M. J. *J. Photochem. Photobiol. A-Chem.* **1997**, *111*, 97-104.
21. Abraham, B.; McMasters, S.; Mullan, M. A.; Kelly, L. A. *J. Am. Chem. Soc.* **2004**, *126*, 4293-4300.
22. Struijk, C. W.; Sieval, A. B.; Dakhorst, J. E. J.; van Dijk, M.; Kimkes, P.; Koehorst, R. B. M.; Donker, H.; Schaafsma, T. J.; Picken, S. J.; van de Craats, A. M.; Warman, J. M.; Zuilhof, H.; Sudhölter, E. J. R. *J. Am. Chem. Soc.* **2000**, *122*, 11057-11066.
23. Green, S.; Fox, M. A. *J. Phys. Chem.* **1995**, *99*, 14752-14757.
24. Veenstra, S. C.; Verhees, W. J. H.; Kroon, J. M.; Koetse, M. M.; Sweelssen, J.; Bastiaansen, J.; Schoo, H. F. M.; Yang, X.; Alexeev, A.; Loos, J.; Schubert, U. S.; Wienk, M. M. *Chem. Mater.* **2004**, *16*, 2503-2508.
25. Al-Ibrahim, M.; Roth, H. K.; Schroedner, M.; Konkin, A.; Zhokhavets, U.; Gobsch, G.; Scharff, P.; Sensfuss, S. *Organic Electronics* **2005**, *6*, 65-77.
26. Onoda, M.; Tada, K.; Zakhidov, A. A.; Yoshino, K. *Thin Solid Films* **1998**, *331*, 76-81.
27. Kim, Y.; Choulis, S. A.; Nelson, J.; Bradley, D. D. C.; Cook, S.; Durrant, J. R. *J. Mater. Sci.* **2005**, *40*, 1371-1376.
28. Padinger, F.; Rittberger, R. S.; Sariciftci, N. S. *Adv. Funct. Mater.* **2003**, *13*, 85-88.
29. Schilinsky, P.; Waldauf, C.; Brabec, C. J. *Appl. Phys. Lett.* **2002**, *81*, 3885-3887.
30. Yang, X. N.; Loos, J.; Veenstra, S. C.; Verhees, W. J. H.; Wienk, M. M.; Kroon, J. M.; Michels, M. A. J.; Janssen, R. A. J. *Nano Lett.* **2005**, *5*, 579-583.
31. Kroeze, J. E.; Savenije, T. J.; Vermeulen, M. J. W.; Warman, J. M. *J. Phys. Chem. B* **2003**, *107*, 7696-7705.
32. Schouten, P. G.; Warman, J. M.; Dehaas, M. P. *J. Phys. Chem.* **1993**, *97*, 9863-9870.

Chapter 3

Femtosecond Time-Resolved Photophysics of 1,4,5,8-Naphthalene Diimides

Abstract

The photophysical properties of a tetrahedral molecule with naphthalene diimide (NDI) moieties, and of two model compounds were investigated. The absorption and fluorescence spectra of dialkyl-substituted NDI are in agreement with literature. While the absorption spectra of phenyl-substituted molecules are similar to all other NDIs, their fluorescence showed a broad band between 500–650 nm. This band is sensitive to the polarity of the solvent, and is attributed to a CT state. The absorption spectrum and lifetime (10 ± 1 ps) of the electronically excited singlet state of a dialkyl-substituted NDI was determined by femtosecond transient absorption spectroscopy, and the latter was confirmed by picosecond fluorescence spectroscopy. Nanosecond flash photolysis showed the subsequent formation of the triplet state. The presence of a phenyl substituent on the imide nitrogen of NDI resulted in faster deactivation of the singlet state (lifetime 0.5 – 1 ps). This is attributed to the formation of a short-lived (30 – 120 ps) CT state, which decays to the local triplet state. This fast deactivation was further confirmed by fluorescence lifetime measurements in solution and in a low-temperature methyl-tetrahydrofuran (MTHF) glass.

3.1. Introduction

During the past decade research on organic electronics has grown enormously. Such organic electronics include OFETs,¹⁻⁵ OLEDs,⁶⁻⁹ and all-organic photovoltaics.¹⁰⁻¹² This research is consistently in need of new types of conductive materials to improve their current efficiencies and deepen the understanding by checking general principles on wider classes of materials. These materials should be either of *p* or of *n*-type, with good electrochemical properties and an air-stable conductivity. Derivatives of 1,4,5,8-naphthalene diimides (NDIs) are known for such air-stable conductivity.¹³ Due to this, NDIs have been used in the study of electron-transfer processes,¹⁴⁻¹⁸ as liquid crystalline and photorefractive materials,¹⁹⁻²¹ as photosynthetic model compounds,²² and for optoelectronic applications.²³

Electrochemical and photophysical properties of NDI have been explored previously by several groups. Penneau *et al.* have reported the dimerization and aggregation behavior of NDI radical anions in aqueous and DMF solutions based on extensive spectroscopic studies (UV–Vis, NIR, IR and ESR).²⁴ Photoprocesses of functionalized NDIs in aqueous media^{25, 26} and in the presence of DNA²⁷ were investigated together with the radical anion formation via photochemical mechanisms. Further investigations on the excited state properties of NDI radical anions were carried out by Gosztola *et al.*²⁸

Green *et al.* reported a detailed study on the photophysical properties of NDI by measuring both the fluorescence and phosphorescence, from which they calculated the singlet and triplet energy levels.²⁹ They attempted to measure the fluorescence lifetime of the NDI, but found it too short to be determined accurately by their equipment, and therefore they estimated it to be < 20 ps. The short singlet lifetime is attributed to fast depopulation of the singlet state via intersystem crossing. Following this report, Barros *et al.* undertook a systematic study on the absorption and fluorescence properties of NDI.³⁰ This study revealed that NDIs stack with aromatic solvents and give rise to exciplex fluorescence. In water, even at low concentrations, a red-shifted fluorescence was observed, which was attributed to ground state aggregation of NDI. Although, the triplet state and radical anion formation are well described in the above mentioned reports, the singlet state dynamics of NDIs have not yet been reported. Since the lifetime of the NDI

singlet state has been reported to be < 20 ps, it is necessary to do measurements in the femtosecond time domain to accurately determine the lifetime.

In Chapter 2, we have reported a novel NDI-based tetrahedral amorphous material, which showed a high conductivity.²³ Though the conductivity of NDIs is not as high as that of other diimides with extended aromatic cores,³¹ conductivities as high as $0.16 \text{ cm}^2 \text{ V}^{-1} \text{ s}^{-1}$ have been reported.¹³ Since this material was intended for optoelectronic applications, such as organic photovoltaics, our interests also extend to the photophysical properties of this material. In this Chapter we report on the ultrafast excited state dynamics of this tetrahedral molecule **3**, and of two model compounds **1** and **2** (Figure 3.1). In order to study their singlet-state dynamics, time-resolved techniques were applied, from the femtosecond to the nanosecond time domains. These studies reveal the singlet state absorption and excited-state lifetimes, and also delineate the deactivation pathways in dependence of the molecular structure. To the best of our knowledge, this is the first report of the NDI singlet state absorption and of accurately determined lifetimes as measured with time-resolved techniques.

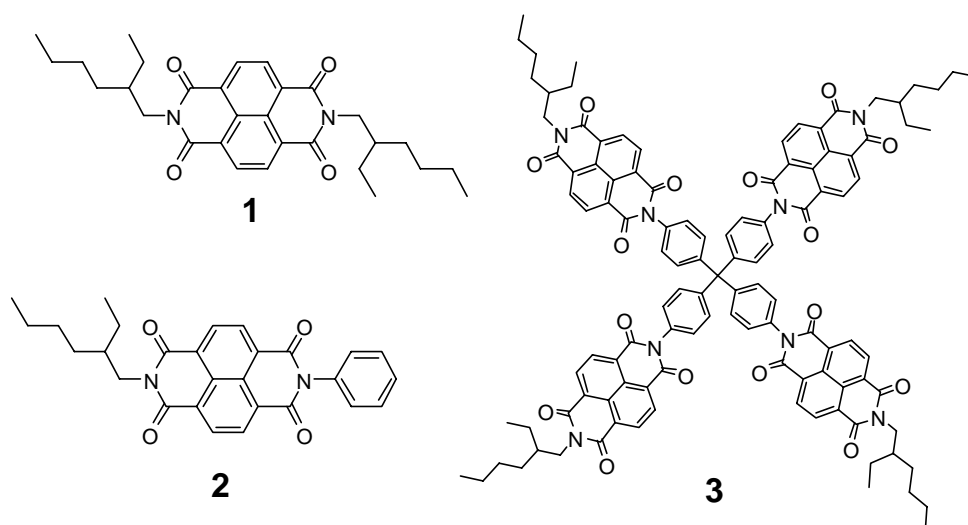


Figure 3.1. Structures of naphthalene diimide derivatives under study.

3.2. Results and Discussion

3.2.1. Steady-state absorption and fluorescence spectra

The steady-state absorption spectra of compounds **1–3** in chloroform (Figure 3.2a) have vibrational features with maxima at 344, 362 and 382 nm, and a high-energy

band at 242 nm. They have high molar extinction coefficients ($\sim 10^4 \text{ M}^{-1} \text{ cm}^{-1}$) indicating that the transition is $\pi-\pi^*$ in nature. The steady-state fluorescence spectra between 380 and 448 nm (Figure 3.2b) form mirror images of the absorption spectra with a small Stokes shift, and reveal fluorescence from the singlet state. The absorption and fluorescence spectra of **1** are in agreement with literature reports for other naphthalene diimides.^{29, 30} In case of **2** and **3** a second broad fluorescence band is observed which has a peak between 500 and 650 nm (Figure 3.2c & 2d). This band shifts to the red upon increasing the polarity of the solvent (from tetrachloromethane to 1,2-dichloroethane), which suggests that it involves partial transfer of charge. This charge-transfer (CT) band is interpreted to indicate that, in the case of **2** and **3**, there is an electron transfer between NDI and the phenyl ring. This is supported by the femtosecond transient absorption measurements (*vide infra*).

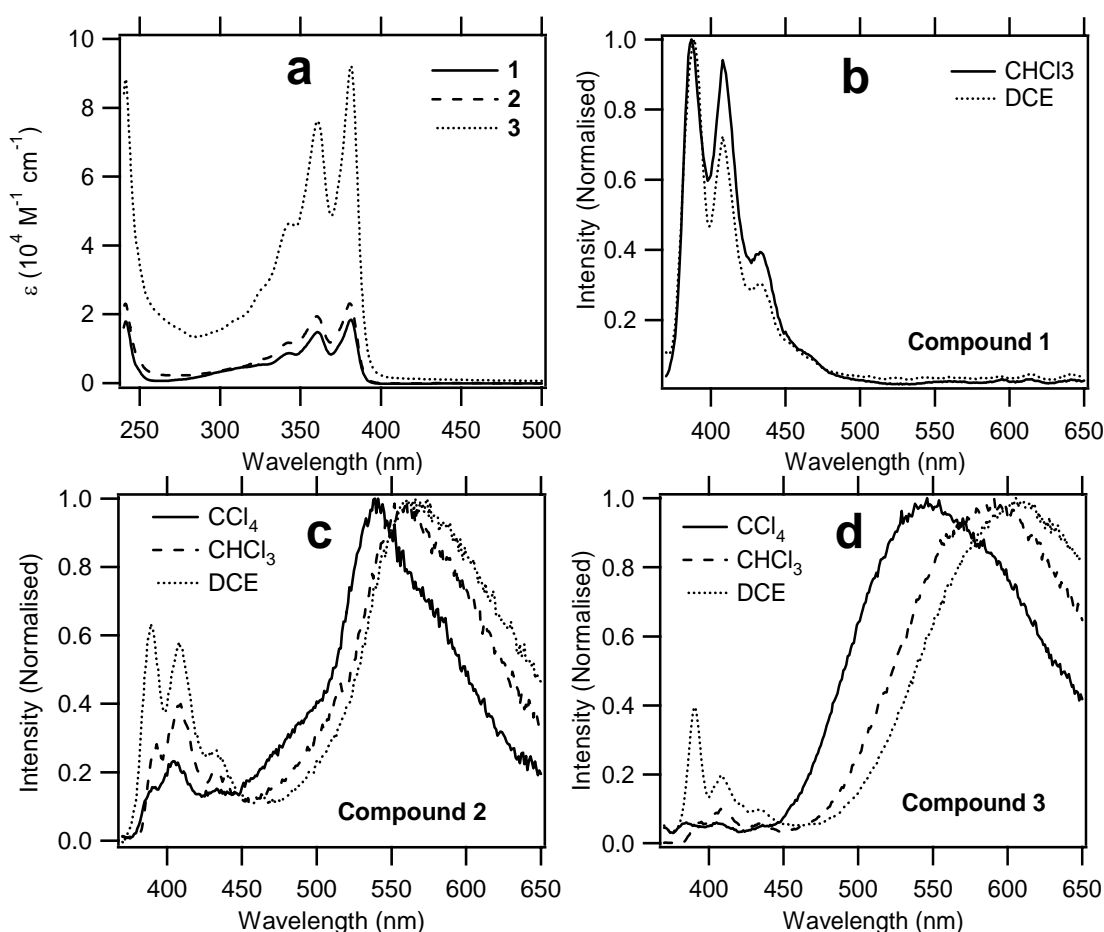


Figure 3.2. Steady-state absorption spectra (a) of **1-3** in chloroform, and fluorescence spectra in solvents of different polarity (b–d; $\lambda_{\text{exc}} = 350 \text{ nm}$), of **1**, **2**, and **3**, respectively.

3.2.2. Nanosecond transient absorption measurements

Laser flash photolysis experiments on a nanosecond timescale were done in chloroform for all 3 compounds, studied under aerated conditions. The spectra obtained are given in Figure 3.3. They show similar transient absorption spectra with two peaks at 450 nm and 480 nm. These spectra are attributed to the triplet state of the naphthalene diimide.^{23, 29} The decays are mono-exponential with lifetimes of 495, 448, and 895 ns, for compounds **1**, **2**, and **3**, respectively. The extended triplet lifetime for compound **3** might be due to restriction in the rotational freedom of the chromophore imposed by the central tetraphenyl methane moiety. On this time scale, no other absorptions were observed than those of the triplet state, within the spectral window employed (up to 800 nm). Femtosecond transient absorption measurements were performed to get more insight into the formation of the triplet state.

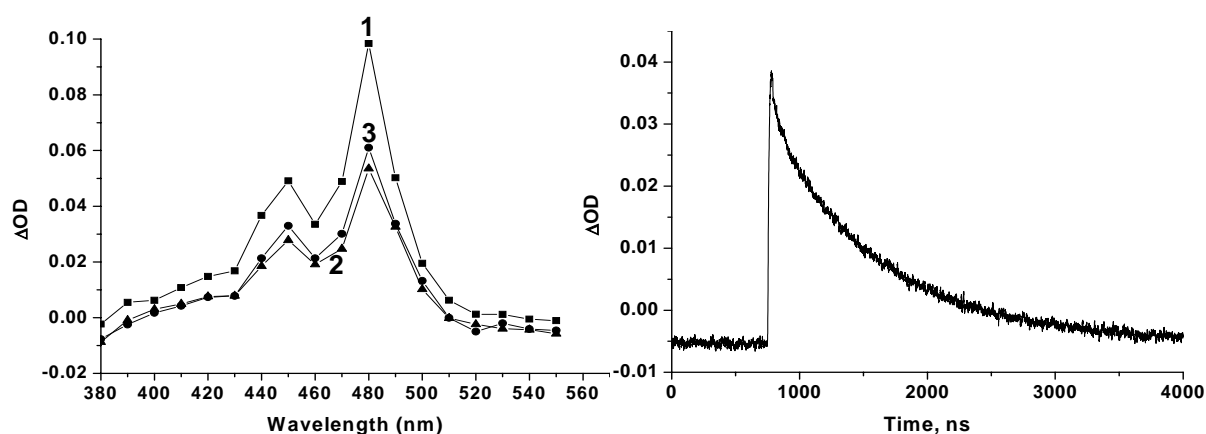


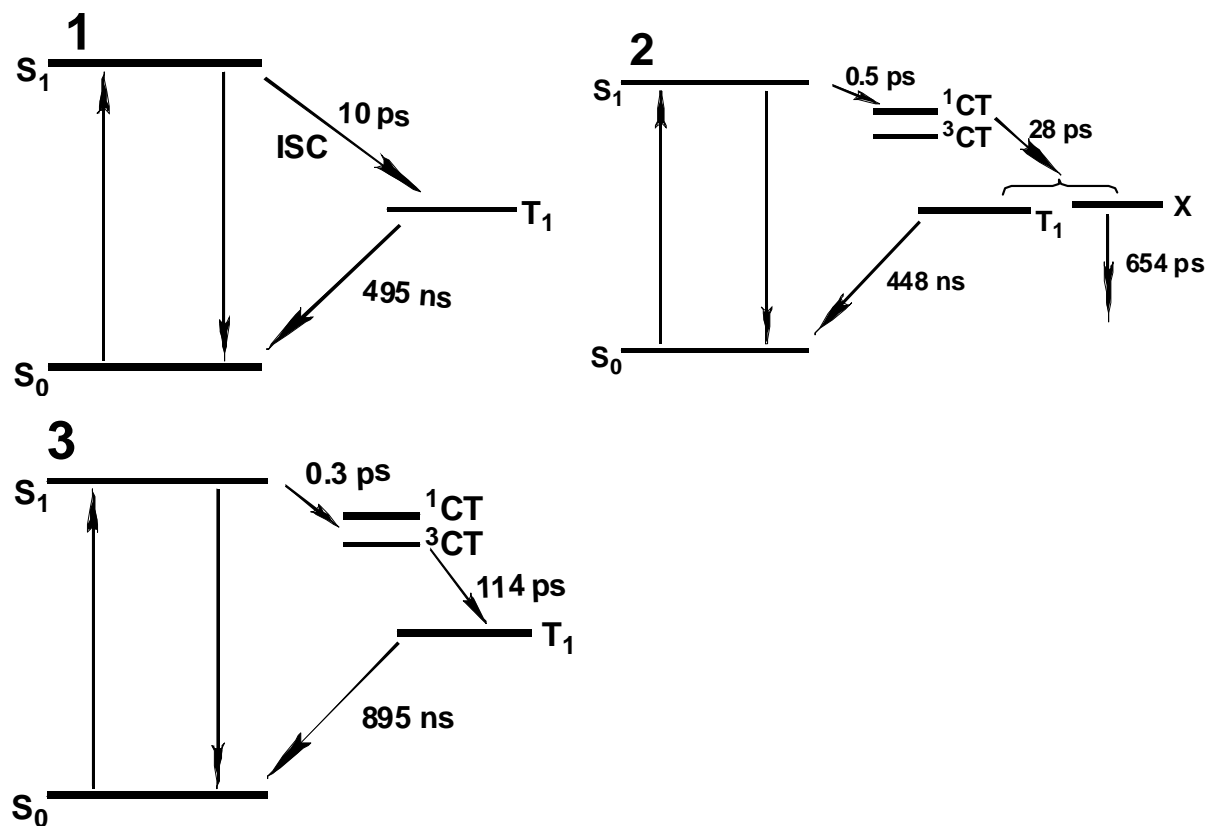
Figure 3.3. (left) Transient absorption spectra obtained with nanosecond laser flash photolysis experiments— 40 ns after the pulse of **1** (square), **2** (triangle) and **3** (circle) in chloroform; (right) Representative decay curve of **3** at 480 nm (concentration $\sim 10^{-5}$ M; $\lambda_{\text{exc}} = 355$ nm).

3.2.3. Femtosecond transient absorption measurements

The time-resolved transient absorption spectra measured with femtosecond pump-probe experiments and the decay-associated difference spectra (DADS), obtained by global analysis of the data,^{32, 33} are depicted in Figure 3.4. In the transient spectra of **1**

(Figure 3.4a), two distinct features are observed in time. Shortly after the pulse an absorption band with a maximum at 606 nm and a shoulder at 720 nm is present. This transient decays with a lifetime of 10 ± 1 ps, and gives rise to a spectrum with absorption maxima at 456 and 488 nm. The DADS associated with the 10 ps decay shows a negative band at 488 nm indicating a direct transition between these two transients.

The long-lived spectrum of **1** does not decay on the time scale of this experiment (up to 1 ns) and is similar to the triplet state spectrum observed with nanosecond flash photolysis (*vide supra*). Therefore, this long-lived transient is attributed to the triplet state of NDI. The triplet state is formed directly from the short lived species as indicated by DADS. So the transient at early times is most likely the singlet excited state of NDI. To the best of our knowledge, this is the first report of the absorption spectrum and lifetime of the NDI singlet state as obtained from femtosecond transients. The photoprocesses of **1** are summarized in an energy level diagram given in Scheme 3.1. Upon excitation of **1** the singlet state is formed, which decays rapidly via intersystem crossing (ISC) to the triplet state.



Scheme 3.1. Energy level diagrams proposed for excited state dynamics of **1**, **2**, and **3**.

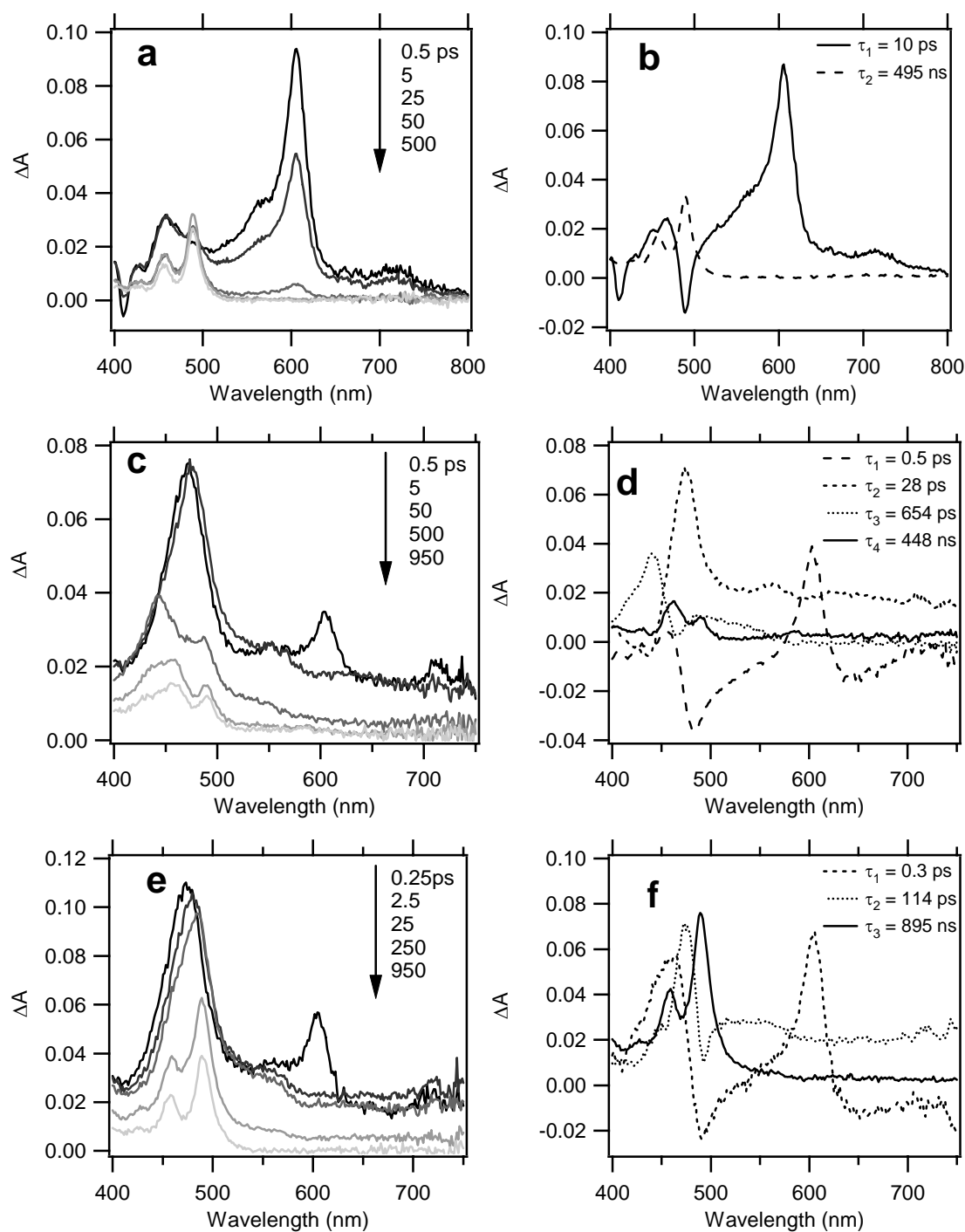


Figure 3.4. Time-resolved femtosecond transient absorption spectra (a, c, e) and decay-associated difference spectra (b, d, f) obtained by global analysis for **1**, **2** and **3**, respectively. The lifetimes associated with the DADS are shown in b, d and f as an inset. The longest components (> 400 ns) are from the nanosecond transient absorption measurements.

The time-resolved spectra and DADS for compound **2** are given in Figure 3.4c and 3.4d. Compared with the spectra for compound **1**, the evolution of the spectra in time is different for **2**. Global analysis gives four different components with corresponding DADS. The component with a maximum at 603 nm and minimum at 481 nm in the DADS decays with a lifetime of ~ 490 fs. The DADS of the second component has a maximum at 475 nm. This spectrum decays in 28 ps and a new spectrum with two maxima at 442 and 486 nm appears simultaneously. The absorption band at 442 nm decays faster (654 ps) than that at 486 nm ($\gg 1$ ns). Although this spectrum looks similar to the triplet state spectrum of **2** (*vide supra*), it does not match exactly. This suggests that the spectrum at ~ 1 ns is a sum of the triplet state absorption and the absorption of a transient with 654 ps lifetime.

The DADS (Figure 3.4d) with lifetime of 0.5 ps has a maximum (603 nm) at the same position as that of the singlet state of **1**. This suggests that this transient also arises from the singlet state. But for compound **2** the singlet state decays much faster and gives rise to a different spectrum than in case of **1**. Apparently, the deactivation of the singlet state of **2** takes another route instead of direct ISC to the triplet state. The transient formed from the singlet state has an absorption maximum at 473 nm, and the absorption extends over the whole spectral range employed (up to 800 nm). We attribute this to the NDI radical anion, which is well described in literature from chemical, electrochemical and photochemical reductions.^{18, 29} Normally this spectrum has a maximum around 470 nm and a weaker absorption band over 600 nm. The weaker absorption band is not clearly present in our data, which is likely due to the lower spectral resolution of the spectrograph and a lower signal-to-noise ratio of the setup employed. The appearance of the NDI radical anion would imply that the singlet state decays via a charge-transfer (CT) process, in which the phenyl moiety acts as electron donor to form a singlet CT state, in line with our previously mentioned hypothesis (*vide supra*).^{34, 35}

The CT state of NDI **2** has a lifetime of ~ 28 ps, and it decays simultaneously to the triplet state and to another unassigned state with a lifetime of 654 ps. However, in the nanosecond flash photolysis experiments only the triplet state spectrum is observed. This means that the triplet state is formed via charge recombination from the CT state. The formation of the triplet requires a spin flip before it can reach the local triplet state (3L). One possibility for this can be through ISC from 1CT to 3CT followed by charge

recombination producing ^3L .³⁶ Another possibility is the direct transition from ^1CT to the local triplet state via spin-orbit coupling between the spin states of the ^1CT and the triplet manifold.³⁷ This mechanism has been proposed for other molecules with a large dihedral angle between the donor and the acceptor moieties.³⁸ A larger dihedral angle gives a significant change in the orbital angular momentum upon charge recombination. This requires a spin flip in order to conserve energy.³⁹ Since the dihedral angle between the phenyl ring and NDI is close to 90° , the direct transition from the ^1CT to a ^3L triplet state might also occur in this case. From our transient absorption data it is not possible to conclude which of the two mechanisms is prevalent in the present case, since the absorption spectra of the ^1CT and the ^3CT could be the same.

Based on this a representative energy level diagram for **2** is given in Scheme 3.1. After excitation the singlet excited state decays via fast electron transfer to a ^1CT state. This state decays to the ^3L via either a ^3CT or a direct transition from ^1CT with simultaneous spin flip. From the ^1CT state also another species is formed, which has a decay time of 663 ps. This is not observed with compound **3** (vide infra), which indicates that it might be caused by some intermediate formed during the decay process specific for **2**. Since we are mainly interested in the lifetimes of the excited singlet state of the molecules under study, detailed determinations of the nature of this intermediate fall outside the scope of this study.

The time-resolved spectra and DADS for the tetrahedral compound **3** are given in Figure 3.4e and 3.4f. Global analysis of the data for **3** shows three components. The first has a lifetime of 340 fs and the DADS has maximum at 606 nm and minimum at 489 nm. The second DADS has a maximum at 476 nm and extends over the whole wavelength range. This species decays with a lifetime of 114 ps to the third spectrum, which shows maxima at 459 and 489 nm. The transients observed are similar to those of **2** except for the unassigned species, which suggest a similar decay pathway by rapid intramolecular electron transfer from the singlet state (340 fs). The formed ^1CT state decays with a lifetime of 114 ps to the triplet state, which has a lifetime of 895 ns as observed in the nanosecond transient absorption measurements. The energy level diagram for **3** is represented as given in Scheme 3.1.

The CT state of **2** has a higher energy than that of **3** (deduced from CT-fluorescence maxima), due to which the driving force for charge recombination is larger

for **2**. The lifetime of the CT state in **2** is shorter than that of **3**, which means that the rate of charge recombination is higher for a CT-state of higher energy (Marcus normal region).⁴⁰⁻⁴²

In summary, the femtosecond transient absorption measurements resulted in the observation of the singlet state absorption and determination of the singlet state dynamics (lifetime and decay routes) of a dialkyl-substituted NDI **1**. Substitution with a phenyl ring (**2** and **3**) on the imide nitrogen of NDI opens an additional decay pathway for the singlet state via intramolecular charge transfer process.

3.2.4. Picosecond fluorescence lifetime measurements

In order to support the singlet lifetimes observed in the femtosecond transient absorption, the corresponding fluorescence lifetimes were determined by time-correlated single photon counting. The fluorescence decay traces following excitation with a 18 ps laser pulse ($\lambda_{\text{exc}}=330$ nm) were monitored at 410 nm. A representative decay curve in chloroform is given in Figure 3.5. The concentrations of the solutions employed were in the order of 10^{-6} M. The data was fitted using iterative reconvolution of the instrument response function with a number of exponentials, generally with four exponentials. The obtained lifetimes are listed in Table 3.1.

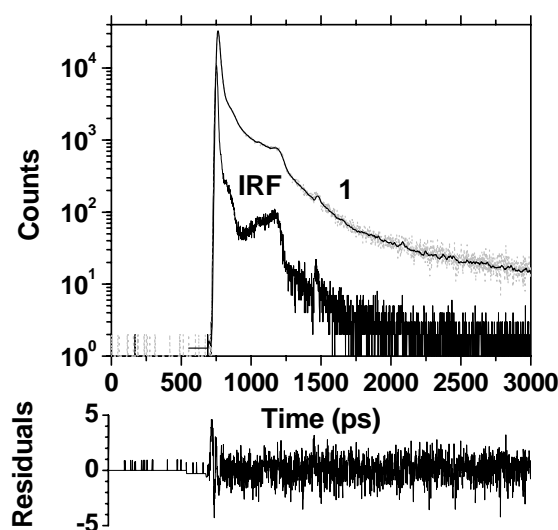


Figure 3.5. Representative picosecond fluorescence decay curve of **1** in chloroform at 410 nm, with fitting residuals.

Table 3.1. Fluorescence lifetimes and relative amplitudes (A) of the components obtained during the analysis of the decay curves observed at 410 nm.

Compound	A (%)	τ_1 (ps)	A (%)	τ_2 (ps)	A (%)	τ_3 (ns)	A (%)	τ_4 (ns)
1	89.5	12 \pm 2	7.3	90 \pm 20	1.7	0.5 \pm 0.1	1.5	3 \pm 1
2	96.2	1 \pm 2	3.6	12 \pm 2	0.1	0.3 \pm 0.1	0.1	2 \pm 1
3	81.7	3 \pm 2	17.7	10 \pm 2	0.4	0.3 \pm 0.1	0.2	1 \pm 1

For compound **1** the first component has a lifetime of ~ 12 ps, which is in agreement with the short component of 10 ps obtained from the femtosecond transient absorption data and confirms that it is from singlet state. Similar analysis of the decay curves obtained for **2** and **3** results in lifetimes of ~ 1 ps and ~ 3 ps, respectively, for the first components. These lifetimes are very short compared to the singlet lifetime of **1** (10 \pm 1 ps). These short lifetimes are not very accurate, since the instrumental response of the fluorescence lifetime measurements is ~ 18 ps (FWHM). Therefore, we interpret these to be in agreement with the femtosecond absorption data obtained for **2** ($\tau = 0.5$ ps) and **3** ($\tau = 0.3$ ps), within the experimental errors. As the lifetime data from the femtosecond absorption data are more reliable on this timescale, those values should be taken as the lifetime of the respective singlet states. These short fluorescence lifetimes confirm that the excited singlet state deactivation is much faster for compounds **2** and **3** than for **1**.

The fluorescence decays of all three compounds are multi-exponentials. The origin of the other components other than the shortest ones is not clear. Excimer formation by diffusion is highly unlikely in view of the short lifetimes observed for the singlet state. They might be attributed to excimer emission from ground state aggregates. However, such ground state aggregates were not visible in the steady state absorption, and are also not expected for the concentrations used ($\sim 10^{-6}$ M) during the single photon counting experiments. If they are present at all, then only in very low quantities. These low quantities of aggregates could have a high luminescence quantum yield giving rise to the observed long components. Also triplet-triplet annihilation leading to delayed fluorescence could contribute to these long lifetimes. The complex nature of the

fluorescence decay is not fully understood, and the details of this fall outside the scope of our present investigation.

The fluorescence lifetimes of the CT emission bands of **2** and **3**, in three different solvents, are presented in Table 3.2. The lifetimes in chloroform qualitatively agree with the lifetimes obtained by the global analysis of the femtosecond transient absorption data. The lifetime of the CT state of compound **2** is shorter than that of **3** as observed in the femtosecond data. The fact that the CT-fluorescence lifetime matches with the lifetimes from transient absorption indicates that the CT state observed in the latter is from ^1CT .

Table 3.2. Fluorescence maxima and lifetimes of the CT emission of **2** and **3**.

Compound	Fluorescence maxima (nm)			Fluorescence lifetime (ps)		
	CCl_4	CHCl_3	DCE	CCl_4	CHCl_3	DCE
2	540	559	570	23	34	49
3	545	589	609	144	172	145

3.2.5. Fluorescence lifetime measurements at 77 K

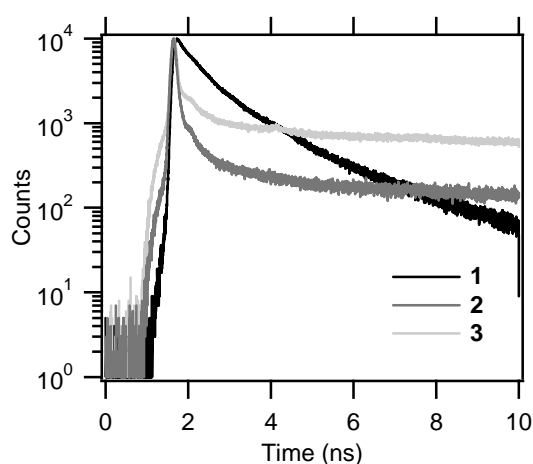


Figure 3.6. Fluorescence decay curves of **1**, **2** and **3** in MTHF at 77 K.

The fluorescence decays in a low temperature (77 K) glass were also measured, to further investigate the influence of the nitrogen substituents on the singlet state deactivation. It is known that the ISC of alkyl-substituted NDIs hinges on the out-of-plane bending modes in carbonyl compounds, and is thus slowed down in glasses.²⁹ This leads to less efficient triplet formation in rigid matrices, where the molecular motion is inhibited. For the phenyl substituents a different deactivation pathway is observed, and therefore it is expected that the rigid matrix does not affect the singlet deactivation process of compounds **2** and **3**. The fluorescence decays in a methyl-tetrahydrofuran (MTHF) glass at 77 K are depicted in Figure 3.6. The fluorescence lifetime of **1** in MTHF at 77 K becomes much longer (\sim ns) due to the slowing down of ISC process. For compounds **2** and **3** the fluorescence lifetimes remain short. This confirms that in case of NDIs substituted with a phenyl group on one of the nitrogen atoms, the singlet state deactivation follows a different decay pathway, namely intramolecular electron transfer from the phenyl ring to the NDI moiety, as already inferred from the transient absorption experiments.

3.3. Experimental

3.3.1. General

The synthesis and characterization of the compounds used are described in detail elsewhere.²³ Steady-state absorption spectra were recorded with a Cary 100 UV-Vis spectrophotometer. Fluorescence spectra were measured with a FLS 920 Spectrophotometer (Edinburgh Instruments, UK) fitted with a red-sensitive PMT (R928, Hamamatsu). All the solvents used in this study are of spectrophotometric grade purchased from Sigma-Aldrich, and freshly distilled over drying agents before use.

3.3.2. Femtosecond transient absorption measurements⁴³

The pump beam was an \sim 100 fs laser pulse train out of an optical parametric amplifiers (OPA) pumped by an amplified Ti:sapphire laser system (Spectra-Physics Hurricane) at a repetition rate of 1 kHz. Probing white light was produced by focusing a small amount of the fundamental beam (800 nm) on a sapphire plate. The probe beam

was then focused on the sample such that the pump beam irradiated a larger area of the sample ($\sim 0.25 \text{ mm}^2$) compared to the probe beam ($\sim 0.1 \text{ mm}^2$) in order to guarantee a homogeneous optical density throughout the probing area. The transmitted light was collected by a photodiode. An Ocean Optics (Si, 2048 px) plug-in card diode array was used for the UV-visible region (200-1100 nm). The samples used for these measurements were prepared so that the absorbance of the samples was about 1 in a cuvette of 1 mm thickness. The solutions were continuously stirred during the measurements to minimize possible thermal effects and photo-degradation.

Global analyses of the transient absorption data were performed using Igor Pro, version 5.0.5A. In all cases three or four exponential functions convoluted with a Gaussian function representing the instrumental response were used to fit a data set.^{32,33,44} The width of the Gaussian was fixed at the best value obtained from the fits at single wavelengths, and its value was about 200 fs (fwhm) in all cases.

3.3.3. Picosecond fluorescence lifetime measurements⁴⁵

Fluorescence decay curves at single wavelengths were measured with picosecond time-correlated single-photon counting (TCSPC). The setup consisted of a mode-locked argon-ion laser (Coherent 486 AS Mode Locker and Coherent Innova 200 laser) which was used to pump a cavity dumped DCM dye-laser (Coherent model 700) synchronously. The output frequency was doubled with a BBO crystal, resulting in $\sim 330 \text{ nm}$ pulses. A Hamamatsu micro-channel plate photomultiplier (R3809) was used as detector. Raman signal of water was taken as the instrument response function [full width at half maximum (fwhm) $\sim 18 \text{ ps}$].

3.3.4. Fluorescence lifetime measurements at 77 K

Low-temperature fluorescence lifetime measurements were performed in a FLS 920 Spectrophotometer (Edinburgh Instruments, UK) fitted with a cooled MCP PMT detector (Hamamatsu, R3809U-50). Samples were excited with a pulsed diode laser (LDH-P-C-375; PicoQuant GmbH, Germany; FWHM = 39 ps; $\lambda_{\text{exc}} = 372 \text{ nm}$), controlled by a pulse controller (PDL 800-B; PicoQuant GmbH, Germany). The instrument response function (FWHM of IRF $\sim 87 \text{ ps}$) was determined from scattering from colloidal silica Ludox (Sigma-Aldrich). The samples were cooled with a cryostat

(Optistat DN; Oxford Instruments, UK), which was controlled with a temperature controller (ITC 503S; Oxford Instruments, UK).

3.3.5. Nanosecond laser flash photolysis

Nanosecond laser flash photolysis studies were carried out using the third harmonic (355 nm, FWHM = 4 ns) of a Nd:YAG laser (Brilliant, Quantal Inc.). The transient spectra were obtained using an LP920 spectrophotometer (Edinburgh Instruments Limited) fitted with a 450 W Xe arc lamp as probe-light source and a red-sensitive photomultiplier (R928, Hamamatsu) and ICCD camera (DH720, Andor Technology) as detectors.

All spectroscopic measurements were carried out under magic-angle condition unless stated otherwise, to avoid the possible influence of rotational motions of the probe molecules.

3.4. Conclusions

NDI derivatives **1**, **2** and **3** were studied with nanosecond to femtosecond time-resolved techniques. For the symmetrically substituted NDI **1** the excited singlet state absorption (600 nm) and lifetime (10 ± 1 ps) are reported for the first time. The singlet state decays to the ground state via efficient ISC. Substitution of the imide nitrogen with a phenyl ring like in the case of **2** and **3** opens an additional decay pathway from the S_1 state to a local 3L triplet state via an intramolecular charge transfer state (1CT) resulting from electron transfer from the phenyl ring to the NDI moiety. As a consequence, the singlet state lifetime is drastically reduced, which is in the range of $\sim 300 - 500$ fs for **2** and **3**. This 1CT state subsequently decays to the triplet state of NDI. The fluorescence lifetimes obtained are in close agreement with the lifetimes of the singlet state found with femtosecond transient absorption measurements. The difference in the singlet state decays between **1** versus **2** and **3** was further proven by fluorescence lifetime measurements at 77 K in an MTHF glass. In MTHF glasses, the singlet state lifetime remained short in case of **2** and **3**, but increased to nanoseconds for **1** due to slowing down of the ISC process.

3.5. References

1. Baeg, K. J.; Noh, Y. Y.; Ghim, J.; Kang, S. J.; Lee, H.; Kim, D. Y. *Adv. Mater.* **2006**, *18*, 3179-3183.
2. Takimiya, K.; Kunugi, Y.; Konda, Y.; Ebata, H.; Toyoshima, Y.; Otsubo, T. *J. Am. Chem. Soc.* **2006**, *128*, 3044-3050.
3. Xiao, K.; Liu, Y. Q.; Qi, T.; Zhang, W.; Wang, F.; Gao, J. H.; Qiu, W. F.; Ma, Y. Q.; Cui, G. L.; Chen, S. Y.; Zhan, X. W.; Yu, G.; Qin, J. G.; Hu, W. P.; Zhu, D. B. *J. Am. Chem. Soc.* **2005**, *127*, 13281-13286.
4. Yasuda, T.; Fujita, K.; Tsutsui, T.; Geng, Y. H.; Culligan, S. W.; Chen, S. H. *Chem. Mat.* **2005**, *17*, 264-268.
5. Anthopoulos, T. D.; Tanase, C.; Setayesh, S.; Meijer, E. J.; Hummelen, J. C.; Blom, P. W. M.; de Leeuw, D. M. *Adv. Mater.* **2004**, *16*, 2174-2179.
6. Hancock, J. M.; Gifford, A. P.; Zhu, Y.; Lou, Y.; Jenekhe, S. A. *Chem. Mat.* **2006**, *18*, 4924-4932.
7. Lee, M. T.; Liao, C. H.; Tsai, C. H.; Chen, C. H. *Adv. Mater.* **2005**, *17*, 2493-2497.
8. Chao, T. C.; Lin, Y. T.; Yang, C. Y.; Hung, T. S.; Chou, H. C.; Wu, C. C.; Wong, K. T. *Adv. Mater.* **2005**, *17*, 992-996.
9. Yeh, S. J.; Wu, M. F.; Chen, C. T.; Song, Y. H.; Chi, Y.; Ho, M. H.; Hsu, S. F.; Chen, C. H. *Adv. Mater.* **2005**, *17*, 285-289.
10. Li, G.; Shrotriya, V.; Huang, J. S.; Yao, Y.; Moriarty, T.; Emery, K.; Yang, Y. *Nat. Mater.* **2005**, *4*, 864-868.
11. Spanggaard, H.; Krebs, F. C. *Sol. Energy Mater. Sol. Cells* **2004**, *83*, 125-146.
12. Brabec, C. J. *Sol. Energy Mater. Sol. Cells* **2004**, *83*, 273-292.
13. Katz, H. E.; Lovinger, A. J.; Johnson, J.; Kloc, C.; Siegrist, T.; Li, W.; Lin, Y. Y.; Dodabalapur, A. *Nature* **2000**, *404*, 478-481.
14. Borgström, M.; Shaikh, N.; Johansson, O.; Anderlund, M. F.; Styring, S.; Akermark, B.; Magnuson, A.; Hammarström, L. *J. Am. Chem. Soc.* **2005**, *127*, 17504-17515.
15. Johansson, O.; Wolpher, H.; Borgström, M.; Hammarström, L.; Bergquist, J.; Sun, L. C.; Akermark, B. *Chem. Commun.* **2004**, 194-195.
16. Guo, X. F.; Gan, Z. H.; Luo, H. X.; Araki, Y.; Zhang, D. Q.; Zhu, D. B.; Ito, O. *J. Phys. Chem. A* **2003**, *107*, 9747-9753.

17. Flamigni, L.; Johnston, M. R.; Giribabu, L. *Chem.-Eur. J.* **2002**, *8*, 3938-3947.
18. Miller, S. E.; Lukas, A. S.; Marsh, E.; Bushard, P.; Wasielewski, M. R. *J. Am. Chem. Soc.* **2000**, *122*, 7802-7810.
19. Ofir, Y.; Zelichenok, A.; Yitzchaik, S. *J. Mater. Chem.* **2006**, *16*, 2142-2149.
20. Koehorst, R. B. M.; Fokkink, R. G.; Stuart, M. C.; Zuilhof, H.; Sudhölter, E. J. R. *Macromolecules* **2002**, *35*, 4226-4228.
21. Wiederrecht, G. P.; Wasielewski, M. R. *J. Am. Chem. Soc.* **1998**, *120*, 3231-3236.
22. Wasielewski, M. R. *J. Org. Chem.* **2006**, *71*, 5051-5066.
23. Ganesan, P.; Yang, X. N.; Loos, J.; Savenije, T. J.; Abellon, R. D.; Zuilhof, H.; Sudhölter, E. J. R. *J. Am. Chem. Soc.* **2005**, *127*, 14530-14531.
24. Penneau, J. F.; Stallman, B. J.; Kasai, P. H.; Miller, L. L. *Chem. Mat.* **1991**, *3*, 791-796.
25. Aveline, B. M.; Matsugo, S.; Redmond, R. W. *J. Am. Chem. Soc.* **1997**, *119*, 11785-11795.
26. Abraham, B.; McMasters, S.; Mullan, M. A.; Kelly, L. A. *J. Am. Chem. Soc.* **2004**, *126*, 4293-4300.
27. Rogers, J. E.; Weiss, S. J.; Kelly, L. A. *J. Am. Chem. Soc.* **2000**, *122*, 427-436.
28. Gosztola, D.; Niemczyk, M. P.; Svec, W.; Lukas, A. S.; Wasielewski, M. R. *J. Phys. Chem. A* **2000**, *104*, 6545-6551.
29. Green, S.; Fox, M. A. *J. Phys. Chem.* **1995**, *99*, 14752-14757.
30. Barros, T. C.; Brochsztain, S.; Toscano, V. G.; Berci, P.; Politi, M. J. *J. Photochem. Photobiol. A-Chem.* **1997**, *111*, 97-104.
31. Struijk, C. W.; Sieval, A. B.; Dakhorst, J. E. J.; van Dijk, M.; Kimkes, P.; Koehorst, R. B. M.; Donker, H.; Schaafsma, T. J.; Picken, S. J.; van de Craats, A. M.; Warman, J. M.; Zuilhof, H.; Sudhölter, E. J. R. *J. Am. Chem. Soc.* **2000**, *122*, 11057-11066.
32. Van Stokkum, I. H. M.; Larsen, D. S.; van Grondelle, R. *Biochim. Biophys. Acta-Bioenerg.* **2004**, *1658*, 262-262.
33. Van Stokkum, I. H. M.; Larsen, D. S.; van Grondelle, R. *Biochim. Biophys. Acta-Bioenerg.* **2004**, *1657*, 82-104.
34. Loveland, J. W.; Dimeler, G. R. *Anal. Chem.* **1961**, *33*, 1196-1201.

35. The NDI has a reduction potential of -0.64 V vs SCE and benzene has an oxidation potential of +2.382 V vs SCE. From these data, a driving force of -0.2 eV is calculated
36. Verhoeven, J. W. J. *Photochem. Photobiol. C-Photochem. Rev.* **2006**, 7, 40-60.
37. Van Dijk, S. I.; Wiering, P. G.; Groen, C. P.; Brouwer, A. M.; Verhoeven, J. W.; Schuddeboom, W.; Warman, J. M. *J. Chem. Soc.-Faraday Trans.* **1995**, 91, 2107-2114.
38. Van Willigen, H.; Jones, G.; Farahat, M. S. *J. Phys. Chem.* **1996**, 100, 3312-3316.
39. Wiederrecht, G. P.; Svec, W. A.; Wasielewski, M. R.; Galili, T.; Levanon, H. *J. Am. Chem. Soc.* **2000**, 122, 9715-9722.
40. Gould, I. R.; Boiani, J. A.; Gaillard, E. B.; Goodman, J. L.; Farid, S. *J. Phys. Chem. A* **2003**, 107, 3515-3524.
41. Gould, I. R.; Farid, S. *Accounts Chem. Res.* **1996**, 29, 522-528.
42. Kavarnos, G. J.; Turro, N. J. *Chem. Rev.* **1986**, 86, 401-449.
43. Poór, B.; Michniewicz, N.; Kállay, M.; Buma, W. J.; Kubinyi, M.; Szemik-Hojniak, A.; Deperasińska, I.; Puszko, A.; Zhang, H. *J. Phys. Chem. A* **2006**, 110, 7086-7091.
44. Poprawa-Smoluch, M.; Baggerman, J.; Zhang, H.; Maas, H. P. A.; De Cola, L.; Brouwer, A. M. *J. Phys. Chem. A* **2006**, 110, 11926-11937.
45. Proposito, P.; Marks, D.; Zhang, H.; Glasbeek, M. *J. Phys. Chem. A* **1998**, 102, 8894-8902.

Chapter 4

Amorphous Siloxanes with Naphthalene Diimide Acceptor Moieties

Abstract

Cyclic siloxanes with pendent naphthalene diimide groups were synthesized via a hydrosilylation reaction, to form amorphous electron-accepting materials. Photophysical measurements of blends of these siloxanes with *p*-type polymers (P3HT, MDMO-PPV) showed >99.9 % fluorescence quenching of the latter polymers. This demonstrates that these siloxanes form a new class of highly efficient electron accepting (*n*-type) materials that additionally provide control over intermolecular interactions. Mixtures of these siloxanes and *p*-type polymers gave homogeneous amorphous films from chloroform solution, and films with micro-crystallinity were obtained from *o*-dichlorobenzene solutions. The time-resolved microwave conductance in films formed from *o*-dichlorobenzene was higher than in films formed from chloroform, which is attributed to nanoscopic phase separation that enhances the interfacial charge separation.

Part of this Chapter was published in –

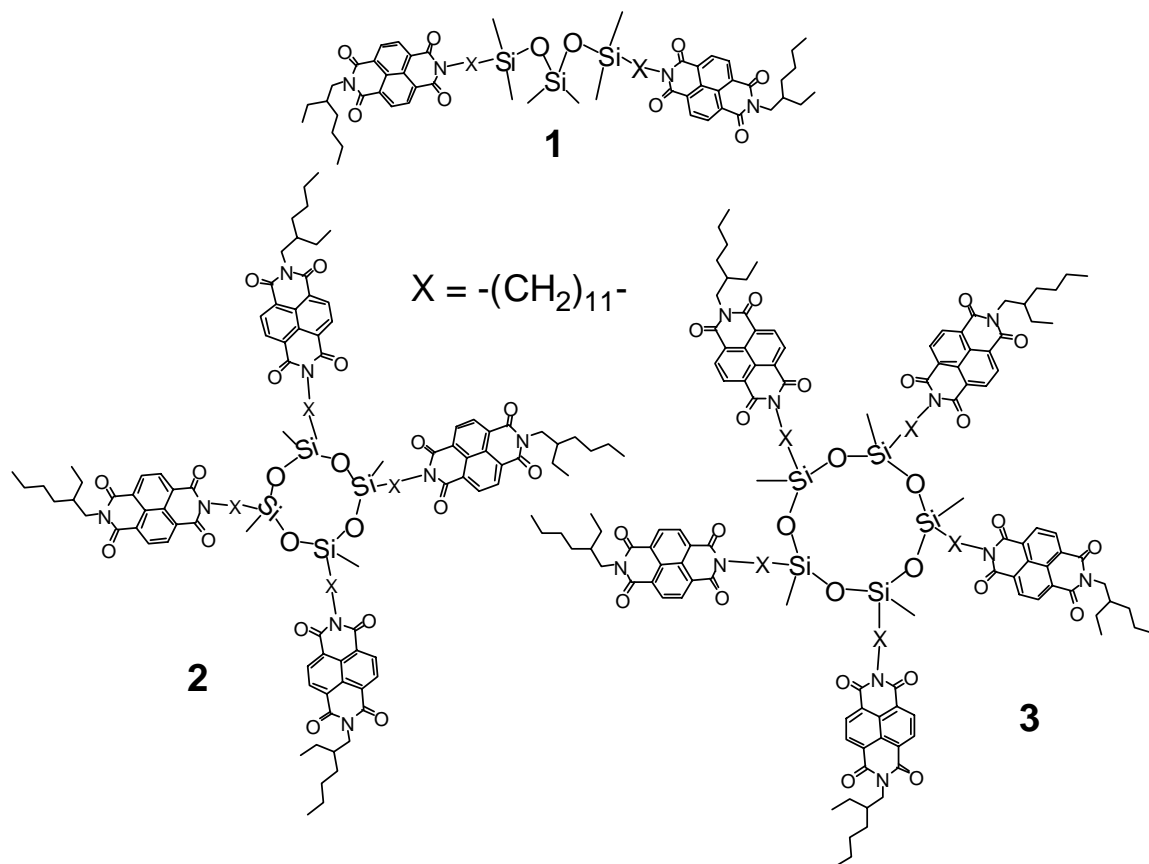
P. Ganesan, B. van Lagen, A. T. M. Marcelis, H. Zuilhof, and E. J. R. Sudhölter, *Org.Lett.* (2007), *In Press*

P. Ganesan, W. Grzegorzczuk, S. S. van Bavel, T. J. Savenije, J. Loos, H. Zuilhof, and E. J. R. Sudhölter
(Manuscript in preparation)

4.1 Introduction

Over the last decade, there is a rapidly increasing interest in the development of organic optoelectronic materials. In devices based on these materials the overall molecular order, structural defects, π - π stacking and (partial) crystallization of the material pose constraints to the properties of such a material.¹ While *nanoscopic* phase separation is essential for the proper performance of *e.g.* organic photovoltaic solar cells, *macroscopic phase separation or crystallization* is undesired. Phase separation between *n*- and *p*-type materials and π - π overlap domains with length scales in the order of the exciton diffusion length are desired for an effective electron-hole separation.² There have been many attempts to bring controlled order in organic optoelectronic materials, and thus improve the morphology of the active materials used for organic FETs,³⁻⁵ LEDs,^{6, 7} and photovoltaic devices.⁸⁻¹² Our interests focus on the prevention of *large-scale* crystallization, and aim to obtain a homogeneous morphology of the photoactive layer by developing amorphous materials. In Chapter 2, we reported on the synthesis and optoelectronic properties of a novel *n*-type amorphous tetrahedral tetraphenylmethane-based material, which yielded upon mixing with *p*-type polymers a homogeneous morphology and a very high conductivity.¹³ While the resulting blend was amorphous in nature, the structural rigidity of this molecule precluded further optimization of the charge transfer paths. Therefore, in this chapter we aimed to develop amorphous *n*-type materials in which the electron-accepting moieties are attached to an inert core via a flexible linker. This should allow intra- and intermolecular structural reorganization that may lead to an improved π - π overlap between adjacent molecules, and thus to more efficient charge transfer channels, without compromising the amorphous nature of the material. Siloxanes are attractive for this purpose, as they have a flexible, yet photochemically and electrically inert backbone. Cyclic oligomeric siloxanes provide the additional benefit of a well-defined size-dependent structure. While they have been used for ion transport,¹⁴ liquid crystalline materials^{15, 16} and organometallic reactions,^{17, 18} this class of materials has still not been used in optoelectronic materials. This chapter describes the synthesis, characterization and photophysical properties of three novel siloxanes with pendent naphthalene diimide (NDI) chromophores (**1** – **3**; Scheme 4.1), together with their fluorescence quenching of *p*-type polymers. For blends of siloxanes with *p*-type polymers, spin coated from *o*-

dichlorobenzene (ODCB) or CHCl_3 solutions, the morphology and TRMC studies are also reported.

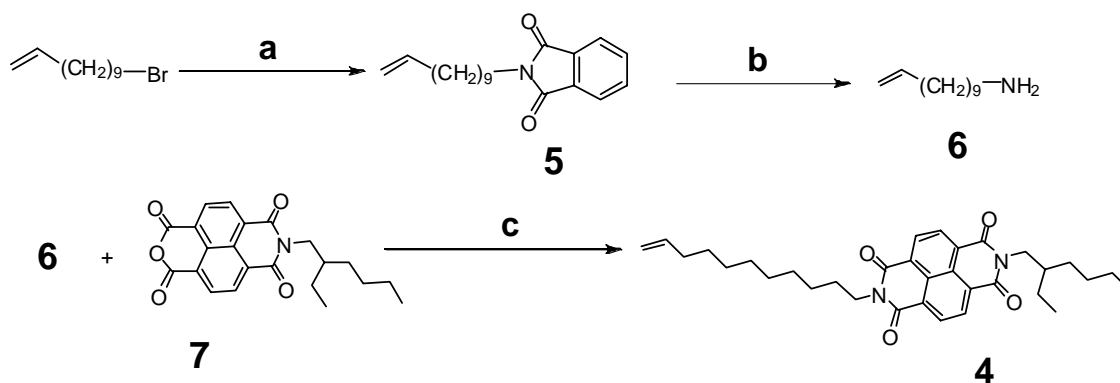


Scheme 4.1. Structures of the siloxanes described in this chapter.

4.2. Results and Discussions

4.2.1. Synthesis

Synthesis of 1-amino-10-undecene **6** was achieved using a literature procedure.¹⁹ The reaction between 1-bromo-10-undecene and potassium phthalimide resulted in compound **5**, which on reduction with hydrazine gave **6** in ~70 % yield. The starting material for the synthesis of siloxanes, the alkene terminated naphthalene diimide (NDI) **4**, was synthesized in good yield by the condensation of **6** with **7** (Scheme 4.2).



Scheme 4.2. Synthesis of starting molecule **4**. (a) potassium phthalimide, DMF, 90 °C, 24 h; (b) hydrazine monohydrate, EtOH, reflux, 3 h; (c) 1,4-dioxane, reflux, 15 h.

Compounds **1-3** were synthesized via hydrosilylation reactions catalyzed by Karstedt's Pt⁰-catalyst in dry toluene under an argon atmosphere at 70 °C (Scheme 4.3). Dimer **1** and tetramer **2** were obtained in an overall yield of around 50%, but pentamer **3** could only be obtained in a very low yield (~1.5%), which we attribute to the following two factors:²⁰

(i) Figure 4.1 shows a representation of a hypothetical double-chair conformation adopted by the siloxane pentamer. A movement of the Si(1) towards the ring, as indicated by the arrow, would induce an outward motion of Si(2) and Si(3). This motion would only have a small effect on Si(4) and Si(5). Having large substituents on Si(2) and Si(3), R=NDI, would also result in an outward movement and consequently an inward movement of Si(1). Si-H(1) then becomes much less accessible for reaction and thus contributes to an overall low yield of **3**. Addition of more alkene **4** and/or catalyst or increase in the reaction temperature did not help to drive the reaction further to completion.

(ii) the difference in polarity between fully substituted and partially substituted siloxanes is small, which make the separation of the desired molecule by chromatographic methods difficult. This difficulty also brought the isolated yield of **3** further down.

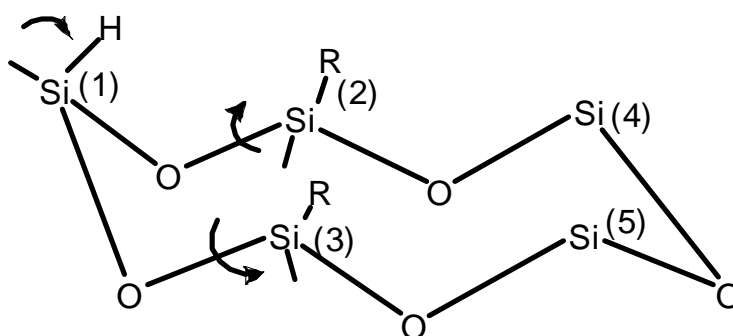
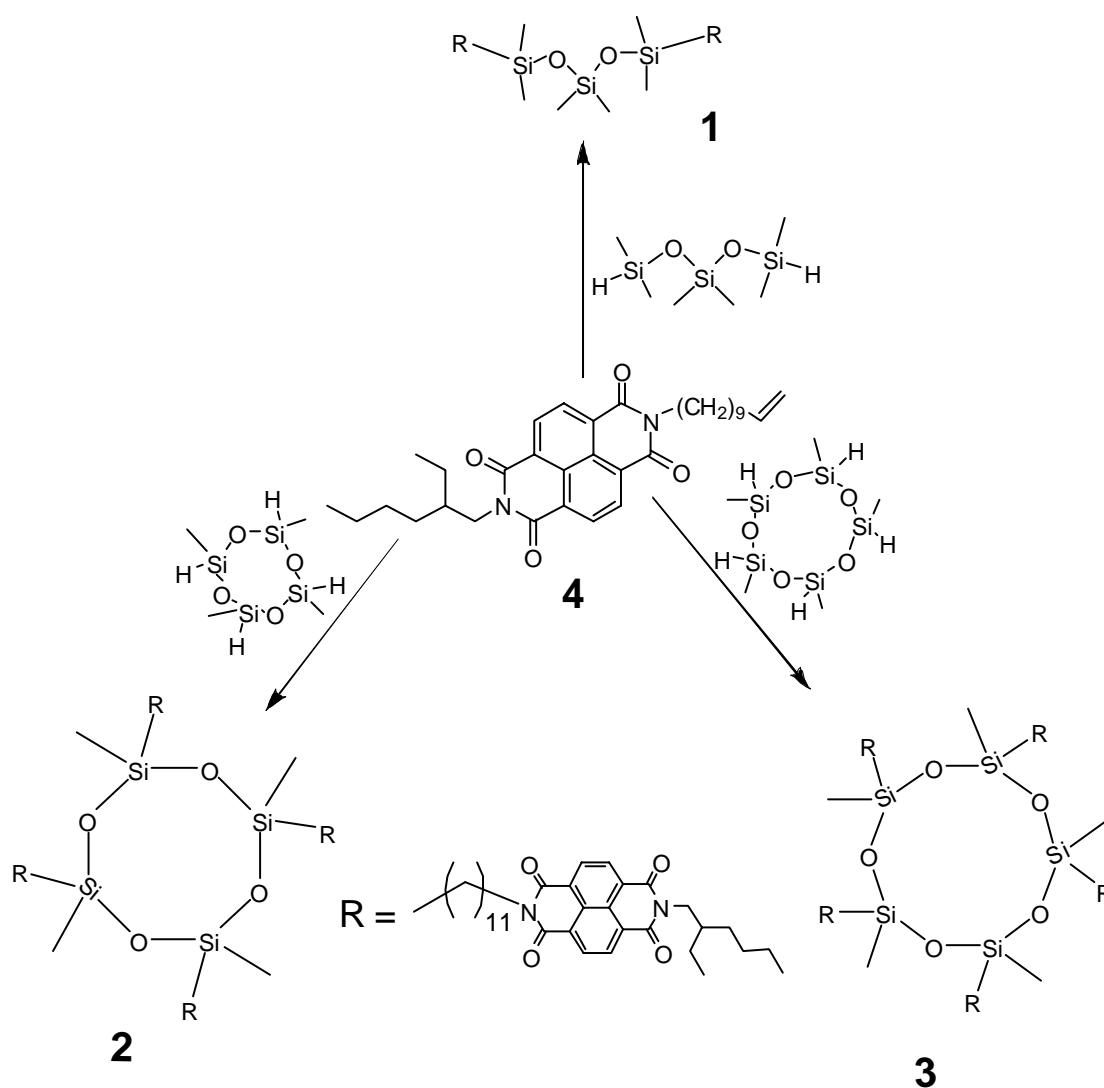


Figure 4.1. Double chair conformation of cyclic siloxane pentamer.



Scheme 4.3. Synthesis of siloxanes **1-3** by hydrosilylation. Reaction conditions: dry toluene, 5 μ l-(platinum(0)-1,3-divinyl-1,1,3,3-tetramethyldisiloxane complex; 0.10 M solution in xylenes, 70 °C, argon atmosphere.

4.2.1.1. Mechanism of hydrosilylation

Recently these two mechanisms were investigated by computational methods and a generalized mechanism was suggested.²¹ According to this (third) mechanism, the silylation mechanism in the synthesis of **1-3** takes a catalytic route as depicted in Figure 4.2. First, two alkene-terminated NDI molecules are non-covalently bound to Pt metal. In the second step, the hydrogen-terminated siloxane binds covalently to Pt by an insertion reaction. Subsequently, a covalent bond is formed between one of the alkene molecules and Pt, while the H atom is transferred from Pt to a β -carbon atom. In the last step, the product eliminates after addition of one more alkene molecule.

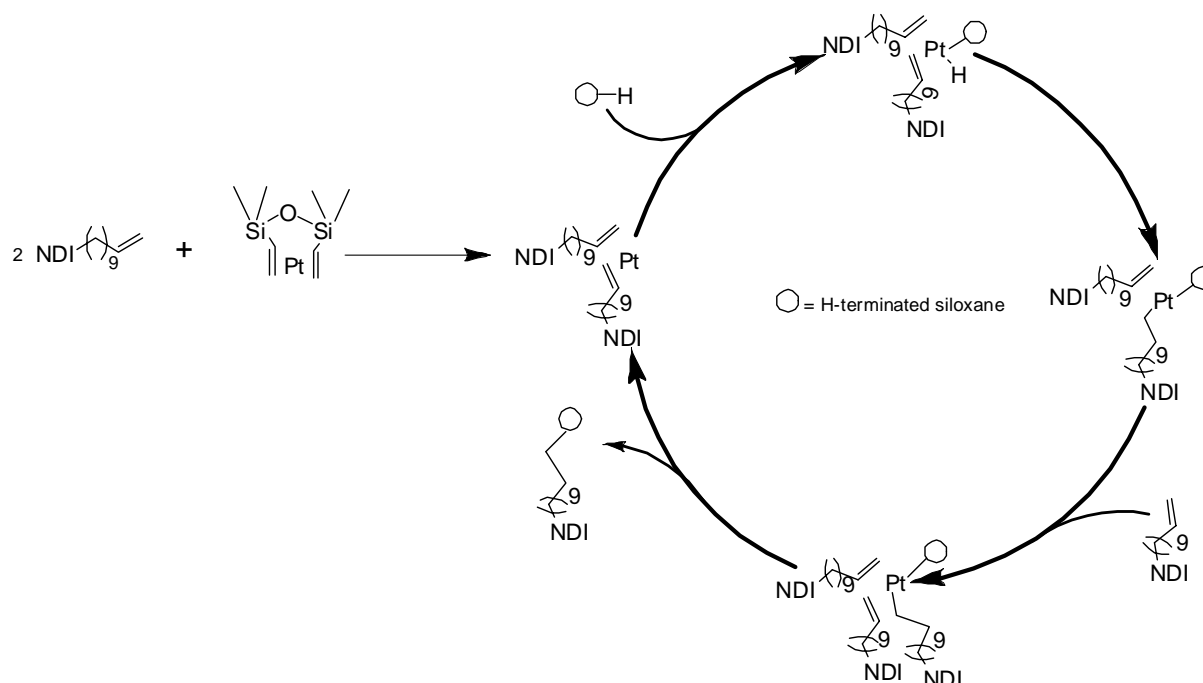


Figure 4.2. Hydrosilylation mechanism.

4.2.2. NMR Studies and Stereoisomers

In contrast to the ¹H-NMR spectrum of compound **1**, the spectra of compounds **2** and **3** display more than one signal for the protons of the naphthalene rings (Figure 4.3). Though the spectrum of **2** and **3** might look like a multiplet splitting because of their symmetrical nature, variation of the frequencies (300 *vs* 400 MHz) revealed a field-dependent spectrum. As a result, the spectra are not due to different proton-proton couplings, but are caused by the presence of different stereoisomers.

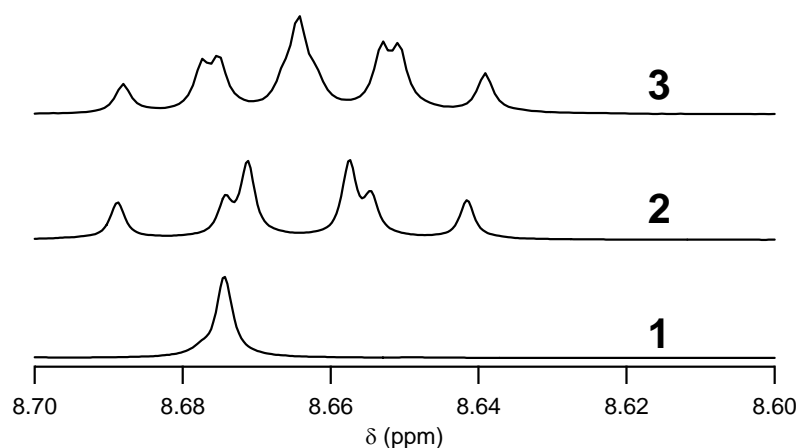


Figure 4.3. ^1H -NMR chemical shifts of siloxanes dimer **1**; tetramer **2**; and pentamer **3** in the aromatic region (300 MHz).

In the case of tetramer **2** four stereoisomers are possible (Figure 4.4) with a statistical distribution of 2 : 4 : 1 : 1. The observed ratios could be different from the statistical distribution, because of epimerization that allows equilibrium distributions.²²⁻²⁴ The observation of six rather than four peaks in the NMR spectrum can be explained from the environments of the NDI rings in isomers **2a-2d**.

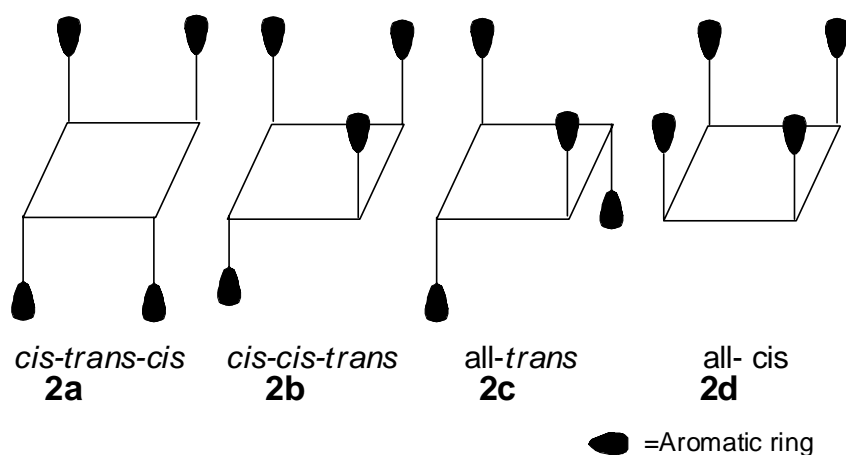


Figure 4.4. Simplified representation of the stereoisomers of cyclic siloxane tetramers **2**.

In compound **2a** every NDI aromatic ring is oriented *cis* to one neighboring ring, and *trans* to the other, while it is oriented *trans* with respect to aromatic ring across the siloxane ring. As a result all aromatic rings are in the same environment, and show up as one peak. Analogous arguments apply for **2c** and **2d**, which yield a spectrum of a single NDI moiety with different chemical shifts. In case of **2b**, the NDI rings are not identical, and show up as three singlets in a ratio of 1:2:1. Given that **2b** statistically amounts to half of the total distribution, 6 signals are to be expected in the ^1H -NMR with a signal ratio of 1:1:2:2:1:1, as experimentally observed. In fact, this is the first reported case in which the ratios match exactly the statistical distribution, since epimerization is completely blocked by the bulky substituents at the Si atom.

Analogously, for pentamer **3** four stereoisomers are possible. This will give rise to ten different environments for the NDI rings due to splitting of peaks of three isomers into a 2 : 2 : 1 ratio (Figure 4.5). Since the addition of the 5th substituent can be highly activated depending on the substitution pattern of the ring (*vide supra*), no statistical mixture is to be expected, in line with the observation of seven peaks in the ^1H -NMR spectrum of **3** with an observed peak ratio (%) of 7.7 : 9.8 : 11.6 : 31.8 : 14.0 : 14.5 : 10.6.

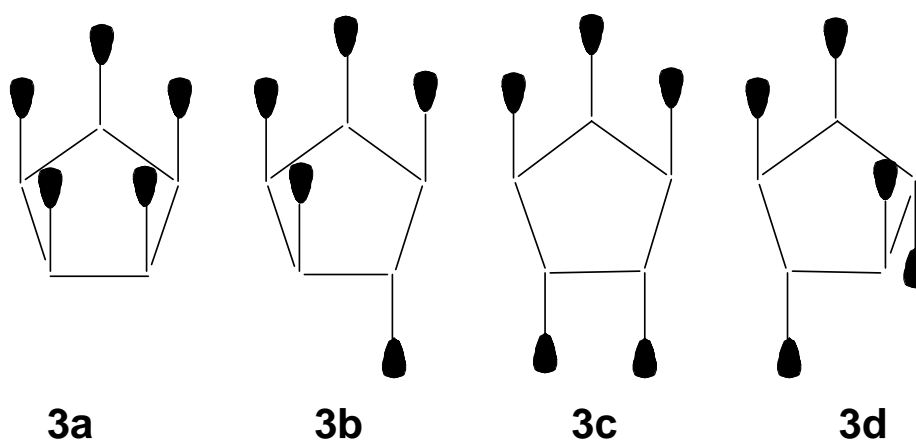


Figure 4.5. Simplified representation of the stereoisomers of cyclic siloxane pentamers **3**.

The naphthalenediimide groups in isomers **3b**, **3c** and **3d** occur in three different environments, each. Therefore, each peak of these three isomers would split at a ratio of 2 : 2 : 1. Thus in total 10 different peaks for the naphthalenediimide aromatics could be

expected. Given the high similarity of some of these environments, it is likely that some of these peaks overlap, which would reduce the number of observed peaks to < 10 . This is indeed our observation (7 peaks are seen).

4.2.3. Photophysics

4.2.3.1. Absorption and Fluorescence spectroscopy

Optical absorption spectra of **1** - **3** obtained at micromolar concentrations in chloroform show a normal absorption of NDI with vibrational features (Figure 4.6a). For **1**, but not for **2** and **3**, an extra absorption band around 450 nm starts to grow upon increasing the concentration to the millimolar range. This is attributed to ground state aggregation (Figure 4.6b). In contrast, the steady-state emission spectra of all three compounds displayed, over the whole measurable concentration range, two distinct features: (i) the monomer (410 nm) and (ii) the exciplex (503 nm) emission. This kind of emission was observed even at sub-micromolar concentrations (10^{-7} M), indicating that the emission at 503 nm is due to intramolecular excimer formation.

The position and intensity of the fluorescence of **1** - **3** are significantly influenced by the solvent (Figure 4.6c). On changing the solvent from chloroform to *o*-dichlorobenzene (ODCB), the monomer fluorescence of **2** enhanced with a shift from 410 to 430 nm, while the intensity of the excimer fluorescence decreased. This phenomenon is attributed to π - π stacking of the aromatic solvent molecules with the chromophores, which competes with excimer formation of **2**.^{25, 26} For low concentrations of compound **1** this π - π stacking in ODCB even leads to disappearance of the excimer peak. This is an indication of intermolecular ground state aggregates in the case of **1**, which is prevented by the solvent molecules. In the case of **2** and **3**, although intermolecular aggregations are prevented, the intramolecular stacking is not prevented by the solvent molecules. Therefore, the excimer emission has not disappeared as in the case of **1**.

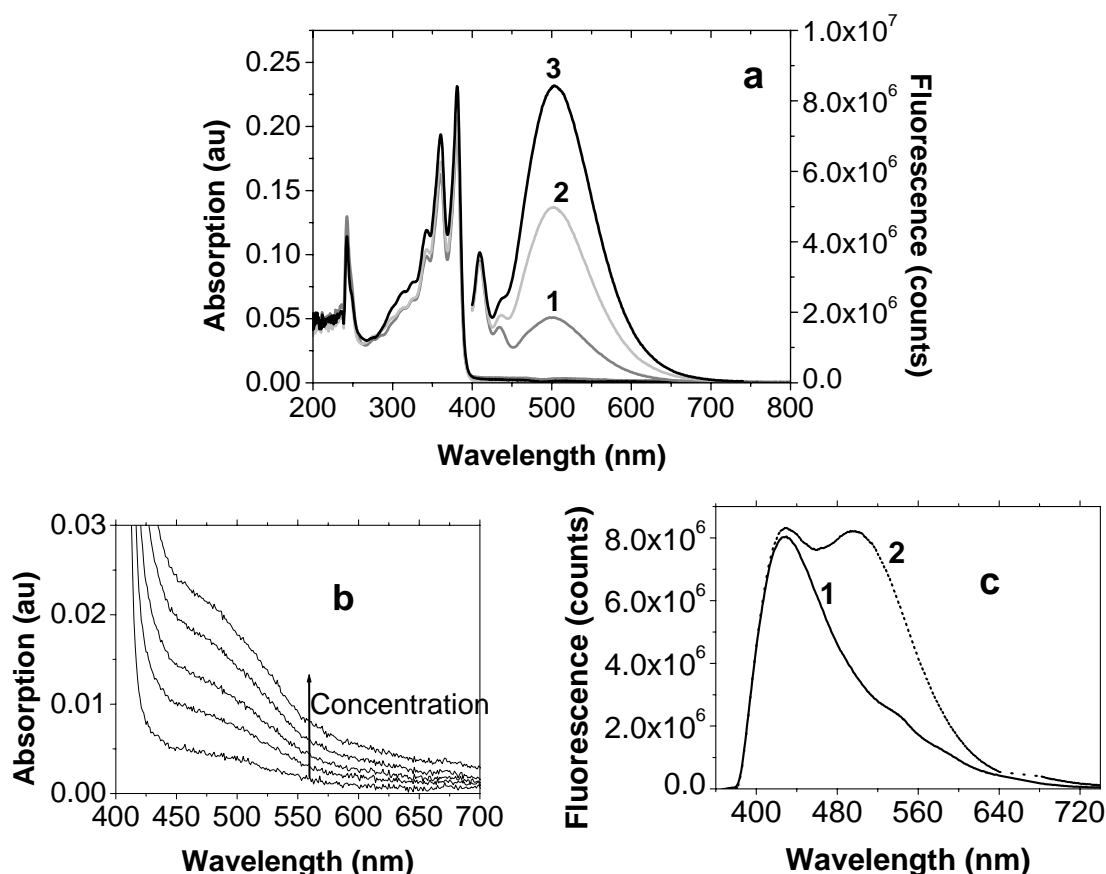


Figure 4.6. (a) Absorption and emission ($\lambda_{\text{exc}} = 381 \text{ nm}$) spectra of dimer **1** ($5.04 \mu\text{M}$), tetramer **2** ($2.54 \mu\text{M}$) and pentamer **3** ($1.96 \mu\text{M}$) in CHCl_3 ; concentrations chosen to yield equal chromophore concentrations. (b) Absorption spectra of dimer **1** at higher concentrations ($2 - 10 \text{ mM}$); (c) Emission spectra of **1** (solid line) and **2** (dotted line) in ODCB ($\sim 8 \mu\text{M}$).

4.2.3.2. Nanosecond transient absorption

Nanosecond laser flash photolysis (LFP) studies on siloxanes **1**, **2**, and **3** in chloroform reveal the triplet spectrum of the NDI moieties (Figure 4.7). As described in Chapter 3, the higher triplet states lie near the excited singlet states; therefore the intersystem (S_1-T_1) crossing is very efficient and shortens the excited singlet state lifetime. This leads to low fluorescence quantum yields.²⁵ These triplet spectra were vibrationally resolved (456 and 485 nm) up to a certain concentration.

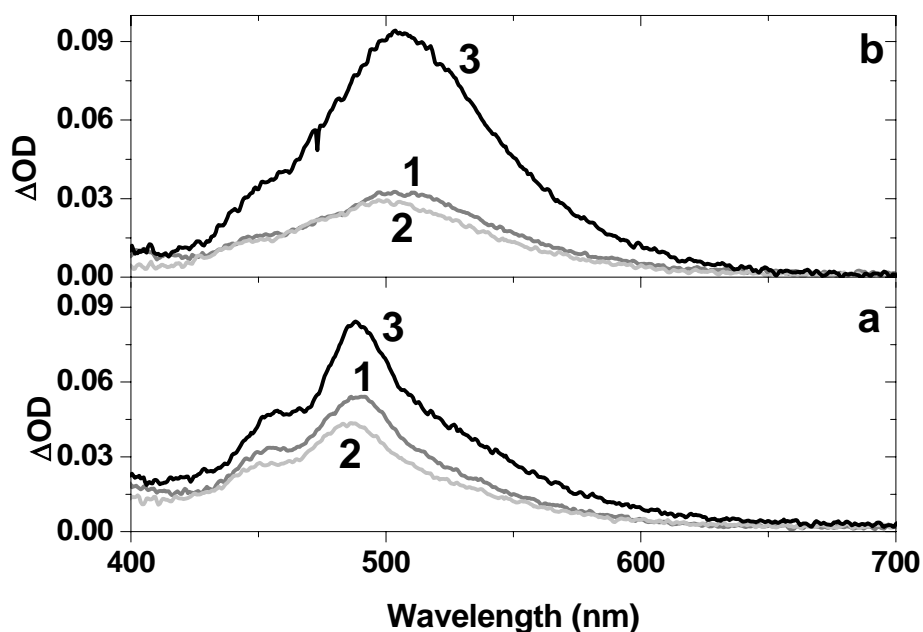


Figure 4.7. Transient absorption spectra of **1** (gray), **2** (light-gray), and **3** (black) in chloroform. a) at low concentration [**1** – 100 μM , **2** – 50 μM and **3** – 20 μM]; b) at higher concentration [**1** – 0.2 mM, **2** – 0.1 mM and **3** – 79 μM ($\lambda_{\text{exc}} = 355 \text{ nm}$; FWHM = 4 ns)].

Above this concentration (for **1**: 0.1 – 0.2 mM; for **2**: 0.005 – 0.01 mM; for **3**: 0.008 – 0.01 mM) the spectra were red-shifted with loss of vibrational resolution. The red shift in the transient absorption maxima (Figure 4.7 b) is more pronounced in dimer **1** (510 nm) than in **2** and **3** (505 nm). At these concentrations, an extra shoulder was seen in the UV-Vis spectrum of **1** at 450 nm, indicating the formation of ground state aggregates as shown in Figure 4.6b. Such a shoulder was not seen in UV-vis spectra of **2** and **3**. However, it is also for these compounds, expected that intermolecular π - π stacking of chromophores becomes more significant at higher concentrations, resulting in both the loss of vibrational features and a red shift in the triplet absorption maxima. Upon a further significant increase in concentration, as in thin solvent-casted films, we can therefore expect intermolecular complexes to be ubiquitously present.

4.2.3.3. Time-resolved fluorescence spectroscopy

The presence of intermolecular interactions at higher concentrations was also confirmed by time-resolved nanosecond fluorescence spectroscopy. Immediately after the

laser pulse, at low concentrations no excimer/excimer peak was seen (4, 5 and 10 μM , for **3**, **2** and **1**, respectively), whereas at 50-fold higher concentrations an excimer component was clearly observed around 500 nm (Figure 4.8; $\lambda_{\text{exc}} = 355$ nm; FWHM = 4 ns). When the fluorescence was measured 6 ns after the pulse, a clear excimer emission is already seen at the lower concentrations. At higher concentrations, the chromophores form ground state dimers, which are excited and yield the excimer emission immediately after the pulse. At lower concentrations excimers are formed after 6 ns from the pulse. Since the lifetime of the excited singlet state is ~ 10 ps (see Chapter 3), it is unlikely that the molecules diffuse together within their singlet lifetime to form excimers. As the triplet lifetime is ~ 1 μs , it is possible that two NDI chromophores diffuse together within the triplet lifetime, to form π -dimers and undergo triplet-triplet annihilation. This yields a singlet excited NDI together with an NDI molecule in its ground state, which will likely form an excited complex, to give an excimer like emission. This explains why the excimer intensity increases over time from directly after the pulse to 6 ns thereafter.

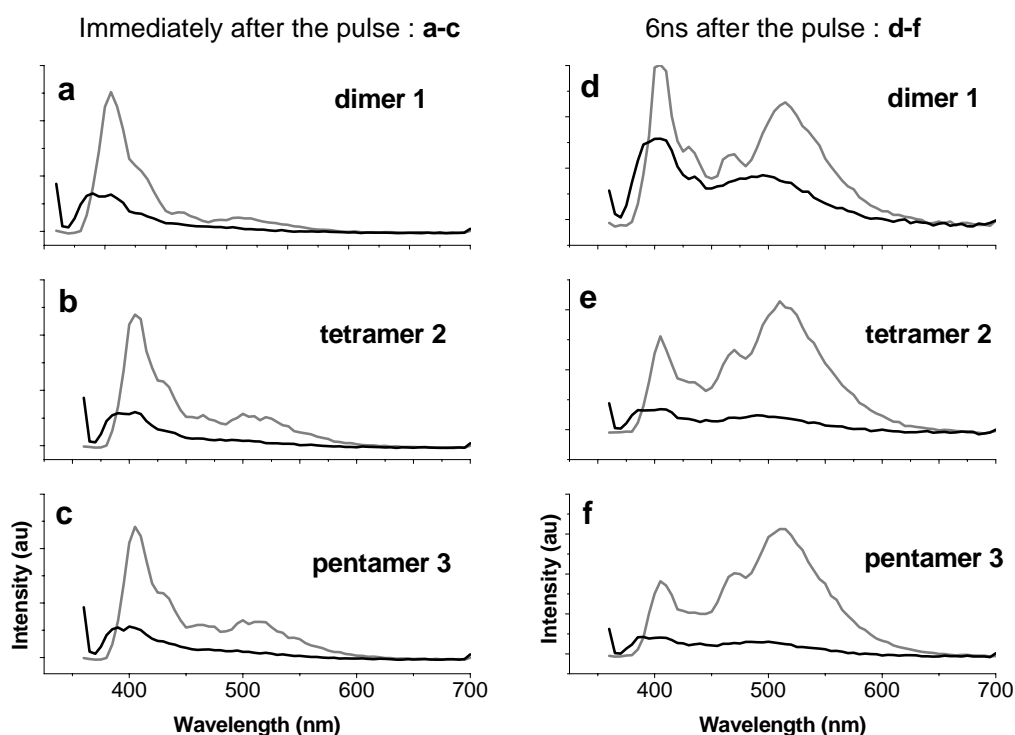


Figure 4.8. Time-resolved emission spectra of siloxanes in chloroform at low- black line (**1** – 10 μM , **2** – 5 μM and **3** – 4 μM) and high – gray line (**1** – 0.5 mM, **2** – 0.25 mM and **3** – 0.2 mM) concentrations, immediately (a-c) and 6 ns (d-f) after the pulse.

Picosecond time-correlated single photon counting measurements (ps-TCSPC) on **1 - 3** in chloroform show a multi-exponential fluorescence decay with lifetimes ranging from 13 ps to 18 ns. These data confirm the complex multi-exponential decay processes involved with the excited singlet state of the NDI chromophores, and are in line with the results described in Chapter 3.

4.2.3.4. Fluorescence quenching

The fluorescence quenching of two *p*-type polymers, MDMO-PPV and P3HT, by siloxanes **1-3**, was tested both in solution and in films. Figure 4.9 shows the fluorescence quenching in a 1 : 1 (wt %) mixture of siloxanes **1-3** with MDMO-PPV and P3HT, respectively in thin films.

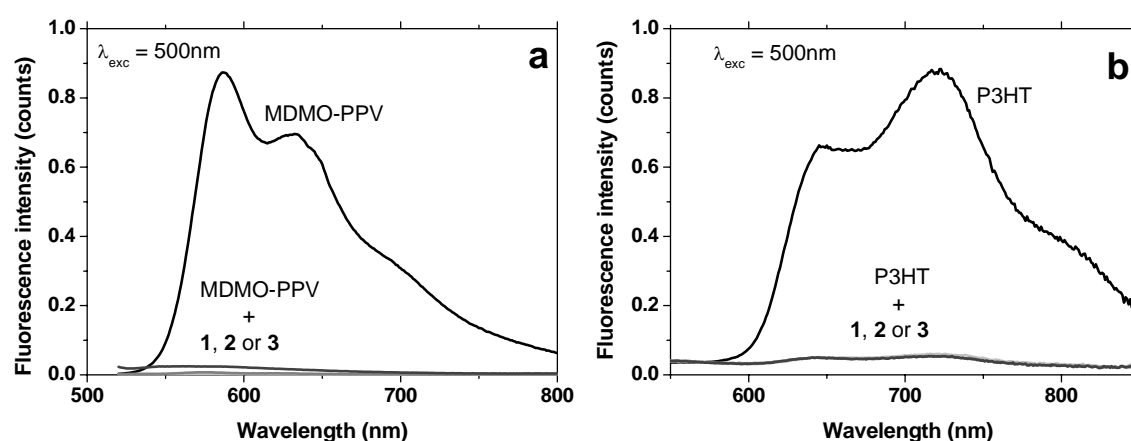


Figure 4.9. Fluorescence quenching of MDMO-PPV (a) and P3HT (b) by **1, 2, and 3** in 1:1 wt.% films spin coated from ODCB at 2000 rpm for 60 s.

All the three siloxanes were very efficient in quenching the singlet excited states of the *p*-type materials. This indicates a highly efficient electron transfer from the *p*-type material to the NDI moieties in **1 - 3**. In fact, MDMO-PPV fluorescence was quenched by **1** and **2** (>99.9 % in 1 : 1 films) even more efficiently than previously reported for the tetrahedral tetraphenylmethane derivative with NDI moieties,¹³ which make them highly promising materials for further (photo-) electrical studies. The quenching efficiencies of all three siloxanes were almost equal upon 1 : 1 (wt %) mixing with P3HT (Figure 4.9b).

These quenching experiments in thin films with two different well-known donor polymers point to the versatility of these siloxanes as an electron-accepting material.

4.2.4. Morphology

Polarized optical microscopy shows that neat films of **1** - **3**, drop-casted from CHCl_3 solutions, are amorphous. This is also the case for films in which these siloxanes are mixed with the polymeric *p*-type materials MDMO-PPV and P3HT. Blends of these materials were spin-coated from two different solvents, chloroform and ODCB, and further investigated with Transmission Electron Microscopy (TEM).

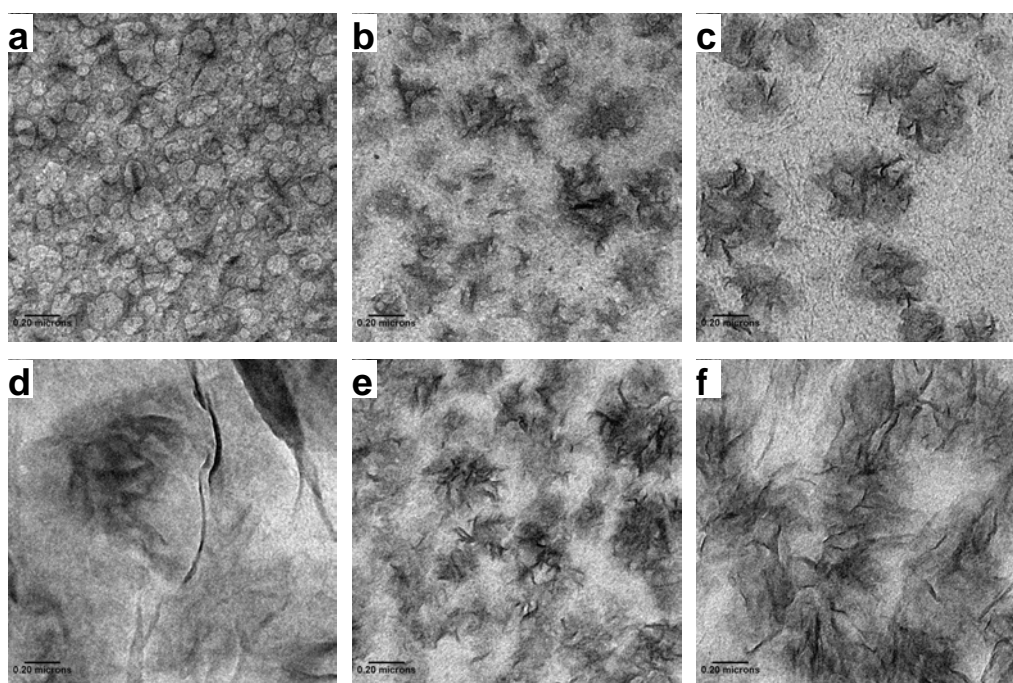


Figure 4.10. TEM images of mixtures P3HT and of **1-3** in 1:1 and 1:4 ratios spin-coated from ODCB. (a) P3HT/**1**-1:1; (b) P3HT/**2**-1:1; (c) P3HT/**3**-1:1; (d) P3HT/**1**-1:4; (e) P3HT/**2**-1:4; (f) P3HT/**3**-1:4. All images are with a scale bar of 0.2 μm .

TEM images of the films of P3HT and siloxanes **1-3** in 1:1 and 1:4 ratios, spin-coated from ODCB are presented in Figure 4.10, where the dark parts arise predominantly from the siloxanes and the gray parts are from P3HT. The films spin-coated from ODCB with a *p:n* ratio of 4:1 showed (images not given) mostly the features

of P3HT. But in case of 1:1 and 1:4 ratio blends, the features of siloxane are also clearly seen as small clusters of 100-200 nm.

The selected-area electron diffraction (SAED) of pure P3HT has a characteristic pattern as seen in Figure 4.11a. When siloxanes **1-3** are blended with P3HT at $p:n$ ratio 1:4, apart from P3HT pattern, new diffraction patterns are seen (Figure 4.11 b, c and d) in the dark regions of the films *i.e.* siloxane-rich regions. This indicates the presence of nano/micro-crystallinity in these predominantly siloxane-rich areas, most likely due to intermolecular interactions of NDI chromophores. This result is in line with time-resolved absorption and fluorescence spectroscopic measurements, which suggested intermolecular interactions at higher concentrations.

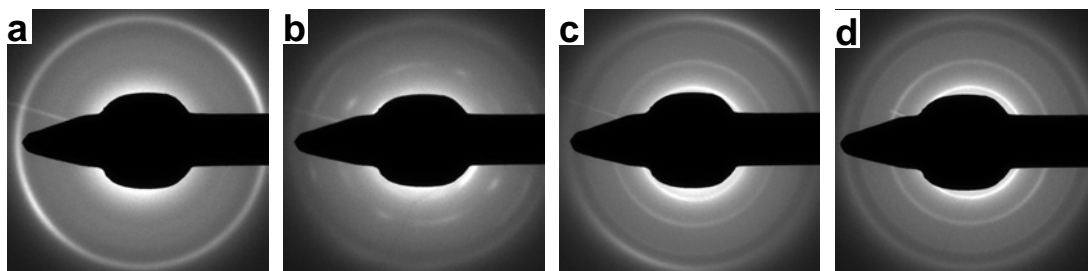


Figure 4.11. SAED of (a) pristine P3HT; (b) P3HT/**1**-1:4; (c) P3HT/**2**-1:4; (d) P3HT/**3**-1:4.

Blends of **1** and **2** with P3HT spin-coated from chloroform showed uniform films. Unlike the ODCB spin-coated films, these films did not show the features of siloxane, (Figure 4.12). Even at higher siloxane contents ($p/n = 1:4$ – Figure 4.12 d and e) the films were quite uniform. However, upon thermal annealing the 1:4 films change from featureless to having clearly visible crystalline regions in μm scale (Figure 4.12 c and f) in case of **2**. Such phase separation upon annealing is also reported in literature for P3HT and C_{60} derivative (PCBM) combinations.^{27, 28}

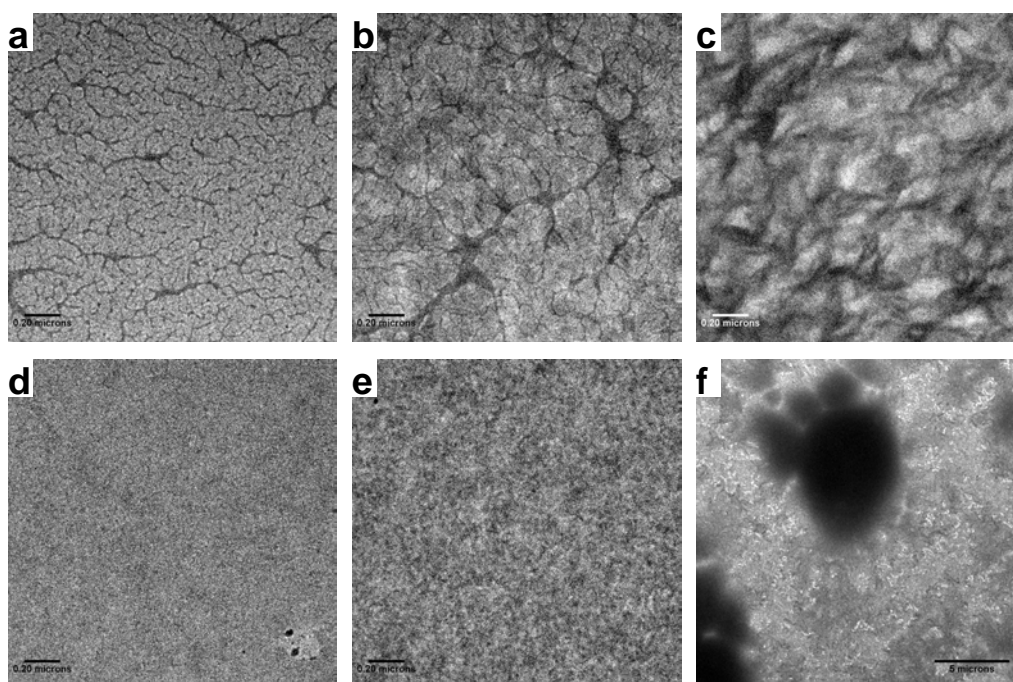


Figure 4.12. TEM images of mixtures of P3HT and **1** and **2** in 1:1 (a and b) and 1:4 (d and e) ratios spin-coated from CHCl₃ and the effect of annealing of 1:4 samples (c and f). (a) P3HT/**1**-1:1; (b) P3HT/**2**-1:1; (d) P3HT/**1**-1:4; (e) P3HT/**2**-1:4; (c) P3HT/**1**-1:4 annealed at 130 °C for 20 min; (f) P3HT/**2**-1:4 annealed at 130 °C for 20 min. Images a-e are with a scale bar of 0.2 μm . Image (f) has a scale bar of 5 μm .

From these morphological studies it could be concluded that the films spin-coated from chloroform yield more uniform films than that of ODCB spin-coated films. From the SAED of these films it is obvious that siloxanes form nano/micro-crystalline regions in the films, arising from intermolecular interactions of NDI, as suggested by the photophysical measurements.

4.2.5. Time-Resolved Microwave Conductivity

The P3HT and siloxanes **1-3** blends were studied using Flash Photolysis-Time Resolved Microwave Conductivity (FP-TRMC) techniques.^{29, 30} The absorption spectra of these blends, spin-coated on quartz substrates, are given in Figure 4.13. In the absorption

spectra of $p:n = 4:1$ blends, the absorption features of P3HT alone are seen. In 1:1 and 1:4 ratio blends, the features of NDI absorption is clearly seen between 300 and 400 nm.

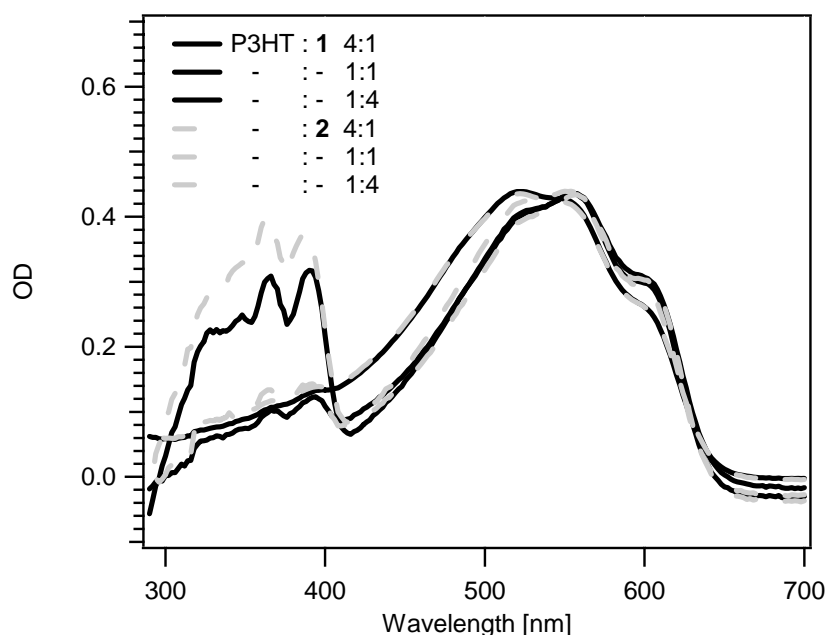


Figure 4.13. Absorption spectra of films of P3HT and siloxanes **1** and **2** spin-coated from ODCB solution on quartz substrates in p/n ratios of 4:1, 1:1 and 1:4. The different ratio curves could be identified with the contribution from NDI- between 300 and 400 nm.

The films were excited with a 500 nm laser pulse and on this excitation, radical ion pairs were created in the films due to electron transfer from the P3HT donor polymer to the NDI acceptor molecules. These ion pairs dissociate into long-lived electrons and holes. The product of the sum of mobilities of these electrons and holes ($\Sigma\mu$) and charge carrier formation quantum yield (Φ) could be deduced from the change in conductivity of the film, with the following equation:

$$\Phi \sum \mu = \frac{\Delta G_{\max}}{I_0 F_A \beta e}$$

where ΔG is the change in conductance, I_0 is the incident light intensity, F_A is the fraction of light actually absorbed by the sample at a given wavelength, e is the elementary charge, and β is a constant specific for the waveguide used. The charge carriers decay either by

charge recombination or by trapping. Therefore, the change in conductance, ΔG , is time dependent. A representative time-dependent charge-carrier decay for the film of P3HT and **2** at 1:4 ratio is given in Figure 4.14. This decay suggests that on photo excitation charge carriers are produced due to electron transfer and that the lifetimes of the thus formed charge-carriers are in the range of tens of microseconds.

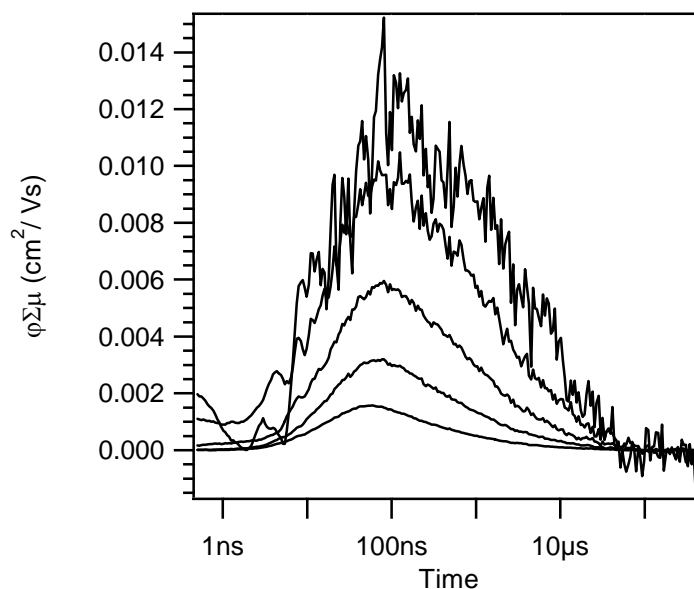


Figure 4.14. Charge carrier decay over time at different incident light intensities for the P3HT : **2** film (1:4) spin-coated from ODCB solution.

Similar time and intensity dependent decays were obtained for all films of blends of P3HT and siloxanes **1-3**, spin-coated either from ODCB or from CHCl_3 . The maxima of the TRMC signals, as a function of the incident laser intensity expressed as $\phi \Sigma \mu$, for the blends of P3HT and **1** and **2** are given in Figure 4.15. The conductivity of pure P3HT is also given for comparison.

Pristine P3HT shows a very low conductivity at all light intensities measured. An increase of almost two orders of magnitude in the TRMC signal was observed on blending the siloxanes with P3HT. This is in line with the highly efficient fluorescence quenching, by electron transfer from the *p*-type polymer to the *n*-type siloxanes, as presented in Figure 4.9. Compared to non-annealed films of P3HT:PCBM blends, the

magnitude of the conductivity of siloxane:P3HT blends are about one order of magnitude lower, while their charge carrier decay lifetimes are an order of magnitude higher.²⁷ This could be attributed to the nanoscopic crystallinity present in the freshly spin-coated films, which helps in the effective charge separation. Both compound **1** and **2** in films with P3HT show less conductivity at higher incident light intensity from the laser. This is mainly due to higher order recombination processes or due to bimolecular charge carrier recombination.

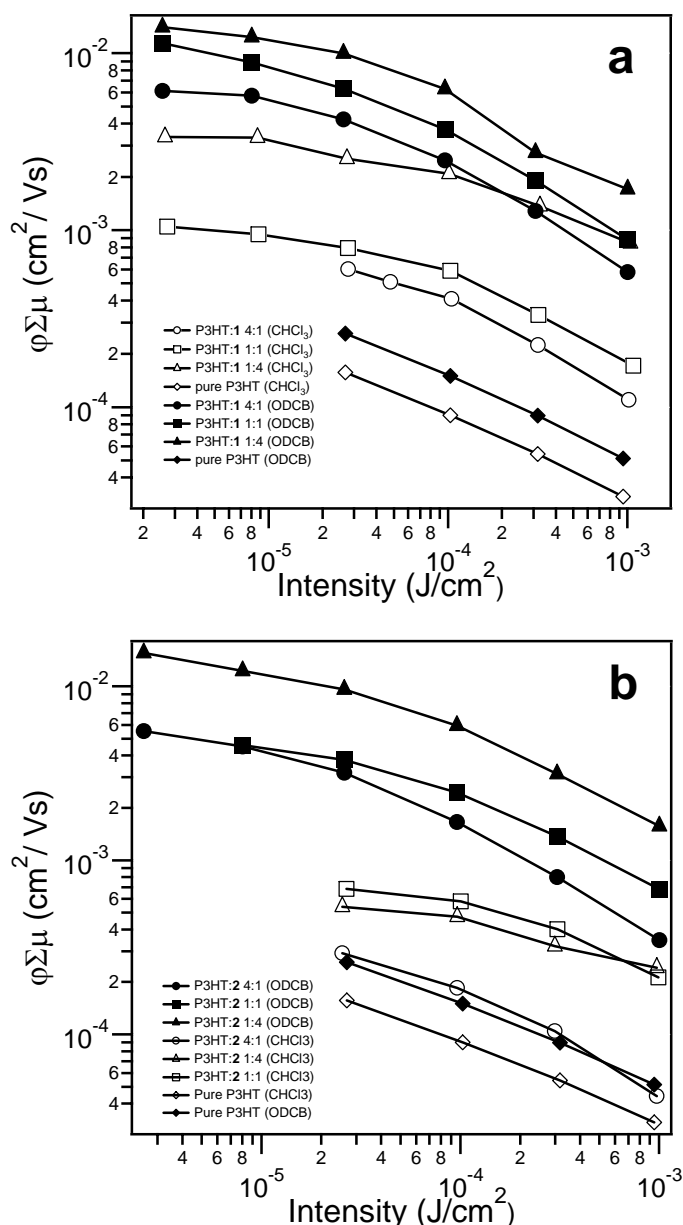


Figure 4.15. Intensity-dependent $\phi\Sigma\mu$ for films of P3HT and (a) **1** or (b) **2** at different ratios spin-coated from CHCl_3 or ODCB.

The morphology of freshly spin-coated films from CHCl_3 was uniform and featureless and the ODCB films had features in the order of 100 – 200 nm. This is linked to the higher conductivity of the ODCB films compared to CHCl_3 derived films: for exciton charge dissociations nano-scale phase separation, as present in these ODCB films, is essential. As the CHCl_3 films are very uniform, rapid charge recombination is most likely very efficient, leading to less long-lived charge dissociations, and a concomitantly observed reduced conductivity in comparison to the films spin-coated from ODCB.

4.3. Experimental

All the chemicals and spectroscopic grade solvents were obtained from Sigma Aldrich. The siloxanes were used after distillation. Spectroscopic grade solvents were freshly distilled over drying agents under nitrogen. ^1H and ^{13}C NMR were measured either with a Bruker DPX 300 or with a Bruker DPX 400 spectrometer. HRMS data were obtained with a Finnigan MAT 95 spectrometer. MALDI-TOF measurements were done with a Bruker-Ultraflex spectrometer with a α -cyano hydroxyl cinnamic acid matrix. UV-vis spectra were measured either with a Varian Cary 50 or with a Cary 100 spectrophotometer. Steady state fluorescence spectra were recorded using a Spex Fluorolog 3.22 spectrophotometer.

Time-resolved fluorescence measurements were carried out using mode-locked continuous wave lasers for excitation and time-correlated photon counting as detection technique. The pump laser was a CW diode-pumped, frequency-doubled Nd:YVO₄ laser (Coherent Inc., Verdi V10). The mode-locked laser was a Ti:sapphire laser (Coherent Inc., Mira 900-D in ps mode, FWHM 3 ps), tuned to 780 nm. The output of the Ti:sapphire laser passed through a pulse picker (APEGmbH, Pulse Select), to bring down the repetition rate of excitation pulses to 3.8×10^6 pulse per second. The output of the pulse picker was directed towards a frequency doubler (Inrad Inc., 5-050, Ultrafast Harmonic Generation System). The excitation pulses did have energies in the nJ region, an excitation wavelength of 390 nm and a pulse duration of less than 0.2 ps. Detection electronics were time-correlated single photon counting modules. With a small portion of the mode-locked light at 780 nm wavelength (left from the harmonics conversion) a fast photodiode (Becker & Hickl model PHD-400) was excited. The output pulses of this photodiode

were fed to one channel of a quad constant fraction discriminator (CFD, Tennelec Inc., Oak Ridge, TS, modified model TC 454), and then used as stop signal for a time-to-amplitude converter (TAC, Tennelec Inc., Oak Ridge, TS, model TC 864). A microchannel plate photomultiplier (Hamamatsu, Hamamatsu, Japan, model R3809U-50 at 3100 V, cooled down by a water bath to a few degrees centigrade) was used for the detection of the fluorescence photons. The single photon responses of this PMT were amplified by a wide-band amplifier (Becker & Hickl GmbH, Berlin, Germany, model ACA-2; 21 dB, 1.8 GHz), analyzed in another channel of the CFD and then used as a start signal for the TAC. The output pulses of the TAC were analyzed by an analogue-to-digital converter (ADC, Nuclear Data Inc., Schaumburg, IL, model 8715, 800 ns fixed dead-time), used in Coincidence and Sampled Voltage Analysis mode, gated by the Valid Conversion Output of the TAC. The output of the ADC was gathered in 4096 channels of a multichannel analyzer (MCA board from Nuclear Data Inc., Schaumburg, IL, model AccuspecB, in a personal computer). The channel time spacing was 5.0 ps.

Nanosecond laser flash photolysis studies and time-resolved fluorescence studies were carried out with an excitation wavelength of 355 nm from the 3 ω of a Nd:YAG laser (Brilliant FWHM = 4 ns, Quanta Inc.) and the signals were detected using LP920-spectrophotometer (Edinburgh Instruments Limited) fitted with 450 W Xe arc lamp as a probe and a red-sensitive photomultiplier (R928, Hamamatsu) and ICCD camera (DH720, Andor Technology) as detectors.

N-(10-Undecenyl)-phthalimide 5: 10.00 g (42.88 mmol) of 1-bromo-10-undecene and 10.33 g (55.77 mmol) of potassium phthalimide were taken in 25 ml of freshly distilled DMF. The resulting mixture was stirred at 90 °C for 24 h. The reaction mixture was cooled to room temperature and 75 ml of water was added. This mixture was extracted with ether (1 \times 75 ml, 2 \times 30 ml). The ether layer was washed with 25 ml of 0.2 N NaOH solution and with 25 ml of brine. The organic layer was dried with MgSO₄ and evaporated. The yellow crude product was recrystallized from distilled methanol to yield 9.70 g (32.39 mmol, 75.5%) of N-(10-undecylenyl)-phthalimide as white crystals.

¹H NMR (300 MHz, CDCl₃) δ 7.83 (m, 2H, Ar), 7.73 (m, 2H, Ar), 5.80 (m, 1H, -CH=CH₂), 4.96 (m, 2H, -CH=CH₂), 3.68 (t, 2H, -N-CH₂-), 2.02 (m, 2H, -CH₂-

CH=CH₂), 1.69 (t, 2H, N-CH₂-CH₂-), 1.32 (m, 12H, 6 × CH₂), in line with reported NMR data.¹⁹

1-Amino-10-undecene 6: To a solution of 9.67 g (32.29 mmol) of N-(10-undecenyl)-phthalimide in 100 ml ethanol, 2.41 g (48.2 mmol) of hydrazine monohydrate was added. This mixture was refluxed for 3 hrs and cooled to room temperature. The pH of the solution was adjusted to 1-2 using 1 M HCl. The white suspension that formed was filtered and washed with 1 M HCl. The filtrate was made alkaline to a pH of 10-11 by addition of NaOH pellets and concentrated to get a turbid aqueous layer. This was extracted with ether (4 × 50 ml). The combined organic layers were washed with 20 ml of 0.2 N NaOH solution and 20 ml of brine containing few ml of 0.2 N NaOH solution. The organic layer was dried over NaOH pellets for two hours and evaporated to yield 3.80 g (22.44 mmol, 69.5 %) of 1-amino-10-undecene as oily substance.

¹H NMR (300 MHz, CDCl₃) δ 5.82 (m, 1H, -CH=CH₂), 4.96 (m, 2H, -CH=CH₂), 2.67 (t, 2H, -N-CH₂-), 2.02 (q, 2H, -CH₂-CH=CH₂), 1.32 (m, 16H, 7 × CH₂ and -NH₂), in line with reported NMR data.¹⁹

N-(2-ethylhexyl)naphthalene monoimide monoanhydride 7:

Naphthalenedianhydride (20.02 g, 74.65 mmol) was taken in a three-necked flask with 200 ml of freshly distilled DMF. The slurry was heated to about 140 °C under N₂ atmosphere. To this mixture 2-ethylhexylamine (9.65 g, 74.64 mmol) was added drop-wise in about 10 minutes and the reaction mixture was refluxed overnight, under a N₂ atmosphere. The reaction mixture was cooled and the precipitated diimide were filtered off. DMF was evaporated under low pressure and the residue dissolved in dichloromethane to remove insoluble material. Dichloromethane evaporated and the crude material was purified on a silica gel column with dichloromethane as eluent to obtain 7.1 g (25 % yield) of the desired product as a pale yellow-orange solid.

¹H NMR (400 MHz, CDCl₃) δ 8.83 (s, 4H, Naphth-H), 4.11 (m, 2H, -N-CH₂-), 1.94 (m, 1H, -CH₂-CH-CH₂), 1.35 (m, 8H, 4 × CH₂), 0.95 (t, 3H, *J* = 7.4 Hz), 0.89 (t, 3H, *J* = 7.2 Hz) in line with reported NMR data.¹³

N-(2-ethylhexyl)-N'-(10-undecenyl)naphthalenediimide 4: To a solution of 1.05 g (2.77 mmol) of N-(2-ethylhexyl)naphthalene monoimide monoanhydride in 1,4-dioxane, 0.47 g (2.77 mmol) of 1-amino-10-undecene in 10 ml of dioxane was added drop wise at about 70 °C. This reaction mixture was refluxed overnight under nitrogen atmosphere. The reaction mixture was cooled to room temperature and the solvent evaporated. The crude product was loaded on a silica gel column and eluted with dichloromethane to get 1.15 g (2.17 mmol, 78%) of the product as a light yellow solid.

¹H NMR (300 MHz, CDCl₃) δ 8.74 (s, 4H, Naphth-H), 5.79 (m, 1H, -CH=CH₂), 5.94 (m, 2H, -CH=CH₂), 4.16 (m, 4H, -N-CH₂-), 2.04 (m, 2H, -CH₂-CH=CH₂), 2.02 (m, 1H, -CH₂-CH-CH₂-), 1.74 (m, 2H, N-CH₂-CH₂-), 1.36 (m, 20H, 10 × CH₂), 0.94 (m, 6H, 2 × CH₃); **¹³C NMR** δ 163.8, 163.42, 139.79, 131.58, 131.52, 127.32, 127.28, 127.20, 45.21, 41.56, 38.54, 34.38, 31.30, 30.03, 29.99, 29.88, 29.67, 29.50, 29.22, 28.67, 27.65, 24.64, 23.62, 14.65, 11.19; **HRMS** calculated for C₃₃H₄₂N₂O₄ 530.3138, found 530.3145.

1,1,3,3,5,5-Hexamethyl-1,5-bis(N-(2-ethylhexyl)-N'-(undecenyl)naphthalenediimide)trisiloxane 1: 1.25 g (2.36 mmol) of N-(2-ethylhexyl)-N'-(10-undecenyl) naphthalenediimide and 0.2 g (0.96 mmol) 1,1,3,3,5,5-hexamethyltrisiloxane were taken in 20 ml of dry toluene. The flask with the reaction mixture was purged with argon while it was warmed up to 70 °C. Then 5 µl of catalyst (platinum(0)-1,3-divinyl-1,1,3,3-tetramethyldisiloxane complex; 0.10 M solution in xylenes) was added using a syringe. This mixture was stirred for 2 h at 70 °C and then cooled to room temperature. Solvent was evaporated under reduced pressure and the crude product was purified using silica gel column with dichloromethane as eluent to get 0.65 g (0.51 mmol, 53.4 %) of the dimer.

¹H NMR (300 MHz, CDCl₃) δ 8.69 (s, 8H, Naphth-H), 4.11 (m, 8H, -N-CH₂-), 1.89 (m, 2H, -CH₂-CH-CH₂-), 1.69 (m, 4H, N-CH₂-CH₂-), 1.33 (m, 48H, 24 × CH₂), 0.89 (m, 12H, 4 × CH₃), 0.45 (t, 4H, -Si-CH₂-), 0.0 (s, 12H, 2 × -CH₂-Si(CH₃)₂-), -0.02 (s, 6H, -O-Si(CH₃)₂-O-); **¹³C NMR** δ 163.00, 162.60, 130.77, 126.47, 44.40, 40.78, 37.73, 33.27, 30.49, 29.44, 29.39, 29.35, 29.20, 29.14, 28.41, 27.89, 26.90, 23.83, 23.03, 22.81, 18.10, 13.84, 10.38, 0.98, 0.00; **MALDI-TOF** calculated for C₇₂H₁₀₄N₄O₁₀Si₃ 1268.706, found 1268.704.

2,4,6,8-Tetramethyl-2,4,6,8-tetra(N-(2-ethylhexyl)-N'-(undecenyl)

naphthalenediimide)cyclotetrasiloxane 2: 1.31 g (2.47 mmol) of N-(2-ethylhexyl)-N'-(10-undecenyl) naphthalenediimide and 0.135 g (0.56 mmol) 2,4,6,8-tetramethylcyclotetrasiloxane were dissolved in 20 ml of dry toluene. The flask with the reaction mixture was purged with argon while it was warmed up to 70 °C. Then 5 µl of catalyst (platinum(0)-1,3-divinyl-1,1,3,3-tetramethyl disiloxane complex; 0.10 M solution in xylenes) was added using a syringe. This mixture was stirred for 40 h at 70 °C and then cooled to room temperature. Solvent was evaporated under reduced pressure and the residue was recrystallized from dichloromethane. The recrystallized product was further purified using a silica gel column with chloroform as eluent to get 0.66 g (0.28 mmol, 50.0 %) of the tetramer.

¹H NMR (300 MHz, CDCl₃) δ 8.69-8.63 (6s, 16H, Naphth-H), 4.10 (m, 16H, -N-CH₂-), 1.89 (m, 4H, -CH₂-CH-CH₂-), 1.65 (m, 8H, N-CH₂-CH₂-), 1.32 (m, 96H, 48×CH₂), 0.85 (m, 24H, 8×CH₃), 0.4 (t, 8H, 4x (-Si-CH₂)), 0.0 (s, 12H, 4x (-O-Si(CH₃)-O-)); **¹³C NMR** δ 163.77, 162.33, 131.49, 127.24, 45.20, 41.58, 38.53, 33.82, 31.29, 30.25, 29.99, 29.65, 28.70, 27.74, 24.63, 23.63, 17.80, 14.66, 11.18, 0.00; **MALDI-TOF** calculated for C₁₃₆H₁₈₄N₈O₂₀Si₄ 2361.270, found 2361.307.

2,4,6,8,10-Pentamethyl-2,4,6,8,10-penta(N-(2-ethylhexyl)-N'-(undecenyl)

naphthalene diimide)cyclopentasiloxane 3: 1.56 g (2.94 mmol) of N-(2-ethylhexyl)-N'-(10-undecenyl)naphthalenediimide and 0.161 g (0.54 mmol) of 2,4,6,8,10-pentamethylcyclopentasiloxane were dissolved in 20 ml of dry toluene. The flask with the reaction mixture was purged with argon while it was warmed up to 70 °C. Then 10 µl of catalyst (platinum(0)-1,3-divinyl-1,1,3,3-tetramethyl disiloxane complex; 0.10 M solution in xylenes) was added using a syringe. This mixture stirred for 60 h at 70 °C and then cooled to room temperature. Solvent was evaporated under reduced pressure. The crude product was purified using a silica gel column with 2 % ethyl acetate in dichloromethane as eluent to get pure pentamer **3**.

¹H NMR (300 MHz, CDCl₃) δ 8.69-8.63 (7s, 20H, Naphth-H), 4.10 (m, 20H, -N-CH₂-), 1.95 (m, 5H, -CH₂-CH-CH₂-), 1.70 (m, 10H, N-CH₂-CH₂-), 1.32 (m, 120H, 60 × CH₂), 0.96 (m, 30H, 10 × CH₃), 0.5 (t, 10H, 5 × (-Si-CH₂)), 0.0 (s, 15H, 5x (-O-Si(CH₃)-O-)); **¹³C NMR** δ 163.21, 162.19, 131.38, 127.11, 45.10, 41.50, 38.45, 33.89, 30.04, 30.01, 29.98,

29.93, 29.14, 28.63, 27.68, 23.64, 23.56, 17.95, 14.60, 11.11, 0.00; **MALDI-TOF** calculated for $C_{170}H_{230}N_{10}O_{25}Si_5$ 2951.588, found 2951.966.

4.4. Conclusions

Three new siloxanes bearing electron-accepting NDI moieties were synthesized. The synthesized materials are amorphous in nature and consist of sets of stereoisomers. The size of NDI moieties prevents the inter-conversion of these isomers, via e.g. epimerization, which for the first time allows the use of cyclic siloxanes to obtain a stable and controllable morphology. Photophysical measurements show that intermolecular interactions of acceptor chromophores occur at higher concentrations. This opens up the possibility to create continuous pathways for charge transport in appropriate films. A major stimulus for such further studies is that highly efficient fluorescence quenching of the excited NDI moieties occurs with different *p*-type polymers, which points to the potential of these amorphous siloxanes as electron accepting materials in applications such as organic solar cells. Morphology studies of blends of P3HT donor polymer with these siloxanes with transmission electron microscopy reveal featureless uniform films when spin-coated from chloroform. In contrast, features in the order of 100-200 nm arising from phase separation of these siloxanes were observed, when the films were spin-coated from ODCB. Due to this nano-crystallinity, attributed to intermolecular interactions of aggregated NDI molecules through π - π stacking, time-resolved conductivity experiments reveal that the ODCB-derived films were better conducting than chloroform-derived films.

4.5. References

1. Katz, H. E.; Bao, Z. N.; Gilat, S. L. *Accounts Chem. Res.* **2001**, *34*, 359-369.
2. Hoppe, H.; Sariciftci, N. S. *J. Mater. Chem.* **2006**, *16*, 45-61.
3. Rittner, M.; Baeuerle, P.; Goetz, G.; Schweizer, H.; Calleja, F. J. B.; Pilkuhn, M. H. *Synth. Met.* **2006**, *156*, 21-26.
4. Singh, T. B.; Meghdadi, T.; Gunes, S.; Marjanovic, N.; Horowitz, G.; Lang, P.; Bauer, S.; Sariciftci, N. S. *Adv. Mater.* **2005**, *17*, 2315-2320.
5. Yang, H. C.; Shin, T. J.; Yang, L.; Cho, K.; Ryu, C. Y.; Bao, Z. N. *Adv. Funct. Mater.* **2005**, *15*, 671-676.

6. Bozano, L. D.; Carter, K. R.; Lee, V. Y.; Miller, R. D.; DiPietro, R.; Scott, J. C. *J. Appl. Phys.* **2003**, *94*, 3061-3068.
7. Fichet, G.; Corcoran, N.; Ho, P. K. H.; Arias, A. C.; MacKenzie, J. D.; Huck, W. T. S.; Friend, R. H. *Adv. Mater.* **2004**, *16*, 1908-1912.
8. Kim, Y.; Cook, S.; Tuladhar, S. M.; Choulis, S. A.; Nelson, J.; Durrant, J. R.; Bradley, D. D. C.; Giles, M.; McCulloch, I.; Ha, C. S.; Ree, M. *Nat. Mater.* **2006**, *5*, 197-203.
9. Ma, W. L.; Yang, C. Y.; Gong, X.; Lee, K.; Heeger, A. J. *Adv. Funct. Mater.* **2005**, *15*, 1617-1622.
10. Sivula, K.; Ball, Z. T.; Watanabe, N.; Frechet, J. M. J. *Adv. Mater.* **2006**, *18*, 206-210.
11. Sun, X. B.; Zhou, Y. H.; Wu, W. C.; Liu, Y. Q.; Tian, W. J.; Yu, G.; Qiu, W. F.; Chen, S. Y.; Zhu, D. B. *J. Phys. Chem. B* **2006**, *110*, 7702-7707.
12. Zhang, F. L.; Jespersen, K. G.; Bjorstrom, C.; Svensson, M.; Andersson, M. R.; Sundstrom, V.; Magnusson, K.; Moons, E.; Yartsev, A.; Inganas, O. *Adv. Funct. Mater.* **2006**, *16*, 667-674.
13. Ganesan, P.; Yang, X. N.; Loos, J.; Savenije, T. J.; Abellon, R. D.; Zuilhof, H.; Sudhölter, E. J. R. *J. Am. Chem. Soc.* **2005**, *127*, 14530-14531.
14. Zhang, Z. C.; Lyons, L. J.; Jin, J. J.; Amine, K.; West, R. *Chem. Mater.* **2005**, *17*, 5646-5650.
15. Lacey, D.; Mann, T. E. *Liq. Cryst.* **2003**, *30*, 1159-1170.
16. Liu, L. M.; Zhang, B. Y.; He, X. Z.; Cheng, C. S. *Liq. Cryst.* **2004**, *31*, 781-786.
17. Decken, A.; Passmore, J.; Wang, X. P. *Angew. Chem.-Int. Edit.* **2006**, *45*, 2773-2777.
18. Ramirez-Oliva, E.; Cuadrado, I.; Casado, C. M.; Losada, J.; Alonso, B. *J. Organomet. Chem.* **2006**, *691*, 1131-1137.
19. Sieval, A. B.; Linke, R.; Heij, G.; Meijer, G.; Zuilhof, H.; Sudhölter, E. J. R. *Langmuir* **2001**, *17*, 7554-7559.
20. Harrod, J. F.; Pelletier, E. *Organometallics* **1984**, *3*, 1064-1069.
21. Faglioni, F.; Blanco, M.; Goddard, W. A.; Saunders, D. *J. Phys. Chem. B* **2002**, *106*, 1714-1721.
22. Moore, C. B.; Dewhurst, H. A. *J. Org. Chem.* **1962**, *27*, 693-694.
23. Pelletier, E.; Harrod, J. F. *Organometallics* **1984**, *3*, 1070-1075.

24. Unno, M.; Kawaguchi, Y.; Kishimoto, Y.; Matsumoto, H. *J. Am. Chem. Soc.* **2005**, *127*, 2256-2263.
25. Barros, T. C.; Brochsztain, S.; Toscano, V. G.; Berci, P.; Politi, M. J. *J. Photochem. Photobiol. A-Chem.* **1997**, *111*, 97-104.
26. Chatterjee, S.; Basu, S.; Ghosh, N.; Chakrabarty, M. *Spectrosc. Acta Pt. A-Molec. Biomolec. Spectr.* **2005**, *61*, 1887-1891.
27. Savenije, T. J.; Kroeze, J. E.; Yang, X. N.; Loos, J. *Adv. Funct. Mater.* **2005**, *15*, 1260-1266.
28. Swinnen, A.; Haeldermans, I.; vande Ven, M.; D'Haen, J.; Vanhoyland, G.; Aresu, S.; D'Olieslaeger, M.; Manca, J. *Adv. Funct. Mater.* **2006**, *16*, 760-765.
29. Kroeze, J. E.; Savenije, T. J.; Warman, J. M. *C. R. Chim.* **2006**, *9*, 667-675.
30. Kroeze, J. E.; Savenije, T. J.; Vermeulen, M. J. W.; Warman, J. M. *J. Phys. Chem. B* **2003**, *107*, 7696-7705.

Chapter 5

Naphthalene Diimide Side-Chain Polymers: Synthesis, Microwave Conductivity and Morphology Studies

Abstract

Four naphthalenediimide (NDI) side-chain polymers were synthesized by grafting NDI onto poly(R-*alt*-maleic anhydride) backbone polymers with various R groups and molecular weights [R= styrene, 1-octene and 1-octadecene], with the aim to tune the morphology of thin films of these materials. Polymers with a degree of substitution up to 60 % were obtained and these polymers showed a high solubility in solvents like chloroform, dichloromethane, etc. Their absorption and fluorescence studies were carried out both in solution and in thin films, with specific attention to the fluorescence quenching of P3HT in thin films. The results show that in all four polymers the NDI chromophores form π -stacked dimers in solution exhibiting excimer fluorescence. The morphology of the blends of the grafted polymers with P3HT was studied at various weight ratios, and showed phase separation in domains of μm dimensions. These blends were also studied using time-resolved microwave-conductivity for their photo-induced charge carrier generation efficiency. They showed appreciable generation of charge carriers, although significantly lower than observed in blends of P3HT with PCBM or oligomeric *n*-type siloxanes.

5.1 Introduction

Thin film morphology plays a key role in the performance of organic electronics such as all-organic photovoltaic cells.¹ The morphology is determined by the phase separation of the chosen electron donor and electron acceptor molecules. A wide range of mixtures of donor and acceptor materials have been employed as the active layer in organic electronics.²⁻⁵ Most commonly, blends of a donor polymer in combination with fullerene-based molecular acceptors have been used in organic photovoltaic applications.⁶⁻⁹ In such thin films, crystallization of the fullerene hampers a further increase of the device efficiency. Apart from fullerene-based acceptors, other types of electron-accepting materials, both oligomers¹⁰ and polymers have also been investigated for use in organic electronics.¹¹⁻¹³

Systems of a donor polymer with covalently linked acceptor moieties have also been investigated to optimize mixing of the two components (double-cable approach).¹⁴⁻¹⁶ In such an approach, a crucial feature is the optimization of the distances between the donor and acceptor parts, in order to minimize the recombination of photo-generated charges. To avoid such optimization steps, the acceptor part can be attached to an inert polymer backbone, to form an interpenetrating polymer network with the donor polymer. Recently, fullerene side-chain polymers have been described, in which the fullerenes were attached to an optically inert backbone and polymerized to give polymers with a high fullerene content and uniform film morphology.¹⁷⁻¹⁹ In Figure 5.1 three different modes of mixing electron donor and electron acceptor materials are represented.

In side-chain polymers, the mechanical and rheological properties are largely determined by the backbone of the polymers, while the optical and electrical properties are determined by the side-chains. Poly(siloxanes),^{20,21} poly(acrylates)²²⁻²⁴ and poly(alkene/styrene co/alternating maleic anhydride)²⁵⁻³⁰ polymers have been used for various purposes. In maleic anhydride-based polymers, usually the anhydride rings are opened for grafting the functional groups.^{27, 30} As a consequence, in the resulting polymers per grafted side chain, a carboxylic functional group is formed that is not used in further functionalizations. For applications in organic electronics, such a high concentration of proton donors is not desirable due to possible reactions with the radical anions of the electron acceptors.

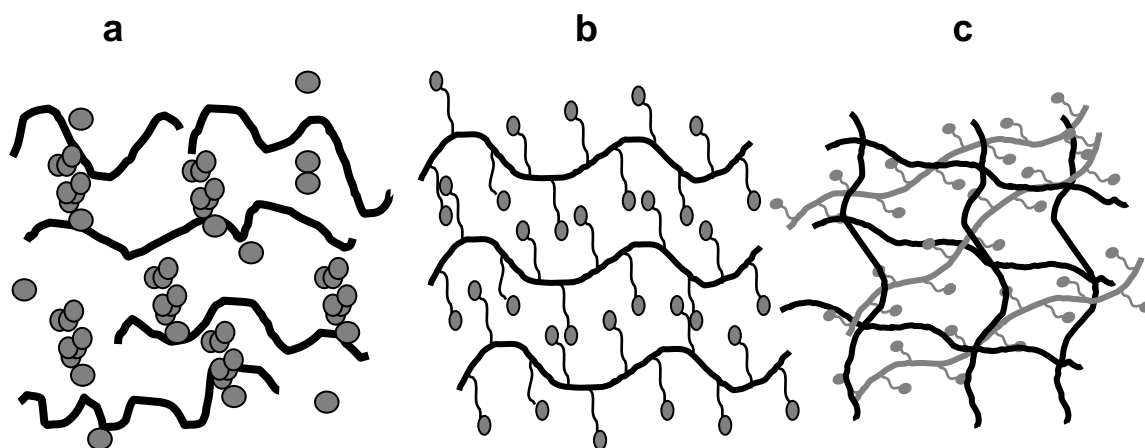
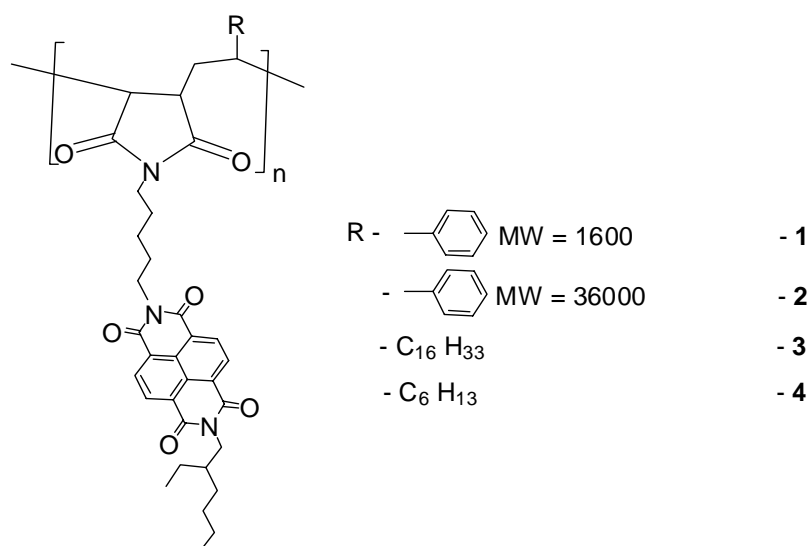


Figure 5.1. Schematic representation of three different bulk heterojunctions (a) *p*-type polymer mixed with molecular acceptors; (b) double-cable approach; (c) interpenetrating network of donor and acceptor polymers. Black lines represent the donor polymer and the gray parts represent the acceptor units.

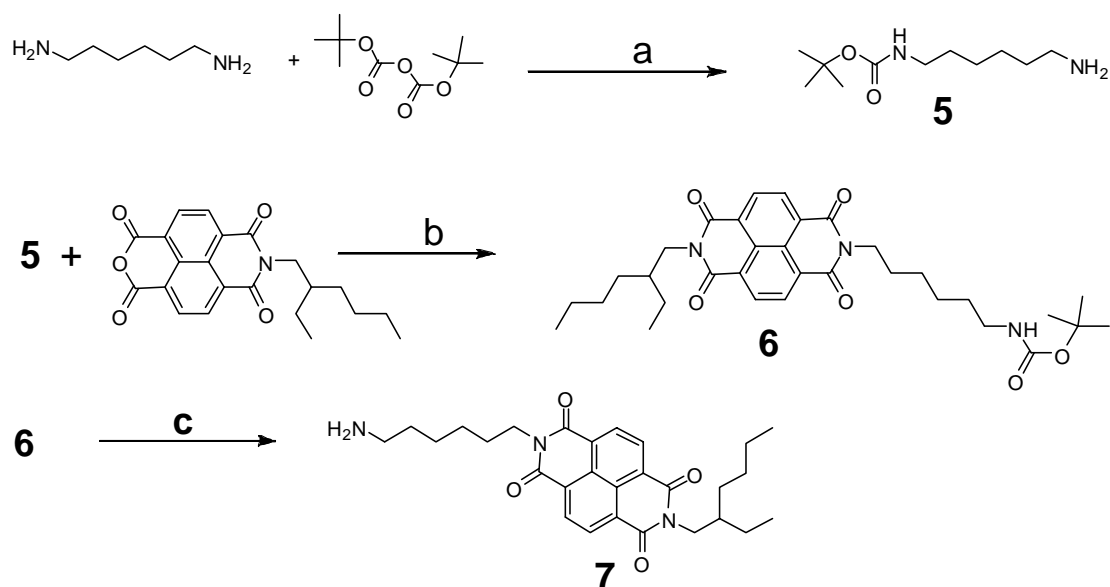
This chapter describes the effect of the structural rigidity of poly(styrene/1-alkene-*alt*-maleic anhydrides) on the morphology and charge carrier generation within bulk-heterojunctions. First, the synthesis of four poly(styrene/alkenes-*alt*-maleic anhydrides) polymers with naphthalenediimide (NDI) pendant groups **1-4** (Scheme 5.1) is reported. During the grafting process the anhydride rings are opened by a nucleophilic attack of an amino-terminated NDI and subsequently closed to form imides. In this way, the persistence of undesired carboxylic acid groups is prevented. Subsequently, the fluorescence quenching, charge carrier generation and morphology studies are discussed with an eye on possibilities and limitations of these materials in the field of organic photovoltaics.



Scheme 5.1. Poly(styrene/alkenes-*alt*-maleic anhydrides) studied in this chapter.

5.2. Results and Discussion

5.2.1. Synthesis

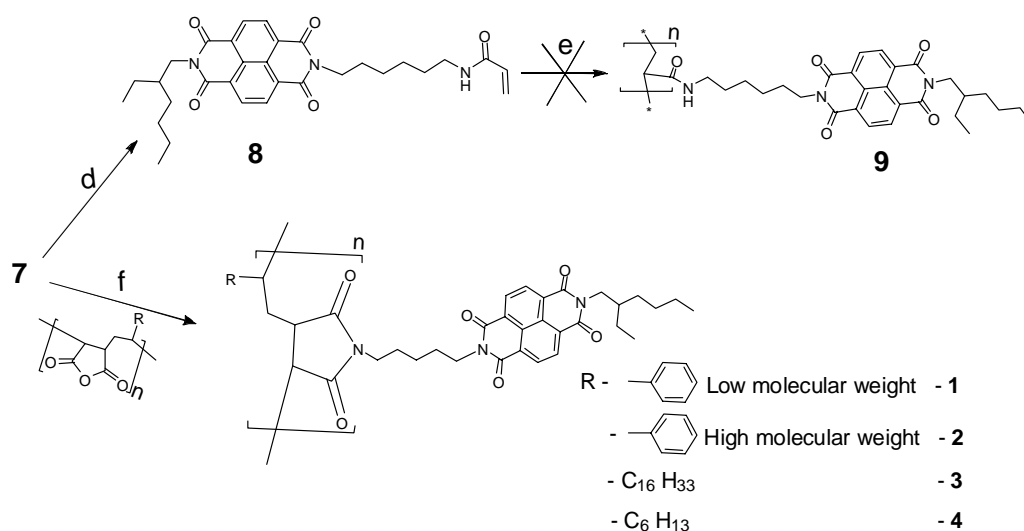


Scheme 5.2. Synthesis of amino-terminated NDI **7**. (a) 1,4-dioxane, 72 h, RT, under argon; (b) DCE, 15 h, reflux, under nitrogen; (c) DCM, excess of TFA, 15 h.

The synthesis of amino-terminated NDI **7** was achieved through the routes shown in Scheme 5.2. The monoprotected diamine **5** was synthesized following a literature procedure starting from 1,6-diaminohexane and di-*tert*-butyl dicarbonate, in a yield of ~60 %.³¹ The amino-terminated NDI **7** was obtained by the reaction between **5** and N-(2-ethylhexyl)-naphthalene monoimide monoanhydride and subsequent removal of the amine-protecting group in **6**. Both reactions proceeded in better than 90 % yield.

Next, compound **7** was functionalized with an acrylic group, by reaction with acryloyl chloride in the presence of triethylamine as a base to yield monomer **8**. Polymerization of **8** using AIBN as the initiator was tried (Scheme 5.3).³² This polymerization was, however, unsuccessful even with higher initiator concentrations, at higher temperature or with a change in solvent. Attempts to copolymerize **8** with methylmethacrylate were also unsuccessful. The probable reason for the failure of these polymerizations is the strong electron-accepting nature of NDIs, which might quench the initiation reaction. In literature, a strong inhibition of AIBN-initiated polymerizations has been described in the presence of fullerenes.³³

As an alternative, grafting the NDI moieties onto maleic anhydride-based polymers was investigated. Four such polymers, **1-4**, of different molecular weight and with different degree of substitution could be prepared (Scheme 5.3).



Scheme 5.3. Synthesis of NDI side-chain polymers. (d) acryloyl chloride, triethylamine, 2 h, -10 °C; (e) AIBN, ~60 °C, 10 h, under argon; (f) DMSO, 40 h, 170 °C, under nitrogen.

In the grafting process a high polar high-boiling solvent such as DMSO has to be employed. The polarity of the solvent helps to increase the solubility of the amine-terminated NDI; the high boiling point enables a high reaction temperature that is required for efficient ring closure to form the final imide. The polymers were isolated after repeated precipitation from chloroform-methanol solutions. The polymers are very well soluble in solvents such as chloroform, dichloromethane, *o*-dichlorobenzene, *etc.*

Broad peaks in the ^1H -NMR spectra of the parent polymers were observed, as a consequence of the backbone rigidity and line broadening due to slower rotation of the polymers (Figure 5.2). Broad peaks for the NDI units and alkyl substituents were also observed in the grafted polymers **1-4**. From the integration of the peaks, the degrees of substitution were calculated and are listed in Table 5.1. It can be seen that the degree of substitution slightly decreases with an increase of the molecular weight of the polymers. Coiling of the higher molecular weight polymers with concomitant increased steric hindrance for the nucleophilic attack might contribute to this phenomenon.

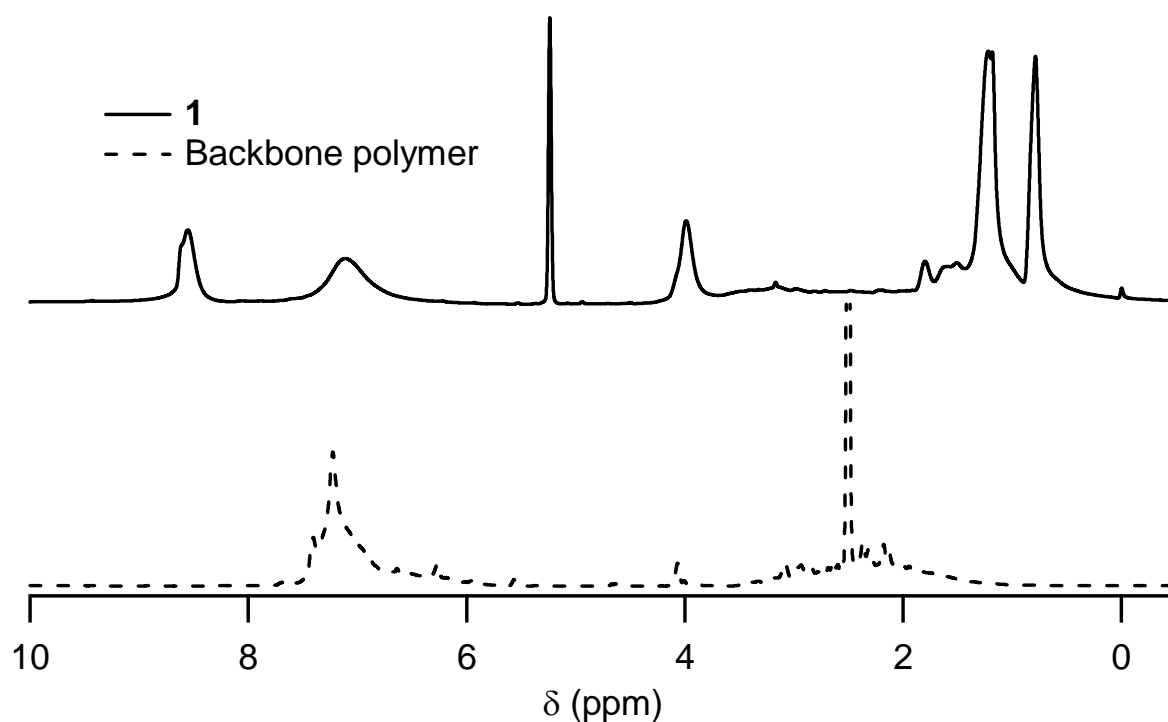
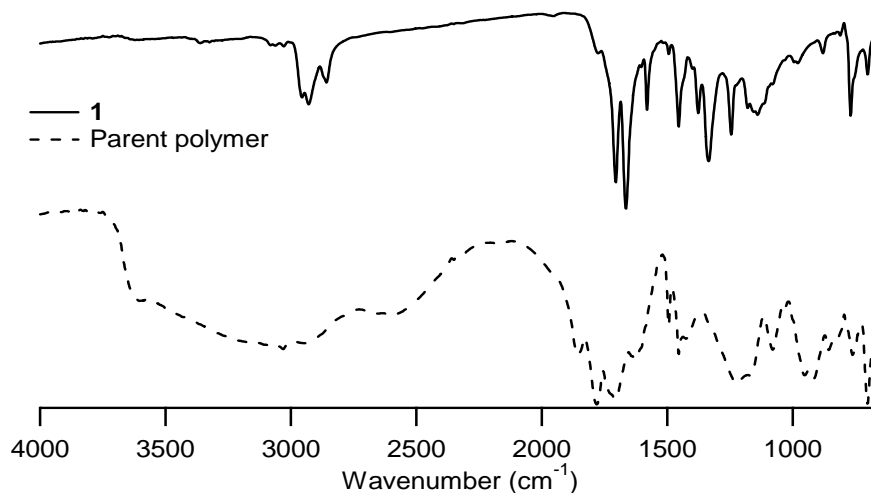


Figure 5.2. ^1H -NMR spectra of backbone polymer (in d_6 -DMSO) and the grafted polymer **1** (in d_2 -DCM).

Table 5.1. Degree of substitution calculated from ^1H NMR spectra.

Polymer	Average molecular weight of parent polymer	Approximate number of repeating units	Degree of substitution
1	~1,600	~8	60 %
2	~36,000	~175	40 %
3	~40,000	~110	52 %
4	~15,000	~70	57 %

**Figure 5.3.** Infrared spectra of backbone polymer and the grafted polymer **1**.

^1H -NMR spectra of **1-4** (Figure 5.2) gave no resonances above 9 ppm, indicating that there are no free carboxylic groups present and that only ring-closed imides are formed. Confirmation of this comes from the infrared spectra of **1-4** in comparison with the spectra of their parent polymers (Figure 5.3). The parent polymer of **1** showed a broad absorption peak between 3000 and 3800 cm^{-1} from the carboxylic group; this arises from some ring opening of the anhydride functionalities. In case of the grafted polymer **1**, the

absence of this peak and the appearance of new peaks for imide stretching between 1450 and 1700 cm^{-1} strongly confirm the ring closure. Some absorptions attributed to the anhydride stretching mode (1780-1855 cm^{-1}) indicate that grafting is not complete.

5.2.2. Absorption and emission spectra

UV-Vis absorption spectra of polymers **1-4**, show the characteristic $\pi-\pi^*$ absorption of the NDI chromophores (Figure 5.4a).

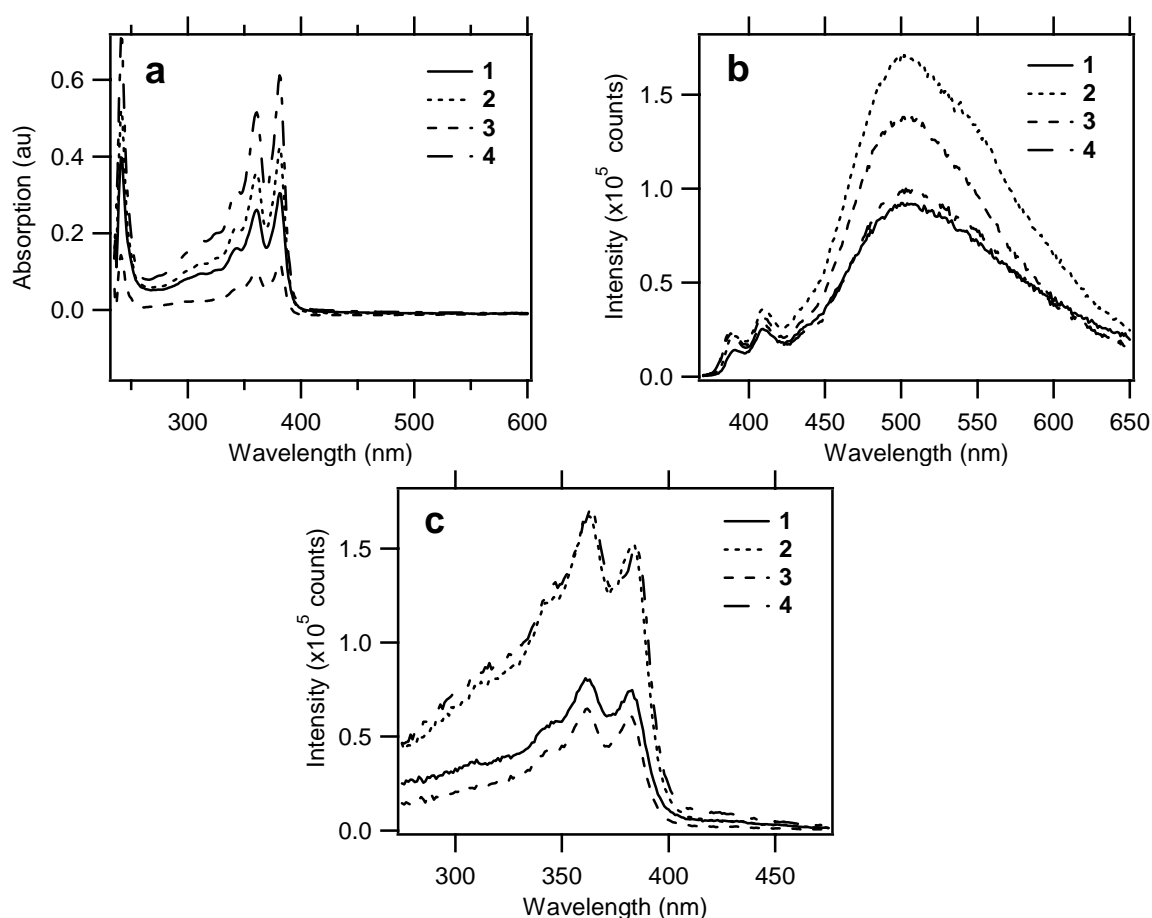


Figure 5.4. (a) Absorption; (b) fluorescence ($\lambda_{\text{exc}} = 350$ nm); (c) excitation spectra ($\lambda_{\text{fluor}} = 500$ nm) of polymers **1-4** in chloroform.

Fluorescence spectra of all four polymers in chloroform solution, showed the singlet (380 – 420 nm) as well as excimer (450 – 600 nm) fluorescence (Figure 5.4b). Such an excimer/excimer peak was also observed in the siloxane-based compounds (Chapter

4) with similar maxima at 503 nm.³⁴ As reported in Chapter 3, the singlet lifetime of NDI is ~ 10 ps and therefore, the peak at 503 nm should arise from the ground-state dimer. Although these ground-state dimers do not show any characteristic absorption in the UV-Vis spectra, their presence was confirmed by the excitation spectra (Figure 5.4c). In the excitation spectra, the peak ratios between the peaks at 361 nm and 381 nm (Figure 5.4a and c) are different from that of steady-state absorption spectra. Such a change in peak ratio is also known in perylene diimides (PDI), which is attributed to the π -dimers or stacking.^{35, 36} Since NDI has a higher affinity for stacking than PDI,³⁷ it is highly likely that there is a ground state dimerization/aggregation in these polymers, which is indeed revealed by the excitation spectra.

5.2.3. Fluorescence quenching

Polymers **1**, **2** and **4** were blended with the *p*-type polymer P3HT to test their fluorescence quenching efficiency. The fluorescence spectra of films of 1:1 weight ratio blends spin-coated from *o*-dichlorobenzene (ODCB) solution are given in Figure 5.5, together with the fluorescence of the same amount of pure P3HT.

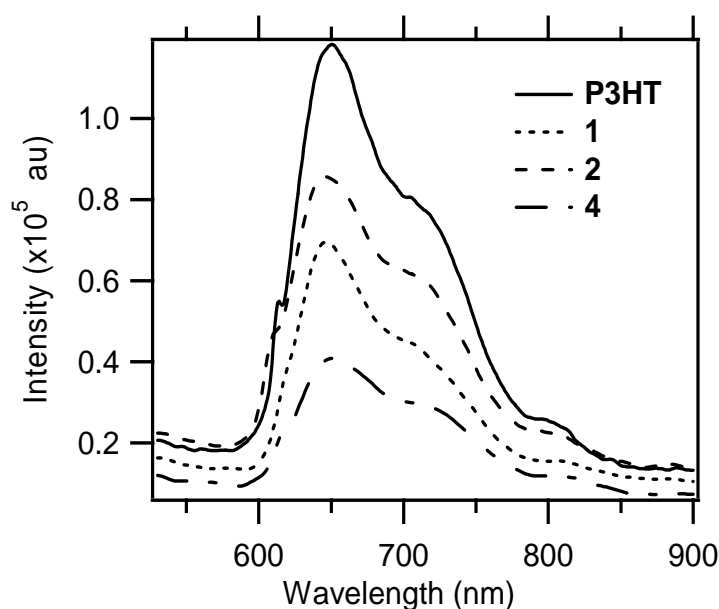


Figure 5.5. Fluorescence quenching ($\lambda_{\text{exc}} = 500$ nm) of P3HT by **1**, **2** and **4**, in 1:1 wt.% films spin coated from ODCB. Normalized for the OD at 500 nm.

The P3HT fluorescence was quenched to about 35-65 % by the acceptor polymers **1**, **2** and **4**. This quenching is significantly less efficient than observed in the cases of the tetrahedral NDI derivative tetra-4-[N-(2-ethylhexyl)naphthalene-1,4,5,8-tetracarboxylic diimide-N'-yl] phenyl methane (Chapter 2) and the oligomeric siloxane-based compounds (Chapter 4), for which near complete quenching of fluorescence was observed. The possible reason for this observation could be the following. Compared to the donor polymer P3HT, the grafted acceptor polymers **1-4** are non-polar and hydrophobic. While the P3HT tend to crystallize to form fibers, the acceptor polymers are amorphous in nature. Due to these physical differences, the miscibility between these polymer systems might be too poor, and therefore donor-only or acceptor-only domain formation is likely. In that case, fluorescence quenching would also be lower. This was investigated further and described below.

5.2.4. Morphology

TEM images $p/n = 1:4$ wt % films, spin-coated from ODCB solution are given in Figure 5.6. These images show large domains of the acceptor (dark regions) polymer in the micrometer dimension range. As already expected, due their structural rigidity, the maleic anhydride-based polymers induce phase separation. In addition, the polarity difference between the P3HT and polymers **1-4** results in demixing of the these two polymers, resulting in phase separation.

The selective-area electron diffraction (SAED) pattern of these films showed the characteristic diffraction of P3HT alone, but no additional diffractions arising from the acceptor part are observed. The absence of such a diffraction pattern means that in the acceptor polymer the NDI chromophores do not stack in the film. This is most likely due to low degree of substitution, where the NDI-NDI distances would be larger and hence the stacking becomes less probable. This large inter-NDI distance is also likely to disturb the continuous pathway for charge transport. This is in contrast to the observation made with the siloxanes as described in Chapter 4. Clearly, in the solid state of **1-4**, no stacking is observed.

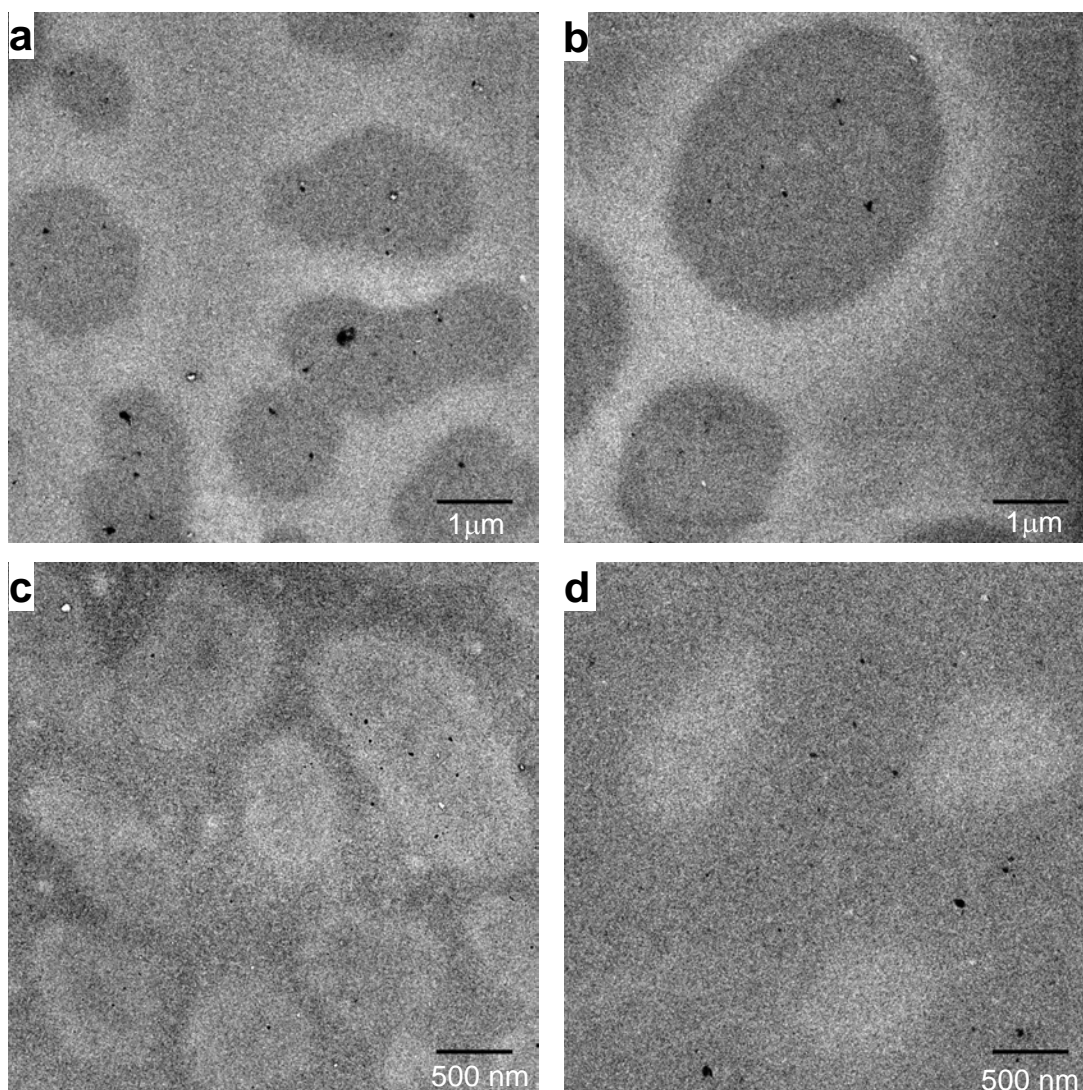


Figure 5.6. TEM images of films of blends of P3HT and polymers **1-4**, spin-coated from ODCB solution. Blends of P3HT ($p/n=1:4$) with (a) **1**; (b) **2**; (c) **3**; (d) **4**. The lighter regions belong to the P3HT and the dark regions belong to **1-4**.

From the TEM images it is obvious that the substitution on the maleic-anhydride polymer backbone has a significant effect on their mixing with P3HT. Polymer **1** and **2** have a phenyl substitution in their backbone and they mix poorly (forms $\sim 5\ \mu\text{m}$ domains) with the P3HT donor polymer. Whereas the polymers **3** and **4** have an alkyl substitution in their backbone and they relatively mix better (forms $\sim 1\ \mu\text{m}$ domains) than **1** and **2** with P3HT. Among **1** and **2**, polymer **2** forms larger domains, likely because of their higher

molecular weight. Among **3** and **4**, polymer **4** seem to mix well with the P3HT polymer most likely due its less hydrophobic nature since it has shorter alkyl chain (C_6) compared to **3**, which has a C_{16} chain. In conclusion, it seems possible that by changing the side-chains in the parent backbone polymer, it is possible to tune the morphology to a desired degree of phase separation.

5.2.5. TRMC conductivity

Photo-induced TRMC measurements were performed on films of blends of P3HT and polymers **1-4**, spin-coated from ODCB solution (Figure 5.7). These measurements revealed a relatively low photo-induced charge carrier generation, which is about an order of magnitude lower compared to the P3HT:siloxane blends and two orders of magnitude less compared to the P3HT:PCBM blends. This is in line with the observed less efficient fluorescence quenching (Figure 5.5).

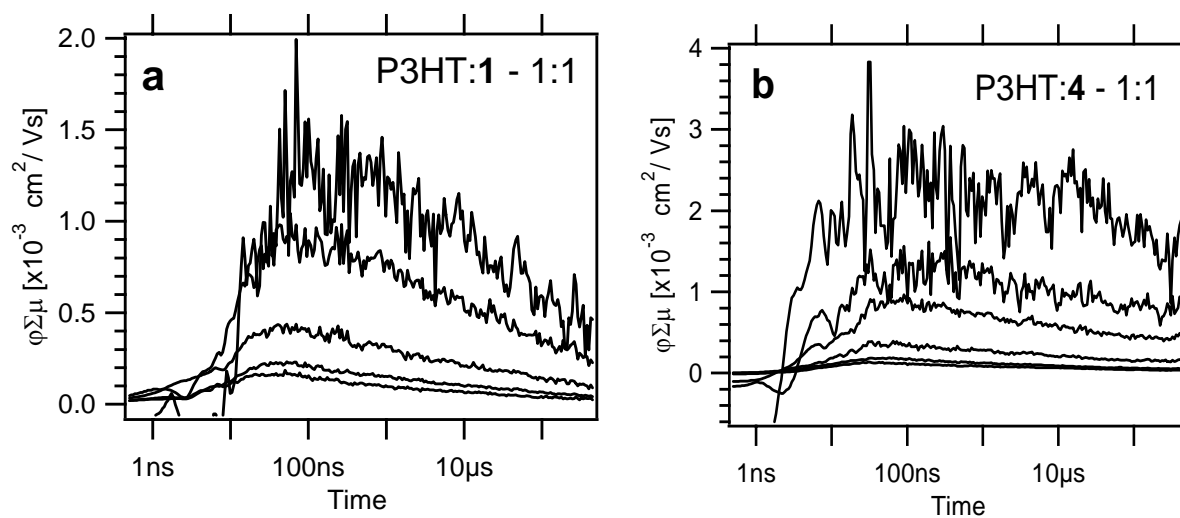


Figure 5.7. Charge carrier decay over time at different incident light intensities for (a) P3HT : **1** film (1:1); (b) P3HT : **1** film (1:1), spin-coated from ODCB solution.

The generated charges also decay much faster than in the case of P3HT : siloxane blends, in which lifetimes were measured for a significant fraction of the charge carriers up to 100 μs (Chapter 4). As discussed in the previous sections, this is likely due to larger

phase separation between donor or acceptor only domains. On increasing the acceptor polymer fraction from 20 wt % to 80 wt % the film formation became increasingly difficult during spin-coating process. This might be due to hydrophobic nature of the acceptor polymer. Due to the same reason it might also be possible that the *n*-type polymer demixes efficiently with P3HT. Such a demixing was highest for polymer **3**, as observed by difficulty in spin-coating and in TEM image (Figure 5.6.c), which is expected to be most hydrophobic due to long alkyl chains (C₁₆) present in the backbone.

5.3. Experimental

5.3.1 General

The parent backbone polymers were purchased from Acros or from Polysciences. All the other chemicals and spectroscopic grade solvents were purchased from Sigma Aldrich. The parent backbone polymers were dried at 100 °C in vacuum oven at 10 mbar for 48 h, before use. ¹H and ¹³C NMR were measured either with a Bruker DPX 300 or with a Bruker DPX 400 spectrometer. HRMS data were obtained with a Finnigan MAT 95 spectrometer. UV-vis spectra were measured either with a Varian Cary 50 or with a Cary 100 spectrophotometer. Steady state fluorescence spectra were recorded using a FLS 920 Spectrophotometer (Edinburgh Instruments, UK) fitted with a red-sensitive PMT (R928, Hamamatsu Photonics) or with a Spex Fluorolog 3.22 spectrophotometer. Sample preparation for TEM investigations was done by spin-coating appropriate solutions on top of PEDOT:PSS / glass substrates. The resulting films were floated onto the surface of demineralized water (with PEDOT:PSS dissolving in water) and picked up with a 400-mesh copper TEM grids. TEM measurements were performed on a TECNAI G2 20 transmission electron microscope (FEI Co., The Netherlands) operated at 200 kV.

5.3.2 Synthesis

***tert*-Butyl *N*-(6-aminohexyl)carbamate 5:** Di-*tert*-butyl dicarbonate [(Boc)₂O] (7.09 g, 32.5 mmol) was dissolved in 80 ml of freshly distilled dioxane and added dropwise over 5-6 h to a stirred solution of 1,6-diaminohexane (28.3 g, 244 mmol) in 250 ml of dioxane under argon atmosphere. The mixture was stirred at room temperature for

3 days. The solution was filtered and the solid residue [*N,N*-bis(*tert*-butoxycarbonyl) diaminohexane] was washed with diethyl ether (3 × 20 ml). The filtrate was concentrated by evaporation, and then 250 ml of water was added to precipitate the residual *N,N'*-bis(*tert*-butoxycarbonyl)-diaminohexane. The precipitate was filtered and washed with water (3 × 20 mL). The filtrate was extracted with CH₂Cl₂ (4×50 ml). The CH₂Cl₂ solution was washed with water, dried over Na₂SO₄ and the solvent evaporated to give 4.3 g (61 %) of pure **5**.

¹H NMR (300 MHz, CDCl₃) δ 4.6 (s, 1H), 2.9 (m, 2H), 1.3 (m, 17p), 0.9 (s, 1H); **¹³C NMR** (300 MHz, CDCl₃) δ 156, 130, 79, 42, 41, 33, 30.3, 29, 27. **HRMS** calculated for C₁₁H₂₄N₂O₂ - 216.1838, found 216.1843.

N- 2-ethylhexyl -N'- [tert-Butyl N-(hexyl)carbamate] naphthalenediimide, 6: Naphthalene monoimide (1.61 g, 4.24 mmol) was dissolved in 20 ml of 1,2-dichloroethane and heated to 80 °C under nitrogen. To this solution, **5** (0.92 g, 4.31 mmol) was added dropwise and refluxed for 15 h. After the reaction mixture had cooled down, the solvent was evaporated under reduced pressure. The crude product was loaded onto a silica column and eluted with 10 % ethylacetate in dichloromethane to get 2.2 g (90 %) of **6**.

¹H NMR (300 MHz; CDCl₃) δ 8.7 (s, 4H), 4.6 (s, 1H), 4.2 (m, 4H), 3.1 (d, 2H), 1.7 (m, 1H), 1.6 (m, 2H), 1.4 (m, 23H), 1.0 (m, 6H); **¹³C NMR** (300 MHz; CDCl₃) δ 63.2, 162.8, 156, 131, 126, 123, 79, 76.5, 44, 40, 38, 30.7, 29.9, 28.6, 28.4, 28, 26.6, 26.4, 24, 23, 14, 10.6. **HRMS** calculated for C₃₃H₄₃N₃O₆ - 577.3153, found 577.3152.

N- (2-ethylhexyl)-N'-(6-aminohexyl)naphthalenediimide, 7: Compound **6** (0.86 g, 1.49 mmol) was dissolved in dichloromethane, and a 100 mol % excess of TFA added slowly and refluxed for 15 h under nitrogen. The mixture was allowed to cool to room temperature, and the solvent was evaporated under reduced pressure. The resulting residue was dissolved in CHCl₃ and washed with saturated NaHCO₃ (3 × 20 ml). Finally, the organic layer was dried over anhydrous Na₂SO₄ and solvent evaporated to get 0.7 g (98 %) of **7**.

¹H NMR (300 MHz, CDCl₃) δ 8.6 (s, 4H), 4 (m, 4H), 2.5 (s, 2H), 1.8 (t, 1H), 1.6 (m, 2H), 1.2 (m, 16H), 0.7 (m, 6H); **¹³C NMR** (300 MHz, CDCl₃) δ 163.6, 163.2, 131, 127, 45, 41,

38, 31, 29, 28, 27, 26.9, 24, 23, 14, 11. **HRMS** calculated for $C_{28}H_{35}N_3O_4$ - 477.2628, found 477.2627.

General synthetic procedure for polymers 1-4: Ca. 0.42 mmol of **7** and 0.38 mmol of the backbone polymer were taken up in 20 ml dry DMSO. This mixture was stirred for 40 h at 170 °C under argon. After cooling the reaction mixture to room temperature, 50 ml of $CHCl_3$ was added to the reaction flask. Then the mixture was washed with water (4 × 50 ml). The organic layer was dried over anhydrous Na_2SO_4 and the solvent was evaporated under reduced pressure, to get a dark brown powder. This crude product was recrystallized three times from $CHCl_3$ and MeOH solvent mixtures. The final filtered precipitate on the filter was dissolved in $CHCl_3$ and the solvent was evaporated to get a dark red/brown polymer powder.

Polymer 1

1H NMR (300 MHz, d_2 -DCM) δ 8.60 (br, 4 H, Naphth-H Aromatic), 7.07 (br, 5H, phenyl-H), 3.95 (br, 6H, 3 × N- CH_2 -), 1.78 (br, m, 1H, - CH_2 -CH- CH_2 -), 1.61 (br, 2H, N- CH_2 - CH_2 -), 1.22 (br, 14H, 7 × CH_2), 0.79 (br, 6H, 2 × CH_3);. **^{13}C NMR** δ 10.74, 14.27, 23.44, 24.33, 26.93, 28.09, 28.99, 31.02, 38.32, 40.99, 44.76, 126.87, 129.05, 131.10, 163.05.

Polymer 2

1H NMR (300 MHz, d_2 -DCM) δ 8.50 (br, 4 H, Naphth-H Aromatic), 7.07 (br, 5H, phenyl-H), 3.96 (br, 6H, 3 × N- CH_2 -), 1.78 (br, m, 1H, - CH_2 -CH- CH_2 -), 1.66 (br, 2H, N- CH_2 - CH_2 -), 1.22 (br, 14H, 7 × CH_2), 0.78 (br, 6H, 2 × CH_3);. **^{13}C NMR** δ 10.74, 14.28, 23.45, 24.34, 26.90, 27.78, 28.11, 28.99, 31.02, 38.33, 40.98, 44.75, 126.83, 128.85, 131.11, 163.04, 163.20, 163.41.

Polymer 3

1H NMR (300 MHz, d_2 -DCM) δ 8.55 (br, 4 H, Naphth-H Aromatic), 3.97 (br, 6H, 3 × N- CH_2 -), 3.3 (2H, - CH_2 -CH(R)-), 1.78 (br, m, 1H, - CH_2 -CH- CH_2 -), 1.59 (br, 2H, N- CH_2 - CH_2 -), 1.12 (br, 14H, 7 × CH_2), 0.78 (br, 9H, 3 × CH_3);. **^{13}C NMR** δ 10.72, 14.26, 23.09, 23.44, 24.32, 26.98, 28.18, 28.98, 29.78, 30.17, 31.01, 32.32, 38.32, 40.97, 44.73, 126.84, 131.08, 163.00.

Polymer 4

¹H NMR (300 MHz, d₂-DCM) δ 8.59 (br, 4 H, Naphth-H Aromatic), 3.96 (br, 6H, 3 \times N-CH₂), 3.35 (2H, -CH₂-CH(R)-), 1.77 (br, m, 1H, -CH₂-CH-CH₂-), 1.60 (br, 2H, N-CH₂-CH₂-), 1.19 (br, 14H, 7 \times CH₂), 0.78 (br, 9H, 3 \times CH₃); **¹³C NMR** δ 10.72, 14.26, 23.03, 23.43, 25.70, 6.91, 27.94, 28.17, 28.98, 30.16, 31.01, 32.20, 38.32, 41.01, 44.75, 126.87, 131.10, 163.04, 163.20, 163.40.

5.4. Conclusion

Maleic anhydride-based side-chain polymers carrying electron-accepting naphthalene diimide groups were synthesized via a grafting procedure, with the aim to tune the morphology of the materials when applied in bulk heterojunctions along with donor polymers. Degrees of substitutions up to 60 % were achieved and the resulting polymers are very well soluble in solvents like chloroform, dichloromethane, *etc.* All these polymers were obtained in their closed-ring imide form.

In fluorescence spectra of these polymers in chloroform solution, excimer fluorescence from NDI was observed and attributed to ground state dimerization in solution. These electron-accepting polymers exhibited about 50 % fluorescence quenching when mixed with P3HT. TEM image of these blends showed large domains in the order of μm scale. The relatively low fluorescence quenching and the lower TRMC signals were accounted for by the reduced miscibility between the donor and acceptor polymers, possibly resulting from the rather hydrophobic nature of the electron-acceptor polymer. Therefore, micrometer-sized donor-only and acceptor-only domains are formed in films. In addition, possible burying of the electron-accepting units within polymer coils might further lower the fluorescence quenching efficiency and photo-induced conductance.

5.5. References

1. Gebeyehu, D.; Brabec, C. J.; Padinger, F.; Fromherz, T.; Hummelen, J. C.; Badt, D.; Schindler, H.; Sariciftci, N. S. *Synth. Met.* **2001**, *118*, 1-9.
2. Angadi, M.; Gosztola, D.; Wasielewski, M. R. *Mater. Sci. Eng. B-Solid State Mater. Adv. Technol.* **1999**, *63*, 191-194.
3. Bellmann, E.; Shaheen, S. E.; Thayumanavan, S.; Barlow, S.; Grubbs, R. H.; Marder, S. R.; Kippelen, B.; Peyghambarian, N. *Chem. Mater.* **1998**, *10*, 1668-1676.
4. Fuchigami, H.; Tsumura, A.; Koezuka, H. *Appl. Phys. Lett.* **1993**, *63*, 1372-1374.
5. Grigalevicius, S. *Synth. Met.* **2006**, *156*, 1-12.
6. Brabec, C. J.; Padinger, F.; Hummelen, J. C.; Janssen, R. A. J.; Sariciftci, N. S. *Synth. Met.* **1999**, *102*, 861-864.
7. Brabec, C. J.; Sariciftci, N. S.; Hummelen, J. C. *Adv. Funct. Mater.* **2001**, *11*, 15-26.
8. Martens, T.; D'Haen, J.; Munters, T.; Beelen, Z.; Goris, L.; Manca, J.; D'Olieslaeger, M.; Vanderzande, D.; De Schepper, L.; Andriessen, R. *Synth. Met.* **2003**, *138*, 243-247.
9. Wienk, M. M.; Kroon, J. M.; Verhees, W. J. H.; Knol, J.; Hummelen, J. C.; van Hal, P. A.; Janssen, R. A. J. *Angew. Chem.-Int. Edit.* **2003**, *42*, 3371-3375.
10. Ganesan, P.; Yang, X. N.; Loos, J.; Savenije, T. J.; Abellon, R. D.; Zuilhof, H.; Sudhölter, E. J. R. *J. Am. Chem. Soc.* **2005**, *127*, 14530-14531.
11. Alam, M. M.; Jenekhe, S. A. *Chem. Mater.* **2004**, *16*, 4647-4656.
12. Alam, M. M.; Tonzola, C. J.; Jenekhe, S. A. *Macromolecules* **2003**, *36*, 6577-6587.
13. Alam, M. M.; Jenekhe, S. A. *J. Phys. Chem. B* **2001**, *105*, 2479-2482.
14. Cravino, A.; Sariciftci, N. S. *J. Mater. Chem.* **2002**, *12*, 1931-1943.
15. Ego, C.; Marsitzky, D.; Becker, S.; Zhang, J. Y.; Grimsdale, A. C.; Mullen, K.; MacKenzie, J. D.; Silva, C.; Friend, R. H. *J. Am. Chem. Soc.* **2003**, *125*, 437-443.
16. Russell, D. M.; Arias, A. C.; Friend, R. H.; Silva, C.; Ego, C.; Grimsdale, A. C.; Mullen, K. *Appl. Phys. Lett.* **2002**, *80*, 2204-2206.
17. Sivula, K.; Ball, Z. T.; Watanabe, N.; Frechet, J. M. J. *Adv. Mater.* **2006**, *18*, 206-210.
18. Ball, Z. T.; Sivula, K.; Frechet, J. M. J. *Macromolecules* **2006**, *39*, 70-72.
19. Ramos, A. M.; Rispen, M. T.; van Duren, J. K. J.; Hummelen, J. C.; Janssen, R. A. J. *J. Am. Chem. Soc.* **2001**, *123*, 6714-6715.

20. Brettar, J.; Burgi, T.; Donnio, B.; Guillon, D.; Klappert, R.; Scharf, T.; Deschenaux, R. *Adv. Funct. Mater.* **2006**, *16*, 260-267.
21. Zheng, Y. Y.; Li, Q. Y.; Zhang, B. Y.; Zhang, L. F. *J. Appl. Polym. Sci.* **2005**, *97*, 2392-2398.
22. Zhu, J.; Wu, L. P.; Zhang, Y. Y.; Jin, X.; He, S. J.; Shi, K. Y.; Guo, X. Z.; Du, Z. J.; Zhang, B. L. *J. Appl. Polym. Sci.* **2006**, *102*, 4565-4572.
23. Kawatsuki, N.; Kawakami, T.; Yamamoto, T. *Adv. Mater.* **2001**, *13*, 1337-1339.
24. Kriz, J.; Plestil, J.; Tuzar, Z.; Pospisil, H.; Brus, J.; Jakes, J.; Masar, B.; Vlcek, P.; Dosekova, D. *Macromolecules* **1999**, *32*, 397-410.
25. Hao, X. J.; Stenzel, M. H.; Barner-Kowollik, C.; Davis, T. P.; Evans, E. *Polymer* **2004**, *45*, 7401-7415.
26. Yan, H.; Zhu, X. *J. Appl. Polym. Sci.* **1999**, *74*, 97-105.
27. Aldea, G.; Chitanu, G. C.; Delaunay, J.; Nunzi, J. M.; Simionescu, B. C.; Cousseau, J. *J. Polym. Sci. Pol. Chem.* **2005**, *43*, 5814-5822.
28. Nieuwhof, R. P.; Koudijs, A.; Marcelis, A. T. M.; Sudholter, E. J. R. *Macromolecules* **1999**, *32*, 6499-6506.
29. McCulloch, I.; DeMartino, R.; Keosian, R.; Leslie, T.; Man, H. T. *Macromol. Chem. Phys.* **1996**, *197*, 687-699.
30. Ikeda, T.; Hasegawa, S.; Sasaki, T.; Miyamoto, T.; Lin, M. P.; Tazuke, S. *Makromol. Chem.* **1991**, *192*, 215-221.
31. Far, S.; Kossanyi, A.; Verchere-Beaur, C.; Gresh, N.; Taillandier, E.; Perree-Fauvet, M. *Eur. J. Org. Chem.* **2004**, 1781-1797.
32. Braks, J. G.; Huang, R. Y. M. *J. Appl. Polym. Sci.* **1978**, *22*, 3111-3120.
33. Mehrotra, S.; Nigam, A.; Malhotra, R. *Chem. Commun.* **1997**, 463-464.
34. Ganesan, P.; Van Lagen, B.; Marcelis, A. T. M.; Zuilhof, H.; Sudhölter, E. *Org. Lett* **2007** (In Press).
35. Chen, Z. J.; Stepanenko, V.; Dehm, V.; Prins, P.; Siebbeles, L. D. A.; Seibt, J.; Marquetand, P.; Engel, V.; Würthner, F. *Chem.-Eur. J.* **2007**, *13*, 436-449.
36. Balakrishnan, K.; Datar, A.; Naddo, T.; Huang, J. L.; Oitker, R.; Yen, M.; Zhao, J. C.; Zang, L. *J. Am. Chem. Soc.* **2006**, *128*, 7390-7398.
37. Barros, T. C.; Brochsztain, S.; Toscano, V. G.; Berci, P.; Politi, M. J. *J. Photochem. Photobiol. A-Chem.* **1997**, *111*, 97-104.

Glossary of Acronyms

BF-TEM	- Bright Field - Transmission Electron Microscopy
CB	- Chlorobenzene
CT	- Charge – Transfer
DADS	- Decay – Associated Difference Spectra
DCM	- Dichloromethane
DMF	- N,N – Dimethylformamide
DMSO	- Dimethylsulfoxide
ESR	- Electron Spin Resonance
FP-TRMC	- Flash Photolysis – Time-Resolved Microwave Conductivity
HOMO	- Highest Occupied Molecular Orbital
IR	- Infrared
ISC	- Inter – System Crossing
LUMO	- Lowest Unoccupied Molecular Orbital
MALDI-TOF	- Matrix-Assisted Laser Desorption/Ionization – Time of Flight
MDMO-PPV	- Poly[2-methoxy-5-(3,7-dimethyloctyloxy)-1,4-phenylenevinylene]
NDI	- 1,4,5,8-naphthalene tetracarboxylic diimide
NIR	- Near – Infrared
ODCB	- 1,2 – Dichlorobenzene
OFET	- Organic Field Effect Transistor
OLED	- Organic Light Emitting Diode
OTFT	- Organic Thin Film Transistor
P3HT	- Poly(3-hexylthiophene)
PCBM	- Phenyl-C61-Butyric acid Methyl ester
PEDOT : PSS	- Poly(3,4-ethylenedioxythiophene) poly(styrenesulfonate)
PR-TRMC	- Pulse Radiolysis - Time-Resolved Microwave Conductivity
PTV	- Poly- (2,5-thienylene vinylene)
PV	- Photovoltaics
SAED	- Selective-Area Electron Diffraction
TCSPC	- Time – Correlated Single - Photon Counting
THF	- Tetrahydrofuran

Summary

The importance of organic materials for use in electronic devices such as OLEDs, OFETs and photovoltaic cells has increased significantly over the past decade. Organic materials have been attractive candidates for such electronic devices because of their compatibility with high-throughput, low-cost processing techniques and their capability to be precisely functionalized to afford desired performance attributes. This has already lead to commercial applications of OLED in car-audio, cell phones and digital cameras. To further improve the performance of these materials, many research groups are focusing on controlling the morphology of the organic films by carefully fine tuning the degree of crystallinity. Synthetic organic chemistry plays a pivotal role in this, as the toolbox of organic chemistry allows the formation of tailor-made materials that form a uniform film in their solid state.

Organic photovoltaics is a rapidly growing field since the exponential growth of energy needs and the rapid depletion of the fossil fuels have led to a compelling demand for alternative sources of energy. The traditional inorganic solar cells are based on silicon. Although energy efficiencies around 25 % have been reached in silicon-based solar cells, for many climatological conditions they are not cost effective since the production of such photovoltaic device requires demanding conditions like high processing temperature, clean room facilities, *etc.*, which prevents the commercially attractive bulk production. Therefore, a significant research efforts are focused on easily processable organic materials for use in photovoltaic devices. Usually the organic photovoltaic devices consist of an electron donating polymer (*p*-type material) and a fullerene-based electron-accepting material (*n*-type material). For such devices energy efficiencies up to 5.2 % have been reported. A significant issue in these devices is the crystallization of fullerenes, which easily leads to excessive phase separation between *p*- and *n*-type materials.

Amorphous molecular materials may exhibit isotropic properties due to the absence of grain boundaries. Naphthalene diimides (NDI) are known to have a high conductivity and electron-accepting capability from a variety of electron donors. This thesis aims at making use of the properties of novel amorphous materials with NDIs to

obtain uniform films without phase separation and crystallization for use in organic solar cells.

Chapter 1 gives an overview of the organic (opto-)electronic materials and of the working principles of several devices that are based on such materials. Solar cells, in particular organic heterojunction cells, are described in detail. The importance of the nanoscale morphology in such heterojunction devices is discussed, together with expected advantages of amorphous materials to obtain films with the desired morphology. Finally the outline of the thesis is given.

A new approach towards the design and synthesis of amorphous *n*-type materials with NDIs is presented in *Chapter 2*. The tetrahedral shape of the molecule yields the amorphous material properties, which are decoupled from its optoelectronic properties. In the first tetrahedral molecule the non-directionality available via tetrahedral cores, as present in tetra(phenyl)methane, is used. This tetrahedral material with 4 NDIs has been characterized for its steady-state and transient optical behavior and for its ground-state electrochemical properties. It has been shown to display a conductivity of $0.03 \text{ cm}^2 \text{ V}^{-1} \text{ s}^{-1}$ in neat film, and exhibited a near-complete quenching of the *p*-type polymer fluorescence. The blended films of this tetrahedral molecule with polymeric *p*-type materials have a very uniform morphology and demonstrated high transient charge carrier mobility.

The photophysical properties of the tetrahedral molecule with naphthalene diimide (NDI) moieties and of two model compounds are described in *Chapter 3*. One of the model compound is a symmetrically dialkyl substituted NDI and the other model compound is an NDI with an alkyl chain and a phenyl ring substitution. The steady-state absorption and fluorescence spectra of dialkyl-substituted NDI are in agreement with literature. While the absorption spectra of the phenyl-substituted molecules are similar to all other NDIs, their fluorescence showed a broad band between 500-650 nm. This band is sensitive to the polarity of the solvent, and is attributed to a charge-transfer (CT) state. The absorption spectra and lifetime ($10 \pm 1 \text{ ps}$) of the electronically excited singlet state of a dialkyl-substituted NDI was determined by femtosecond transient absorption spectroscopy, and the latter was confirmed by picosecond fluorescence spectroscopy. Nanosecond flash photolysis showed the subsequent formation of the triplet state. The presence of a phenyl substituent on the imide nitrogen of NDI resulted in faster deactivation of the singlet state (lifetime $0.5 - 1 \text{ ps}$). This is attributed to the formation of

a short-lived CT state, which decays to the local triplet state. The faster deactivation was confirmed by fluorescence-lifetime measurements in solution and in a low-temperature methyl-tetrahydrofuran (MTHF) glass.

Another new class of amorphous materials with NDIs is described in *Chapter 4*. Cyclic siloxanes are known to exhibit a size-dependent structure with amorphous properties. Novel cyclic siloxanes with pendent naphthalene diimides were synthesized via a hydrosilylation reaction, to form amorphous electron-accepting materials. These materials were studied for their basic photophysical properties using steady state and time-resolved techniques. The fluorescence spectra revealed the formation of excimers, which was shown to be solvent dependent. Fluorescence quenching studies of blends of these siloxanes with *p*-type polymers (P3HT, MDMO-PPV) showed >99.9 % fluorescence quenching of the latter polymers. Mixtures of these siloxanes and *p*-type polymers gave homogeneous amorphous films from chloroform solution, and films with micro-crystallinity were obtained from *o*-dichlorobenzene solutions. The time-resolved microwave conductance in films formed from *o*-dichlorobenzene was higher than in films formed from chloroform, which is attributed to nanoscopic phase separation that enhances the interfacial charge separation. Due to this reason, they also showed a better conductivity than the tetrahedral molecule.

For a good charge transport in the active organic heterojunction films, it is necessary to have a bicontinuous film with nanoscale phase separation. For this reason it is essential that the NDIs are interacting with each other. In order to achieve this, four novel naphthalenediimide (NDI) side-chain polymers were synthesized by grafting NDI onto poly(*R-alt*-maleic anhydride) backbone polymers with various R groups and molecular weights [R= styrene, 1-octene and 1-octadecene]. The synthesis and other characterizations of these materials are described in *Chapter 5*. These polymers were obtained with a degree of substitution up to 60 %, and showed a high solubility in solvents like chloroform. Their absorption and fluorescence spectra were studied both in solution and in thin films, with specific attention to the fluorescence quenching of P3HT in thin films. The results show that in all four polymers the NDI chromophores form π -stacked dimers in solution exhibiting excimer fluorescence. The morphology of the blends of the grafted polymers with P3HT was studied at various weight ratios, and revealed phase separation into domains of μm dimensions. These blends were also

Summary

studied using time-resolved microwave-conductivity for their photo-induced charge carrier generation efficiency, which showed appreciable generation of charge carriers, although significantly lower than observed in blends of P3HT with PCBM or oligomeric *n*-type siloxanes described in the previous chapter.

Overall it could be summarized that the formation of amorphous films with structural elements based on a tetrahedral organization or flexible siloxane rings provide a novel way to construct materials that can be used as *p*-type or *n*-type materials in optoelectronic devices. Use of these elements with appropriate aromatic systems containing more extended π -systems seems a viable route to further improve the potential of organic optoelectronic materials.

Samenvatting

Het belang van organische materialen voor gebruik in opto-elektronische componenten zoals OLED's, OFET's en fotonische cellen is het afgelopen decennium sterk toegenomen. Organische materialen zijn interessante kandidaten voor zulke elektronische toepassingen, omdat ze geschikt zijn voor productie en verwerking in grote hoeveelheden tegen lage kosten en met de mogelijkheid om ze precies te functionaliseren volgens gewenste prestatie/gedrag specificaties. Dit heeft al geleid tot commerciële toepassingen van OLED's in autoradio's, mobiele telefoons en digitale camera's. Om de prestaties van deze materialen verder te verbeteren, richten veel onderzoeksgroepen zich op controle van de morfologie van organische films door zorgvuldige afstemming van de mate van kristallisatie. Synthetische organische chemie speelt een centrale rol in dit proces, omdat de organische chemie de vorming mogelijk maakt van op maat gedefinieerde materialen, die een uniforme film vormen in de vaste toestand.

Onderzoek naar organische fotonische materialen is een snel groeiend veld omdat de exponentiële groei van de energiebehoefte en de snelle afname van fossiele brandstoffen heeft geleid tot een grotere vraag naar alternatieve energiebronnen. De traditionele anorganische zonnecellen zijn gebaseerd op silicium. Hoewel een energieoverdrachteefficiëntie van rond de 25% is gehaald met op silicium gebaseerde zonnecellen, zijn deze voor veel klimatologische omstandigheden niet kostendekkend. De productie van deze fotonische componenten vereist dure condities, zoals ultrazuiver materiaal, hoge verwerkingstemperaturen, cleanroom faciliteiten, etc. Dit belemmert de commercieel aantrekkelijke bulkproductie. Daarom zijn veel onderzoeksinspanningen gericht op eenvoudig te verwerken organische materialen voor gebruik in fotonische cellen. Vaak bestaan organische fotonische cellen uit een electrondonerend polymeer (*p*-type materiaal) en een op fulleren gebaseerd elektronaccepterend materiaal (*n*-type materiaal). Voor deze cellen zijn efficiënties tot 5,2 % gerapporteerd. Een significant aandachtspunt van deze cellen is de kristallisatie van fullerenen, welke makkelijk kan leiden tot overmatige fasenscheiding tussen *p*- en *n*-type materialen.

Amorfe moleculaire materialen kunnen isotrope eigenschappen vertonen door de afwezigheid van korrelgrenzen. Het is bekend dat naftaleendiïmides (NDI) een hoge ladingsgeleidbaarheid en elektronaccepterend vermogen hebben in combinatie met een verscheidenheid aan elektrondonoren. Dit proefschrift is gericht op het gebruik maken van de eigenschappen van nieuwe amorfe materialen met NDI groepen om uniforme films te krijgen zonder macroscopische fasenscheiding en kristallisatie voor toepassing in organische zonnecellen

Hoofdstuk 1 geeft een overzicht van organische (opto-)elektronische materialen en de werkingsprincipes van verschillende elektronische componenten die gebaseerd zijn op zulke materialen. Zonnecellen, in het bijzonder organische heterojunctie-cellen, worden gedetailleerd beschreven. Het belang van morfologie op de nanoschaal in zulke heterojunctie-cellen wordt besproken samen met de verwachte voordelen van amorfe materialen voor het verkrijgen van films met de gewenste morfologie. Ten slotte wordt een overzicht van het proefschrift gegeven.

Een nieuwe benadering gericht op ontwerp en synthese van amorfe *n*-type materialen met NDI's wordt gepresenteerd in *hoofdstuk 2*. De tetraëdrische vorm van het molecuul leidt tot amorfe materiaaleigenschappen, die –in tegenstelling tot fullerenen- ontkoppeld zijn van de opto-electronische eigenschappen. In het eerste tetraëdrische molecuul wordt gebruik gemaakt van de afwezigheid van oriëntatie in tetraëdrische centra zoals tetra(phenyl)methaan. Dit tetraëdrische materiaal met vier NDI's is gekarakteriseerd met betrekking tot zijn “steady-state” en tijdsopgeloste optische gedrag, en de elektrochemische eigenschappen in de grondtoestand. Het materiaal vertoonde een ladingsmobiliteit van $0,03 \text{ cm}^2 \text{ V}^{-1} \text{ s}^{-1}$ als pure film en een bijna complete doving van de *p*-type polymeer fluorescentie. De gemengde films van dit tetraëdrische molecuul met polymere *p*-type materialen hebben een zeer uniforme morfologie en vertoonden een hoge licht-geïnduceerde ladingdragers mobiliteit.

De fotofysische eigenschappen van het tetraëdrische molecuul met naftaleendiïmide eenheden en twee modelverbindingen worden beschreven in *hoofdstuk 3*. Eén van de modelverbindingen is een symmetrisch dialkyl-gesubstitueerde NDI en de andere modelverbinding is een NDI gesubstitueerd met zowel een alkylketen als een fenyling. De “steady-state” absorptie en fluorescentie spectra van de dialkyl-gesubstitueerde NDI zijn in overeenstemming met de literatuur. Terwijl de

absorptiespectra van de phenylgesubstitueerde moleculen vergelijkbaar zijn met alle andere NDI's is in de fluorescentie spectra een brede extra band tussen 500-650 nm te zien. Deze band is gevoelig voor de polariteit van het oplosmiddel en wordt toegeschreven aan een ladingsgescheiden (CT) toestand. Het absorptiespectrum en de levensduur (10 ± 1 ps) van de elektronisch aangeslagen singlet toestand van een dialkyl gesubstitueerde NDI zijn bepaald met femtoseconde tijdsopgeloste absorptiespectroscopie en bevestigd met picoseconde tijdsopgeloste fluorescentiespectroscopie. Nanoseconde flitsfotolyse spectroscopie liet de daaropvolgende vorming van de triplet toestand zien. De aanwezigheid van een phenylsubstituent aan de imide stikstof van NDI resulteerde in een snellere deactivering van de singlet toestand (levensduur 0.5 - 1 ps). Dit wordt toegeschreven aan de vorming van een kortlevende CT-toestand die verval naar de lokale triplet toestand. De snellere deactivering werd ondersteund door fluorescentie-levensduur metingen in oplossing en in een methylnetrahydro-furaan glas bij lage temperatuur.

Een andere nieuwe klasse van amorfe materialen met NDI's wordt beschreven in *hoofdstuk 4*. Cyclische siloxanen zijn bekend vanwege hun grootte-afhankelijke structuur met amorfe eigenschappen. Nieuwe cyclische siloxanen met daaraan naftaleendiimides werden gesynthetiseerd via een hydrosilyleringsreactie, resulterend in amorfe elektronaccepterende materialen. Deze materialen werden bestudeerd met betrekking tot de basale fotofysische eigenschappen met "steady-state" en tijdsopgeloste technieken. De fluorescentiespectra onthulden de vorming van excimeren, die oplosmiddel afhankelijk was. Fluorescentiedoving studies van mengsels van deze siloxanen met *p*-type polymeren (P3HT en MDMO-PPV) lieten een doving van meer dan 99,9% van de fluorescentie van genoemde polymeren zien. Mengsels van deze siloxanen en *p*-type polymeren gaven homogene amorfe films uit chloroform oplossingen en films met micro-kristallijneiteit werden verkregen uit *o*-dichloorbenzeen oplossingen. De tijdsopgeloste microgolfgeleidbaarheid in films uit *o*-dichloorbenzeen was hoger dan in films gevormd uit chloroform, wat wordt toegeschreven aan nanoscopische fasenscheiding die ladingsscheiding op het grensvlak versterkt. Om deze reden vertoonden deze films ook een betere geleidbaarheid dan die met het tetraëdrische molecuul.

Voor een goed ladingstransport in de actieve organische heterojunctiefilms is het noodzakelijk om een bicontinue film met nanoschaal fasenscheiding te hebben. Om deze

reden is het essentieel dat de NDI's onderling interactie hebben. Om dit te bereiken zijn vier nieuwe naftaleendiimide (NDI) zijketen-polymeren gesynthetiseerd, door NDI te koppelen aan polymeren met een poly(R-*alt*-maleinezuuranhydride) hoofdketen met verschillende restgroepen [R=styreen, 1-octeen en 1-octadeceen]. De synthese en overige karakterisaties van deze materialen zijn beschreven in *hoofdstuk 5*. Deze polymeren werden verkregen met een substitutiegraad van $\sim 60\%$ en vertoonden een hoge oplosbaarheid in oplosmiddelen zoals chloroform. De absorptie- en fluorescentiespectra werden bestudeerd in zowel oplossing als dunne films met specifieke aandacht voor de fluorescentie doving van P3HT in dunne films. De resultaten laten zien dat de NDI chromoforen in alle vier de polymeren in oplossing π -gestapelde dimeren vormen, die elk excimeer fluorescentie vertonen. De morfologie van de mengsels van de gekoppelde polymeren met P3HT werd bestudeerd bij verschillende gewichtsratio's en onthulde fasenscheiding in domeinen met μm dimensies. Deze mengsels werden ook bestudeerd met tijdsopgeloste microgolf geleidbaarheid voor de bepaling van de efficiëntie van lichtgeïnduceerde ladingsdragers vorming. Dit liet een meetbare vorming van ladingsdragers zien, hoewel significant lager dan waargenomen in mengsels van P3HT met PCBM of oligomere *n*-type siloxanen zoals beschreven in hoofdstuk 4.

Alles samengenomen kan worden gezegd dat de vorming van amorfe films met structuurelementen gebaseerd op tetraëdrische organisatie of flexible siloxaan ringen een nieuwe weg ontsluiten voor de constructie van materialen die kunnen worden gebruikt als *p*-type of *n*-type materialen in optoelectronische toepassingen. Gebruik van deze elementen met geschikte aromatische systemen die meer uitgebreide π -systemen bevatten lijkt een kansrijke route om het potentieel van organische optoelectronische materialen verder te vergroten.

Curriculum Vitae

Ganesan Palaniswamy was born in Coimbatore district, India, on May 7, 1975. He studied Chemistry at Sri Ramakrishna Mission Vidyalaya – College of Arts and Science and received his Bachelors degree in 1996. He completed his Masters program in Applied Chemistry at Coimbatore Institute of Technology in 1998. After his Masters degree he worked at the National Centre for Ultrafast Processes, University of Madras (May 1998-Sept. 2002) as a Project Assistant. Later he joined the Laboratory of Organic Chemistry, Wageningen University for PhD under the supervision of Professor E.J.R. Sudhölter and Professor H.Zuilhof. He worked on a Dutch Polymer Institute (DPI) sponsored project under the project cluster “Polymer photovoltaics”.

List of Publications

Tetrahedral n-Type Materials: Efficient Quenching of the Excitation of *p*-Type Polymers in Amorphous Films, Palaniswamy Ganesan, Xiaoniu Yang, Joachim Loos, Tom J. Savenije, Ruben D. Abellon, Han Zuilhof, and Ernst J. R. Sudhölter, *J. Am. Chem. Soc.*, **2005**, 127, 14530-14531.

Synthesis and fluorescence quenching of amorphous siloxanes with naphthalenediimide acceptor moieties, Palaniswamy Ganesan, Barend van Lagen, Antonius T. M. Marcelis, Han Zuilhof, and Ernst J. R. Sudhölter, *Org. Lett.* (**2007**), *In Press*.

Ultrafast photoprocesses of naphthalenediimide based tetrahedral molecule, Palaniswamy Ganesan, Jacob Baggerman, Hong Zhang, Han Zuilhof, and Ernst J. R. Sudhölter *J. Phys. Chem. A.* (**2007**), *In Press*.

Siloxanes with naphthalenediimides : relation between structure, morphology and microwave-conductivity, Palaniswamy Ganesan, Wojciech Grzegorzczuk, Svetlana S. van Bavel, Tom Savenije, Joachim Loos, Han Zuilhof, and Ernst J. R. Sudhölter (Manuscript in preparation).

Naphthalene Diimide Side-chain Polymers: Synthesis, Microwave Conductivity and Morphology Studies, Palaniswamy Ganesan, Wojciech Grzegorzczuk, Svetlana S. van Bavel, Tom Savenije, Joachim Loos, Han Zuilhof, and Ernst J. R. Sudhölter (Manuscript in preparation).

Naphthalenediimide – triphenylene based diads and triads : Synthesis and electron-transfer studies, Palaniswamy Ganesan, Ioan Paraschiv, Antonius T. M. Marcelis, Han Zuilhof, and Ernst J. R. Sudhölter (Manuscript in preparation).

Acknowledgments

During my preliminary school, at class four, my interests in science was induced by my teacher with very simple basic scientific experiments. Since then, I am more and more attracted to science and this force of attraction drove me to do a PhD. Now I am at the brink of getting my PhD degree, although reaching to a bachelor's level was already a dream to me during my school days. Looking back at all the hurdles, twists and turns that I have crossed at various stages in my life, I honestly agree it is not only me who did everything to reach this stage. At each difficult moment there has been someone who rescued me. Likewise, this thesis is also an outcome of many collaborations and cooperations. I take this space to thank all who stood with me during my PhD period not only in professional life but also in social life.

At the outset I would like to thank my promoters Professor Ernst J. R. Sudhölter and Professor Han Zuilhof for the opportunity to work in their group and for all the help that they rendered from day one till today. I would like to thank Professor Zuilhof for his trust and patience to wait for about 13 months, before I could start in the laboratory. Han, I think I learnt a lot from you not only from the answers that you gave me, but also from the questions that you asked me. Your training taught me how to be more precise and accurate in what I do and say. Han, I did enjoy working with you with all the freedom and thanks for everything that you did for me.

I have always seen Professor Sudhölter as an optimistic person. At the point when I was stuck in the project you gave me your helping hand and assured that “we will see you going out of this lab as a doctor”. You have not stopped with that assurance but also made sure that it is really happening and now it is becoming a reality. I thank Professor Sudhölter for his positive energy and all the help during my PhD.

As I mentioned in the beginning, this thesis would not have been possible without the cooperations and collaborations especially with the group of Professor L.D.A Siebbeles and Dr. Tom Savenije (TU Delft), Dr. Hong Zhang (UvA) and Dr. Joachim Loos (TU/e), Dr. Jan M. Kroon (ECN). I thank all of them for their readiness to study the materials that I have synthesized. My visits to their laboratory and working with people like Wojciech Grzegorzcyk (TU Delft), Svetlana van Bavel and Xiaoni Yang

Acknowledgments

(TU/e), Elio Cecchetto, Michiel Groeneveld, Dick Bebelaar (UvA) and Sjoerd Veenstra (ECN) gave me good experience and knowledge in different fields. I thank all of you for your great efforts especially to Wojciech and Svetlana for studying lots of samples described in Chapters 4 and 5, within a short notice. I thank all the people in the DPI project clusters for fruitful constructive discussions during the meetings.

I would like to thank Dr. Ton Marcelis for his inputs, discussions and all the help at various stages during my PhD especially with Chapter 4. Many thanks are to Barend van Lagen for his NMR and photophysical measurements. I would like to thank Jacob Baggerman for all his contributions in Chapter 3 and also for making the Dutch version of the summary.

It was a nice experience to work with students of school and university levels. I thank Linda, Saskia and Patrick who worked in this project at different times.

I will always cherish my PhD period at the Laboratory of Organic Chemistry. I thank all the colleagues and friends - Ioan, Kishore, Remko, Tina, Cindy, Michael, Louis, Agnes, Gregor, Dawei, Bin, Ruud, Floor, Frederique, Michel, Milena, Aliaksei, Rosalie, Suzanne, Annemarie, Ahmed, Giedrius, Feng, Qiaoyu, Maud, Loes, Luc, Jurjen, Bart and Asif for the pleasant time. I enjoyed the talks and discussions during borrels, AIO events and barbeques. The great times during our AIO trips to Swiss and USA and during lab-trips I will never forget.

I would like to thank Beb van Veldhuizen for his help with NMR, Elbert van der Klift for the elemental analysis and HPLC measurements, Dr. Maarten A. Posthumus for mass measurements, Edwin Bakx at the Food Chemistry Department for MALDI-TOF measurements, Rob Koehorst and Arie van Hoek at the Biophysics department for their help with steady-state fluorescence and fluorescence lifetime measurements. I thank Elly Geurtsen for her help with residence permit and other official matters.

The typical loneliness of each foreigner in Wageningen makes them to look for people who are in similar situation and make a good friendship. In that way Wageningen is the place, where I made lots of Indian friends from different parts of India, which I would not have managed if I were in India. I will always cherish the good times that I had with valuable friends like Anand, Ajay, Kishore, Sangita, and Anjal. I thank Shibu, Karishma, Basav, Shital, Manickam, Namasivayam, Vanniarajan, Anu, Arijit, Arun, Byjesh,

Acknowledgments

Srinivas, Aarti, Ram, Sharad, Bobby, Palwinder, Senthil and Selvi, for their encouragement and support. My thanks to Shibu for his layout tips.

Haarweg 81 has become a home away from home for me during my stay in Wageningen. I should thank my corridor mates Tony, Marco, Roel, Monique, Martijn, Jean, Marjolein, Joep, Sander and Wouter, with whom I spent a memorable time inside and outside the corridor. I appreciate the care and help I received from Senthil, Vasanth, Vigneswaran, Kugan and their family, during my stay in Wageningen. I thank the captain Alex and members of Wageningen Cricket Club, for the opportunity to play my passion game in Netherlands.

Distance did not separate me from Gowri, Shankar, Santhosh, Rajaram, Saravanakumar, Sureshkumar who are in different parts of the world, still are in constant touch and cheering me up all the time. Dear friends, thanks for standing with me during all walks of my life.

To my family, எந்தவிதமான எதிர்பார்ப்புகளுமின்றி என் விருப்பத்தை நிறைவேற்றுவதற்காக தங்கள் சிரமங்களையும் பொருட்படுத்தாமல் தங்களால் முடிந்த அனைத்து உதவிகளையும் செய்து என் தாய் முத்தம்மாள், தந்தை பழனிச்சாமி, அண்ணன் வடிவேல், அண்ணி சுமதி, அக்கா கலாமணி, பாவா பழனிச்சாமி, அக்கா இந்திராணி மற்றும் பாவா மல்லீஸ்வரன் ஆகியோருக்கு நான் என்றென்றும் நன்றிக்கடன் பட்டுள்ளேன்.

Ganesan

Overview of completed training activities

Discipline specific activities

Courses

European Commission Winter School on Organic Reactivity Bressanone, Italy, 2003
DPI Winter School on Organic and Polymer Photovoltaics, The Netherlands 2003
European Photochemistry Association- Summer School, The Netherlands 2003
110th International Summer Course organised by BASF, Germany, 2005

Meetings

NWO Ontwerp en Synthese, Structuur en Reactiviteit, Biomoleculaire Chemie conference, The Netherlands, February 2003
DPI Workshop on Automated Synthesis and High-Throughput Experimentation in Polymer and Materials Research, Eindhoven University of Technology, The Netherlands, 2003
NWO Ontwerp en Synthese Structuur en Reactiviteit Biomoleculaire Chemie conference, The Netherlands, October 2003
Ph.D. Study trip, organised by the Laboratory of Organic Chemistry, Switzerland, 2003
20th Wageningen Symposium of Organic Chemistry, The Netherlands, 2004
Seminar on Solar cell research in the Netherlands, The Netherlands, 2004
NWO Ontwerp en Synthese Structuur en Reactiviteit Biomoleculaire Chemie conference, The Netherlands, 2004
Ph.D. Study trip, organised by the Laboratory of Organic Chemistry, USA, 2003
DPI-Functional Polymer System mini symposium, The Netherlands, 2006
21st Wageningen Symposium of Organic Chemistry, The Netherlands, 2006
CW-studiegroep Spectroscopie en Theorie, The Netherlands, 2007

General courses

Dutch Language courses (2 levels), Language School, Wageningen University, 2003
VLAG PhD week, 2003
Organising and supervising MSc thesis projects, Wageningen University, 2004

Optionals

Preparation PhD research proposal
Literature study – Laboratory of Organic Chemistry, Wageningen University, 2002

The research described in this thesis was financially supported by the Dutch Polymer Institute (DPI) (project number 324).